

CATALYTIC OXIDATION OF CARBON  
MONOXIDE AND DIMETHYL ETHER SYNTHESIS  
OVER GOLD-CONTAINING CATALYSTS

Thabang Abraham Ntho

A thesis submitted to the faculty of Science, University of the Witwatersrand,  
Johannesburg, in fulfilment of the requirements for the degree of Doctor of Philosophy.

Johannesburg, 2008

## Declaration

I declare that this is my own, unaided work. It is being submitted for the Degree of Doctor of Philosophy in the University of the Witwatersrand, Johannesburg. It has not been submitted before for any degree or examination in any other University.

---

Signature of candidate

\_\_\_\_\_ day of February 2008

## Abstract

In recent years, the catalytic properties of finely dispersed gold particles on oxide support materials have attracted much attention. Such catalysts are active for several types of oxidation reactions, in particular low-temperature carbon monoxide oxidation. The water-gas-shift (WGS) reaction and the selective oxidation of CO in the presence of hydrogen are possible applications of gold-based catalysts.

In this thesis we attempted to detail the key issues relevant to the deactivation of supported gold catalysts. A new aspect of the CO oxidation deactivation mechanism was comprehensively discussed. It was found that titanate nanotube supported gold catalyst (Au/TN), prepared by deposition precipitation, deactivated due to the formation of bicarbonate species on gold-sites. Moisture prevented the formation and accumulation of these species and also promoted the reaction. The Au/TN catalyst was characterised by HRTEM, *in-situ* DRIFTS-Mass spectrometry, BET, etc.

Titanium dioxide ( $\text{TiO}_2$ ) is widely used as support material for various important industrial catalysts and its modification may suite specific catalytic requirements. In this work we have confirmed that the incorporation of nitrogen (N) into  $\text{TiO}_2$  increases the concentration of oxygen ion vacancies. When tested for CO oxidation, the nitrogen-doped titania supported gold catalyst,  $\text{Au/TiO}_{2-x}\text{N}_x$ , was found to be a poor and unstable catalyst compared to the pure titania supported gold catalyst,  $\text{Au/TiO}_2$ . Both catalysts were characterised by XRD, Raman spectroscopy, DRS-UV visible spectroscopy, TPO, BET, HRTEM etc.

New Cu-based methanol synthesis catalysts, prepared by co-precipitation and deposition precipitation, were physically mixed with  $\gamma\text{-Al}_2\text{O}_3$  and tested for the direct single-step DME synthesis from syngas. The catalysts exhibited good CO conversion and DME selectivity. The loading of gold on the methanol synthesis components of the bifunctional catalysts promoted CO conversion and the WGS reaction. In addition, Au suppressed

methanation on the bifunctional catalysts. The catalysts were characterised by TPR, XRD, BET and XRF spectroscopy.

Dedicated to: 'Majoale Jeanette Ntho

## Publications and Presentation related to this work

### Publications

1. T. A. Ntho, J. A. Anderson and M. S. Scurrrell, “*CO oxidation over titanate nanotube supported Au: Deactivation due to bicarbonate*” **To be submitted.**
2. R. Sakhthivel, T. A. Ntho and M. S. Scurrrell, “*CO oxidation over anatase TiO<sub>2</sub> supported Au: Effect of nitrogen doping*” **To be submitted.**
3. T. A. Ntho and M. S. Scurrrell, “*Effect of Au on copper-based catalysts for the direct synthesis of DME from syngas*” **To be submitted.**
4. R. Sakhthivel, T. A. Ntho and M. S. Scurrrell, “*CO oxidation over TiO<sub>2</sub>-CeO<sub>2</sub> supported gold: enhancing effect of CuO*” **To be submitted.**

### Presentations

#### A. Posters

1. RSC SURCAT 2006 Meeting, Cardiff University, Wales, UK.
2. CATSA 2005, Midrand, Johannesburg, S.A.

#### B. Oral

1. CATSA 2006, Mosselbay, Western Cape, S. A.

## Acknowledgements

I am greatfull to the following persons and institutions:

1. My supervisor, Professor Michael S. Scurrrell, for the opportunity and challenge.
2. Basil Chassoulas, for moral and technical support.
3. Professor Jim Anderson, for his teachings on infrared spectroscopy.
4. Dr Sakhthivel Ramasamy, for useful discussions on solid state chemistry.
5. My family: Mots'oane, Connie, Thapelo, Palesa and Nyakallo Ntho; I love you all!
6. All my Catomat friends. Thank you all.
7. Puleng Morake, for all the love, support and typing. Thanks a million.
8. My buddies Tefo (T-bone), Edwin, Gatawa, Maz, Monyane, Tau and the Lolos crew.
9. University of the Witwatersrand
10. Mintek
11. DAAD
12. Canon Collins Education Trust
13. National Manpower Development Secretariat of Lesotho

# Table of Contents

Declaration.....	ii
Abstract.....	iii
Dedicated .....	v
Publications and Presentation related to this work .....	vi
Acknowledgements.....	vii
List of Tables .....	xii
List of Figures .....	xiii
<b>Chapter 1 Introduction.....</b>	<b>1</b>
<b>Chapter 2 Literature Review .....</b>	<b>3</b>
<i>2.1 Reactions catalysed by gold.....</i>	<i>3</i>
<i>2.2 CO oxidation .....</i>	<i>5</i>
2.2.1 Factors that affect activity.....	5
2.2.2 Controversial issues .....	14
2.2.2.1 Oxidation state of active Au .....	14
2.2.2.2 Activation of molecular oxygen (O <sub>2</sub> ).....	15
2.2.2.3 Role of moisture.....	18
2.2.2.4 The active site .....	20
<i>2.3 Direct synthesis of dimethyl ether from syngas .....</i>	<i>24</i>
2.3.1 What is DME?.....	24
2.3.2 Process thermodynamics.....	25
2.3.3 Choice of reactor.....	26
<i>2.4 References .....</i>	<i>28</i>

<b>Chapter 3 Experimental Procedures.....</b>	<b>32</b>
<i>3.1 Catalyst preparation .....</i>	<i>32</i>
3.1.1 Synthesis of titanate nanotube support .....	32
3.1.2 Preparation of titanate nanotube-supported Au catalyst.....	32
3.1.3 Synthesis of nitrogen-doped anatase TiO <sub>2</sub> : TiO <sub>2-x</sub> N <sub>x</sub> .....	33
3.1.4 Preparation of the Au/TiO <sub>2-x</sub> N <sub>x</sub> and Au/TiO <sub>2</sub> catalysts .....	33
3.1.5 Methanol synthesis catalysts.....	33
3.1.5.1 Preparation of the CuO-ZnO-Al <sub>2</sub> O <sub>3</sub> catalyst.....	33
3.1.5.2 Preparation of CuO-ZnO-Al <sub>2</sub> O <sub>3</sub> -Cr <sub>2</sub> O <sub>3</sub> -ZrO <sub>2</sub> -CeO <sub>2</sub> .....	34
<i>3.2 Catalyst characterization.....</i>	<i>35</i>
3.2.1 Surface area determination: BET.....	35
3.2.2 Diffuse Reflectance Infrared Fourier Transform (DRIFT) Spectroscopy .....	35
3.2.3 Temperature Programmed Desorption (TPD) .....	36
3.2.4 Temperature Programmed Oxidation (TPO) .....	36
3.2.5 High Resolution Transmission Electron Microscope (HR-TEM) .....	36
3.2.6 X-ray Diffraction (XRD) measurements .....	36
3.2.7 Diffuse Reflectance spectroscopy (DRS-UV-Vis) and Raman .....	37
3.2.8 X-ray Florescence (XRF) spectroscopy.....	37
<i>3.3 Catalytic evaluation .....</i>	<i>38</i>
3.3.1 CO Oxidation .....	38
3.3.1.1 Activity measurement of Au/TN .....	38
3.3.1.2 Activity measurement of Au/TiO <sub>2</sub> and Au/TiO <sub>2-x</sub> N <sub>x</sub> .....	38
3.3.2 Direct DME synthesis.....	39
3.3.2.1 Product analysis: the rig.....	40
3.3.2.2 Quantification of products .....	41
<i>3.4 References .....</i>	<i>43</i>

**Chapter 4 CO oxidation over titanate nanotube supported gold: Deactivation due to bicarbonate species. .... 44**

4.1. *Introduction*..... 44

4.2. *Results* ..... 45

    4.2.1 Characterization of the support and catalyst..... 45

    4.2.2 CO oxidation..... 47

    4.2.3 CO<sub>2</sub>-TPD..... 49

        4.2.3.1 Titanate nanotube (TN)..... 49

        4.2.3.2 Au/TN catalyst..... 50

    4.2.4 DRIFT spectroscopic measurements ..... 52

4.3. *Discussion*..... 56

4.4. *Conclusions*..... 59

4.5. *References* ..... 60

**Chapter 5 CO oxidation over anatase TiO<sub>2</sub> supported Au: Effect of nitrogen doping. .... 62**

5.1. *Introduction*..... 62

5.2. *Results* ..... 63

    5.2.1 Phase characterization, surface properties and HRTEM studies ..... 63

    5.2.2 Optical properties..... 66

    5.2.3 Ability of oxygen uptake by the supports ..... 67

    5.2.4 Oxidation of CO..... 68

        5.2.4.1 Effect of pre-treatment..... 68

        5.2.4.2 Effect of moisture ..... 71

        5.2.4.3 Regeneration of activity..... 72

        5.2.4.3 Effect of temperature ..... 75

5.3. *Discussion*..... 77

5.4. *Conclusions*..... 81

5.4. *Conclusions*..... 81

5.5. References .....	82
5.5. References .....	82
<b>Chapter 6 Effect of gold on copper-based catalysts for the direct synthesis of DME from syngas.....</b>	<b>85</b>
6.1 Introduction.....	85
6.2 Results .....	87
6.2.1 Surface area.....	87
6.2.2 X-ray analyses.....	88
6.2.3 H <sub>2</sub> -TPR analyses .....	90
6.2.4 Effect of addition of Au on catalytic activities .....	91
6.3 Discussion .....	95
6.4 Conclusions.....	97
6.5 References .....	98
<b>Chapter 7 General Conclusions.....</b>	<b>100</b>

# List of Tables

## Chapter 2

**Table 1** : Examples of reactions catalysed by gold. .... 5

**Table 2**: Activity of gold catalysts prepared by co-precipitation and calcined at 673 K. .. 8

**Table 3**: Catalytic activities of gold catalysts prepared by laser vaporization method .... 10

**Table 4**: Reaction formulae involved in the direct synthesis of DME from syngas. .... 26

## Chapter 3

**Table 1**: Composition of the Cu-S5 catalyst. .... 35

## Chapter 5

**Table 1**: Physical properties of the catalysts studied..... 64

## Chapter 6

**Table 1**: BET surface areas of the various Cu-based methanol synthesis catalysts..... 87

**Table 2**: Effect of Au lading on the catalytic activity of the Cu-Zn-Al catalyst. .... 93

**Table 3**: Effect of Au loading on the catalytic activity of Cu-S5 catalyst. .... 93

# List of Figures

## Chapter 2

<b>Figure 1:</b> . Rates at 273 K over different Au catalysts as a function of average gold particle diameter.....	11
<b>Figure 2:</b> The effect of mean particle size of gold on the activity of CO oxidation .....	12
<b>Figure 3:</b> The dissociative chemisorption energies for oxygen on transition metal surfaces with respect to a molecule in vacuum calculated by density functional theory (DFT). .....	16
<b>Figure 4:</b> The correlation between the binding energies for O <sub>2</sub> , O and CO on Au and the coordination number of the Au atoms in different surfaces and clusters. ....	17
<b>Figure 5:</b> Turnover frequencies per surface gold atom at 273 K for CO oxidation over: (a) Au/TiO <sub>2</sub> , (b) Au/Al <sub>2</sub> O <sub>3</sub> and (c) Au/SiO <sub>2</sub> as a function of moisture concentration. Upright arrow indicates the saturation of CO conversion. ....	20
<b>Figure 6:</b> Mechanism of low temperature CO oxidation on Au catalysts.....	21
<b>Figure 7:</b> The mechanism proposed by Bond and Thompson. ....	22
<b>Figure 8:</b> Reaction mechanisms proposed for CO oxidation over Au/TiO <sub>2</sub> . ....	23
<b>Figure 9:</b> Potential raw materials which can be used to synthesize DME and its potential markets.....	25

## Chapter 3

<b>Figure 1:</b> Flowchart depicting the preparation of CuO-ZnO-Al <sub>2</sub> O <sub>3</sub> -Cr <sub>2</sub> O <sub>3</sub> -ZrO <sub>2</sub> -CeO <sub>2</sub> methanol synthesis catalyst (abbreviated Cu-S5). ....	34
<b>Figure 2:</b> Schematic representation of the reactor used in the direct DME synthesis. ....	39
<b>Figure 3:</b> Schematic representation of the rig used in the direct DME synthesis process. ....	40

## Chapter 4

<b>Figure 1:</b> The TEM images of the titanate nanotube support (right) and the catalyst Au/TN (left). .....	46
<b>Figure 2:</b> EDS spectrum of the titanate nanotube support confirming the presence of potassium in the material. ....	47
<b>Figure 3:</b> Deactivation of the Au/TN catalyst during time-on-line of the oxidation of CO at 70 °C.....	48
<b>Figure 4:</b> Effect of water (100 µL) on the catalytic activity of the Au/TN catalyst measured in a DRIFTS cell: (a) promotion of the oxidation of CO reaction by added water, (b) graph showing the quantification of the CO <sub>2</sub> produced. ....	49
<b>Figure 5:</b> CO <sub>2</sub> -TPD spectra for the titanate nanotube (TN) support: (a) CO + O <sub>2</sub> co-adsorbed, (b) CO <sub>2</sub> adsorbed. ....	50
<b>Figure 6:</b> CO <sub>2</sub> -TPD spectra for the catalyst (Au/TN): (a) CO + O <sub>2</sub> co-adsorbed under dry conditions, (b) CO +O <sub>2</sub> co-adsorbed under wet conditions (~ 2 % vol/vol H <sub>2</sub> O). ....	51
<b>Figure 7:</b> CO <sub>2</sub> -TPD for the Au/TN catalyst after adsorption of CO <sub>2</sub> at 70 °C.....	52
<b>Figure 8:</b> FTIR spectra scanned before and after the addition of water (100 µL) into the feed stream: (a) Spectra showing the growth of the peak at 1290 cm <sup>-1</sup> in the absence of water in the feed, (b) Plot of CO <sub>2</sub> yield vs. the intensity of the peak at 1290 cm <sup>-1</sup> . ....	53
<b>Figure 9:</b> FT-IR spectrum scanned on the titanate nanotube (TN) support under 2 % CO + 5 % O <sub>2</sub> (balance He) flow at 70 °C.....	54
<b>Figure 10:</b> FT-IR spectrum scanned on the Au/TN catalyst under 2 % CO + 5 % O <sub>2</sub> (balance He) flow at 70 °C: (a) 100 min. after addition of water (100 µL), (b) 28 min. of reaction under dry conditions.....	55

## Chapter 5

<b>Figure 1:</b> XRD patterns of (a) Au/TiO <sub>2</sub> and (b) Au/TiO <sub>2-x</sub> N <sub>x</sub> .....	64
<b>Figure 2:</b> Raman spectra of (a) Au/TiO <sub>2</sub> and (b) Au/TiO <sub>2-x</sub> N <sub>x</sub> . ....	65
<b>Figure 3:</b> HR-TEM pictures of Au/TiO <sub>2</sub> and Au/TiO <sub>2-x</sub> N <sub>x</sub> . ....	66
<b>Figure 4:</b> DRS-UV vis spectra of (a) TiO <sub>2</sub> and (b) TiO <sub>2-x</sub> N <sub>x</sub> .....	67

<b>Figure 5:</b> Temperature programmed oxidation (TPO) of (a) TiO <sub>2</sub> and TiO <sub>2-x</sub> N <sub>x</sub> . .....	68
<b>Figure 6:</b> Deactivation of the as-prepared catalysts during time-on-line of CO oxidation: (a) Au/TiO <sub>2</sub> and (b) Au/TiO <sub>2-x</sub> N <sub>x</sub> . Reactions were run at 70 °C.....	69
<b>Figure 7:</b> Deactivation of catalysts pre-treated at 300 °C in 5 % O <sub>2</sub> (balance He): (a) Au/TiO <sub>2</sub> and (b) Au/TiO <sub>2-x</sub> N <sub>x</sub> . Reactions were run at 40 °C. ....	70
<b>Figure 8:</b> CO oxidation activity of catalysts pre-treated at 300 °C in 5 % H <sub>2</sub> (balance He): (a) Au/TiO <sub>2</sub> and (b) Au/TiO <sub>2-x</sub> N <sub>x</sub> . Reactions were run at 70 °C.....	71
<b>Figure 9:</b> Effect of moisture on the catalytic activities of catalysts pre-treated in different atmospheres: (a) Au/TiO <sub>2</sub> and (b) Au/TiO <sub>2-x</sub> N <sub>x</sub> . Reactions were run at 70 °C.....	72
<b>Figure 10:</b> Regeneration of catalytic activities of catalysts pre-treated in 5 % O <sub>2</sub> (balance He): (a) Au/TiO <sub>2</sub> and (b) Au/TiO <sub>2-x</sub> N <sub>x</sub> . Reactions were run at 70 °C.....	74
<b>Figure 11:</b> CO conversion versus temperature ramp over as-prepared catalysts: (a) Au/TiO <sub>2</sub> and (b) Au/TiO <sub>2-x</sub> N <sub>x</sub> . .....	75
<b>Figure 12:</b> CO conversion versus temperature ramp over catalysts pre-treated in (i) 5 % O <sub>2</sub> , (ii) 5 % H <sub>2</sub> both balance in He: (a) Au/TiO <sub>2</sub> and (b) Au/TiO <sub>2-x</sub> N <sub>x</sub> .....	76

## Chapter 6

<b>Figure 1:</b> X-ray diffractograms of various Cu-based methanol synthesis catalysts (• CuO).....	89
<b>Figure 2:</b> Hydrogen temperature-programmed reduction (H <sub>2</sub> -TPR) profiles of various Cu-based methanol synthesis catalysts. ....	91
<b>Figure 3:</b> Effect of temperature on DME synthesis reaction over various catalysts: all catalysts mixed with γ-Al <sub>2</sub> O <sub>3</sub> (1:1), pressure 5.0 MPa, H <sub>2</sub> : CO = 2, GHSV = 343 h <sup>-1</sup> . ....	94

# Chapter 1

## Introduction

Noble metal catalysts, particularly Pt and Pd, have already been used for many years with major success in the chemical and petroleum industries and in automotive pollution control. The noticeable exception has been gold. This noble metal has almost no applications in catalysis although it is much more abundant than the other noble metals. Recent innovative research indicates that new gold-based catalysts could be effectively employed in hydrogen processing and related fuel cell systems. The removal of carbon monoxide impurities from hydrogen feedstock consumed by fuel cells is one of the most probable first uses for gold catalysts in this industry. However, gold-based catalysts used for CO oxidation have also been shown to suffer from rapid deactivation within the first few hours of time-on-line. Further optimization studies to establish greater reproducibility with respect to catalyst preparation, stability and poison resistance are necessary.

Indeed carbon monoxide oxidation has been the most studied reaction catalysed by gold. In addition to fuel cell technology, this reaction can also be of relevance in several applications such as carbon dioxide lasers, gas sensors and many environmental applications. Also the fact that it is a simple reaction to follow, with modest equipment requirements, might explain the huge attention it has received. However, for such a simple reaction, its mechanism has proved to be an extraordinarily tough nut to crack. In close relation to the mechanism of CO oxidation, the mechanisms of deactivation and regeneration of supported gold catalysts are poorly understood. The decline of activity with time-on-line is a crucial factor that could hamper the industrial development of gold-based catalysts.

It has frequently been demonstrated that carbonate-like species (namely, carbonate groups,  $\text{CO}_3$ ; bicarbonate groups,  $\text{HCO}_3$ ; and formate/carboxylate/hydroxycarbonyl

groups,  $\text{HCO}_2$ ) are formed during CO adsorption and CO reaction with oxygen. These species are thought to gradually poison the periphery of particles that contains the  $\text{O}_2$  activation sites. In Chapter 4 of this work, new findings which offer further information concerning the mechanism of deactivation are presented. The role of moisture in promoting the CO oxidation and preventing deactivation is also extensively discussed in the same chapter.

Chapter 5 presents data which emphasizes how sensitive gold catalysts are to parameters such as pre-treatment conditions, humidity and electro-optical properties of the support. The issue of the role of oxygen vacancies in gold catalysis is discussed in relation to the change in optical properties of the support and its structural complexity.

Many commercial catalysts are bimetallic or multi-component, or additives are used to improve their catalytic performance. The additives may act as either promoters or inhibitors. Promoters are additives that improve the activity and/or the selectivity of the catalyst or improve the catalyst life-time. Inhibitors are additives which are used to inhibit unwanted, chemical reactions and hence improve the selectivity to the desired reaction or catalyst life-time. Chapter 6 presents new findings on the effects of Au added to a copper-based methanol synthesis component of the bifunctional catalysts used in the direct single-step dimethyl ether (DME) synthesis from syngas.

Chapter 7 gives a summary of the general conclusions from all the work carried out and presented in this thesis.

# Chapter 2

## Literature Review

### *2.1 Reactions catalysed by gold*

Bulk gold has always been regarded as catalytically inert when compared to the more traditional Platinum Group (PGM) catalysts such as Pt, Pd and Rh. However, gold is recognized as an extremely unique and highly active metal when prepared in the form of supported nano particles [1]. The consensus among researchers working in gold catalysis is that the two key factors that are believed to convert the 'inert gold' into a highly active catalyst are: the reduced dimensions of the metal particles and a strong interaction of Au with the support. Thus, supports such as  $\text{Co}_3\text{O}_4$ ,  $\text{ZnO}$ ,  $\text{TiO}_2$ ,  $\text{Fe}_2\text{O}_3$  and nano crystalline  $\text{Ce}_2\text{O}_3$  are considered to be some of the materials adequate for preparing highly active supported gold catalysts [2].

In the last decade gold has been well established in the catalysis community as a catalyst of choice for many chemical transformations; with much focus put into new gold-catalysed reactions for industrial applications and green technology. Supported gold has been found to be an extremely active and selective oxidation and hydrogenation catalyst. Gold catalysts have also been shown to be active for selective oxidation reactions, oxidative decomposition of halogen compounds, catalytic combustion of hydrocarbons, hydrogenation of carbon oxides, and reduction of nitrogen oxides with propane, carbon monoxide or hydrogen [3]. However, water gas shift (WGS), hydro-chlorination of ethyne and carbon monoxide oxidation remain the most prominent examples of reactions catalysed by gold.

Selective hydrogenation to remove dienes and alkynes from mono-olefin streams is crucial to prevent poisoning of polymerization catalysts [4]. Supported gold catalysts offer interesting potential in such reactions that exhibit a selectivity problem, e.g.

hydrogenation of two C=C bonds or in differentiating C=C versus C=O group reactivity. The preferred hydrogenation of one of these groups, leading to monoenes, unsaturated alcohols and unsaturated ketones, is the advantage gold catalysts hold [5]. With further technology development, gold catalysts have a potential to play a key role in chemical processing of a range of bulk and specialty chemicals. The current targets for green (oxidation) reactions include:

- alkanes to alkenes
- alkenes to epoxides
- alcohols to aldehydes
- direct oxidation of methane to methanol
- direct oxidation of hydrogen to H<sub>2</sub>O<sub>2</sub>
- direct oxidation of alkanes to alcohols.

Table 1 gives a summary of some of the reactions that have so far been successfully carried out over gold catalysts [1]. Whilst the science of catalysis is still quite new compared to research focused on the PGMs, it has been demonstrated that gold can show high catalytic activity for some reactions, including the oxidation of carbon monoxide and the hydrochlorination of ethyne. There is a strong feeling amongst catalysis researchers that in a number of specific areas, gold catalysts have a potential to be applied commercially, including in pollution control.

**Table 1** : Examples of reactions catalysed by gold [1].

Reaction	Temperature (K)	Typical support
Oxidation of CO and hydrocarbons	200-400	Fe <sub>2</sub> O <sub>3</sub> , TiO <sub>2</sub>
Water Gas Shift (WGS)	400-500	CeO <sub>2</sub>
Reduction of NO with propene, CO or H <sub>2</sub>	450-800	Al <sub>2</sub> O <sub>3</sub>
Water or H <sub>2</sub> O <sub>2</sub> production from H <sub>2</sub> and O <sub>2</sub>	275-283	Al <sub>2</sub> O <sub>3</sub>
Removal of CO from H <sub>2</sub> streams	200-350	TiO <sub>2</sub>
Hydrochlorination of ethyne	373-393	Al <sub>2</sub> O <sub>3</sub> , SiO, TiO <sub>2</sub>
Selective oxidation, e.g. epoxidation of olefins	323-473	TiO <sub>2</sub>
Hydrogenation of CO and CO <sub>2</sub>	473-673	ZnO

The oxidation of CO at ambient temperature is an immensely important reaction in purification systems and breathing apparatus. Also the oxidation of CO could be a key aspect of using methanol or hydrocarbons as fuels for fuel cells. The reformat from these materials contains traces of CO which are poisonous for electrodes and need to be removed and gold can provide a mechanism to remove these trace amounts. Some of the parameters that influence the activity of supported gold catalysts, used for CO oxidation and other reactions, are discussed in the next section.

## **2.2 CO oxidation**

### **2.2.1 Factors that affect activity**

The genesis of nano particles represents the focal point of current technological research activities, as such; nano particles have been identified as having potential applications in areas such as sensors, medicine etc. [6]. Lately, synthesis procedures have been developed with the purpose of producing in one step gold nano particles with the

requisite characteristics and biocompatibility. The key to exploring gold nano particles in heterogeneous catalysis is the ability to control size, shape, surface and interparticle properties [2]. Hence the choice of preparation method in gold catalysis is crucial if nano particles of high monodispersity are ultimately to be synthesized. All these factors are crucial in the oxidation of carbon monoxide over gold-based catalysts.

There are two possible routes for the synthesis of nano-particles. The first method is the classic mechanical disintegration of larger solid phases into nano-sized materials (e.g. through milling), even though this approach has severe limitations in practice. The second method is the nucleation from gas/vapor or liquid phase and growth to nano-size units. Gold nano particles can be produced directly via the latter route, forming first the nano-sized dispersion of a precursor entity that can be transformed into the metal by chemical reaction. In all cases the nano-size dispersion of gold needs stabilization against aggregation, e.g. by the use of a support or special ligand shell around the particles.

Numerous methods have been documented for the preparation of supported gold catalysts [1]. Mostly, the following traditional preparative methods are used to synthesize gold nano particle catalysts for CO oxidation:

- (i) impregnation of a preformed support with a solution of chloroauric acid followed by drying and reduction,
- (ii) cation exchange with the support by cationic gold complexes followed by washing, drying and reduction,
- (iii) co-precipitation of hydroxides of both support and gold followed by drying, calcination, and reduction,
- (iv) deposition-precipitation of gold hydroxide to a suspension of the support followed by drying, calcination and reduction,
- (v) chemical vapor deposition of a volatile compound of gold to a high surface area support through an inert gas.

In general, the preparation of naked gold nano-particles on the support using traditional approaches is very advantageous in terms of exposing the nano-crystal surface sites to reactant species. However, the main drawback of these methods is the lack of control over size, shape and stability of the produced nano particles.

It has also been reported that one of the critical central issues in gold catalysts used for CO oxidation is the nature of the support material as well as its physical state [7-10]. Generally transition metal oxides are used as supports in heterogeneous catalysis. Metal oxides exhibit a vast range of electronic properties than they do surface geometries [11]. Their electrical behavior ranges from the best insulators (e.g.  $\text{Al}_2\text{O}_3$  and  $\text{MgO}$ ) through wide band-gap and narrow band-gap semiconductors ( $\text{TiO}_2$  and  $\text{Ti}_2\text{O}_3$ , respectively) to metals ( $\text{V}_2\text{O}_3$ ,  $\text{Na}_x\text{WO}_3$  and  $\text{ReO}_3$ ) and to superconductors like (reduced)  $\text{SrTiO}_3$ . Some metals are ferroelectric ( $\text{BaTiO}_3$ ) and others anti-ferroelectric ( $\text{WO}_3$ ) and their magnetic properties include ferromagnetism ( $\text{CrO}_2$ ), anti-ferromagnetism ( $\text{FeO}$ ), paramagnetism ( $\text{RuO}_2$ ) and highly complex mixed magnetic properties ( $\text{Y}_3\text{Fe}_5\text{O}_{12}$ ) [11]. This range of behavior clearly has an impact on the surface properties of these materials and consequently their chemisorption behavior will more-or-less be directly influenced, affecting their abilities as catalysts/supports.

Metal oxides with a high heat of formation ( $>100$  kcal/mol) such as  $\text{SiO}_2$ ,  $\text{TiO}_2$ ,  $\text{ZrO}_2$ ,  $\text{Al}_2\text{O}_3$ ,  $\text{CeO}_2$ ,  $\text{Nb}_2\text{O}_3$ ,  $\text{MgO}$ ,  $\text{La}_2\text{O}_3$  etc, are usually used as catalyst supports because they are rather difficult to reduce [12]. Metal catalysts supported on non-reducible supports such as  $\text{SiO}_2$  and  $\text{Al}_2\text{O}_3$  generally exhibit little effect of the presence of the support [11]. When metal catalysts are supported on reducible transition metal oxides, a strong interaction can occur that alters the catalytic behavior of the supported metal.

Extensive studies have been made to understand the extent and nature of the influence of the support material on gold catalysts tested for CO oxidation. The best supported gold catalysts, prepared by co-precipitation (Table 2), were those supported on oxides of the base metals of Groups 8-10 and the hydroxides of alkaline earth metals; followed by the

semi-conducting oxides of sp-metals (not d<sup>0</sup>) [10]. These were followed in ability by oxides of other transition metals, with the least effective supports being SiO and Al<sub>2</sub>O<sub>3</sub>.

**Table 2:** Activity of gold catalysts prepared by co-precipitation and calcined at 673 K [10].

Types of supports	Oxides or hydroxides	T <sub>50%</sub> (K)
Oxides of Group VIII 3d transition metals	Fe <sub>2</sub> O <sub>3</sub> , NiO, Co <sub>3</sub> O <sub>4</sub>	<266
Hydroxides of alkaline earth metals	Be(OH) <sub>2</sub> , Mg(OH) <sub>2</sub>	<266
Semiconductor oxides	CuO, ZnO, In <sub>2</sub> O <sub>3</sub> , SnO <sub>2</sub> , CdO	266-298
Oxides of other transition Metals	Sc <sub>2</sub> O <sub>3</sub> , La <sub>2</sub> O <sub>3</sub> , TiO <sub>2</sub> , ZrO <sub>2</sub> , Cr <sub>2</sub> O <sub>3</sub>	333-433
Insulating oxides	Al <sub>2</sub> O <sub>3</sub>	357
	SiO <sub>2</sub>	477

T<sub>50%</sub>: temperature for 50 % conversion, 5 wt% Au except with NiO (10 wt%). Reactions conditions: 200 mg of catalyst, CO = 1 % in air, 66 mls<sup>-1</sup>, SV = 20 000 mlh<sup>-1</sup>g<sup>-1</sup><sub>cat</sub>.

Over the last decade quite a number of contradicting conjectures have appeared in the literature regarding the exact role of the support in the oxidation of CO over supported gold nano-particles. Schubert et al. [9] attempted to put the matter to rest by trying to clarify how the choice of support material influences the activity of a gold catalyst for the CO oxidation reaction. They classified supports as either ‘inert’ or ‘active’ in terms of their role for oxygen supply during reaction. Irreducible (inert) supports such as Al<sub>2</sub>O<sub>3</sub> and MgO were found to have low TOFs because of their poor ability to adsorb or store

oxygen. On the other hand, there were catalysts supported on reducible (active) metal oxides, such as  $\text{Fe}_2\text{O}_3$  and  $\text{TiO}_2$  which exhibited a superior catalytic activity. For the reducible (active) oxides the size of the gold particles was deemed to play only a secondary role to that of the support.

However, Comotti et al. [13] have openly criticized and opposed the classification of supports proposed by Schubert et al. [9]. Based on their work, where they compared a more active  $\gamma$ -alumina (inert support) to a less active ZnO (active support) catalyst, Comotti et al. [13] suggested that the reducibility of the support and its ability to activate oxygen did not seem to be the decisive factor in determining activity. They also concluded that since in their study almost identical particle size distributions on different supports resulted in different activities for CO oxidation, metal support interaction strongly influenced the catalytic properties of the final materials. This influence did not follow the reducibility and oxygen activation ability of the supports.

Again, in contradiction to Schubert et al. [9], the role of the support was said to be limited to determining the final gold particle shape through the interface energy [14]. A high density of nucleation sites (oxygen vacancies) may result in a high dispersion of the gold nano-particles or even in smaller particles, despite low interfacial energy, and result in a different overall catalytic activity.

It is obvious from the forgoing arguments that the role and importance of the support in the oxidation of CO over gold catalysts will continue to be debated well into the foreseeable future. However, the compelling work done by Arii et al. [15] emphasized the importance of the nature of the support on the CO oxidation reaction catalysed by Au. In this work they practically eliminated particle diameter, Au loading and oxidation state of Au as variables to demonstrate the importance and uniqueness of different supports in dictating the rate of the CO oxidation reaction. Their results are summarized in Table 3.

**Table 3:** Catalytic activities of gold catalysts prepared by laser vaporization method [15].

Support	d <sub>Au</sub> (nm)	[Au] (wt%)	T <sub>50%</sub> (K)	TOF at 393 K(s <sup>-1</sup> )
Al <sub>2</sub> O <sub>3</sub>	2.6	0.08	603	2-7 x 10 <sup>-2</sup>
ZrO <sub>2</sub>	2.9	0.05	463	2.81 x 10 <sup>-1</sup>
TiO <sub>2</sub>	2.9	0.02	413	1.1

Reaction conditions: 800-1200 mg of catalyst, 2 % CO, 2 % O<sub>2</sub> in He, 50 mlmin<sup>-1</sup>.

In the above mentioned examples, it has been shown that a huge body of literature exists in which it is shown how small gold particles can be generated in various heterogeneous systems. The properties and homogeneity of the support surface determine the final particle size and size distribution, ultimately controlling the catalytic activity. However, recent findings have clearly demonstrated that particle size plays a more overriding role than the nature of the support in determining catalytic activity [10]. Figure 1 illustrates the summarized findings of various workers. These results clearly demonstrate that particle size is potentially more important than the type of support used.

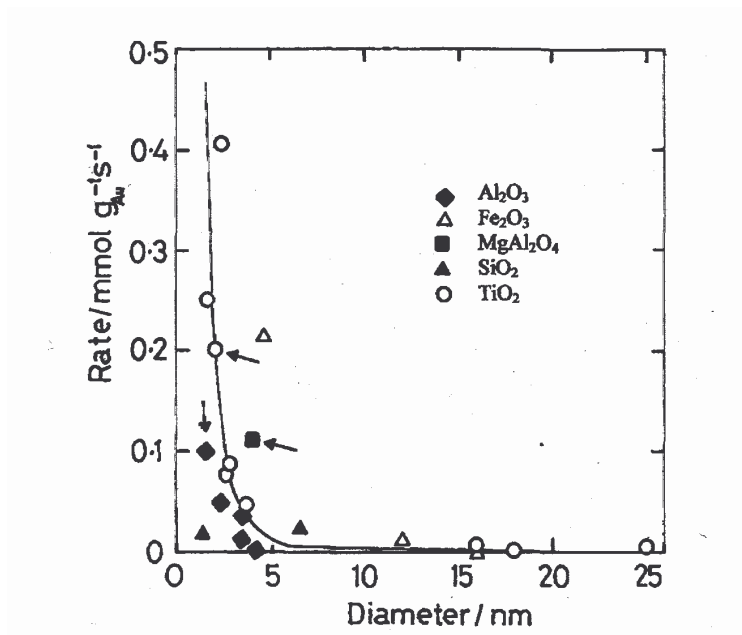


**Figure 1:** Rates at 273 K over different Au catalysts as a function of average gold particle diameter [10].

The importance of metal particle size versus metal support effects on catalytic reactivity is probably best illustrated by examining the current flurry of work in the literature on the catalysis of supported Au nano-particles [16]. It is known that bulk gold and large Au particles cannot chemisorb most reactant molecules. Chemisorption occurs only when a satisfactory number of low-coordinated surface atoms are present, preferably on smaller particles lacking complete metallic character [2]. Recent literature reports on gold catalysis have emphasized the importance of the ability to control size and composition in the 1-10 nm size range. This is important because it is in this size range that metal nano-particles undergo a transition from atomic to metallic properties [2].

In moving from large metal particles to nanometer size particles, the electronic structure changes from one which is comprised of valence and conduction bands to one which is made up of individual molecular states, thus leading to a metal-insulator transition [16]. Also, as the size of a particle approaches the range of a few nanometers, both surface area-to-volume ratio and surface-to-bulk atom ratio dramatically increases. This increase leads to a high concentration of corner and edge atoms, low coordination numbers of

surface atoms, and unique electronic properties (e.g. quantum transition). For gold nanoparticles of ~1 nm size, more than ~70 % atoms are at corners or edges [2].

However, decreasing the particle size to very small atomic ensembles, can sometimes lead to reduced activity. This point is emphasized by the work done by Valden et al. [17] (Figure 2). The observed activity reduction can be related to two factors. Metal atoms in the cluster which have very low coordination form very strong bonds with the adsorbate to compensate for the smaller number of metal-metal bonds [16]. The increased binding energy between the metal and the adsorbate leads to higher reduction temperatures. In addition to the enhanced metal-adsorbent bonding, the bonding between the metal and the oxide support becomes stronger and as such, may begin to deactivate the metal nano-clusters.

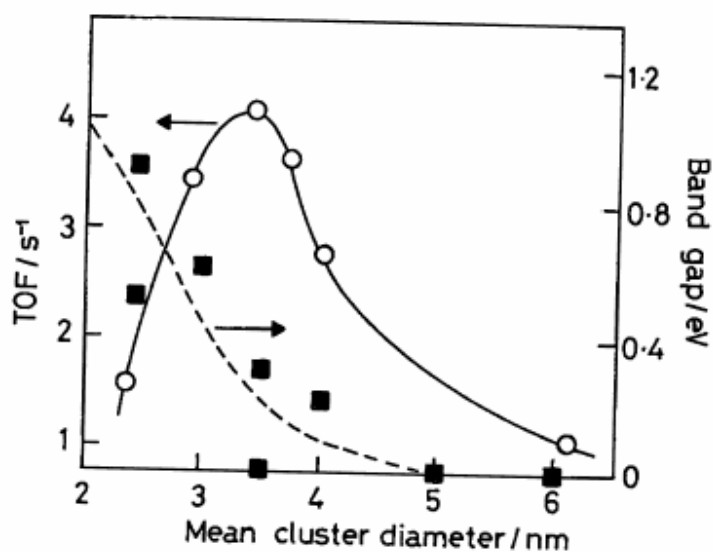


**Figure 2:** The effect of mean particle size of gold on the activity of CO oxidation [10 and references therein].

Small Au particle size is not the only necessary criterion to ensure high catalytic activity. It was shown that for the same Au particle size of around 6 nm, an Au/TiO<sub>2</sub> catalyst

prepared by deposition-precipitation [18] was four orders of magnitude more active than those prepared by photo-decomposition [19]. These studies demonstrated that on the same support and with similar Au particle size, Au catalysts can behave quite differently depending on the preparation methods used.

The preparation method plays a dominant role in determining the structure and the composition of the finished catalyst, and hence its activity for the oxidation of carbon monoxide [10]. The support effect varies from one support to another, as has been discussed above, but different preparation procedures will generally result in different catalysts on the same support in terms of their morphology and other physiochemical properties. The sensitivity of the CO oxidation reaction to the preparation procedures manifests itself in the fact that there is a wide variation in the reported CO oxidation activities over gold catalysts [20].

Many preparation methods are used in the gold catalysis community [10]. However, the deposition-precipitation procedure remains the most popular. Chloride-containing chloroauric acid precursors have been used to make the Au catalysts. Dimethyl gold acetone [21], gold-phosphine complexes [22], and gold ethylene diamine complexes [23] have all been used as well. The disadvantage of the chloride-containing precursors is that the residual chloride facilitates the agglomeration of Au particles during heat treatment [24], and it directly inhibits catalytic activity by poisoning the active sites [25].

In the deposition-precipitation procedure, the support acts as the nucleation initiator, whereby the negatively charged Au complexes  $\text{Au}(\text{OH})_x\text{Cl}_{4-x}$  are attached to the positively charged, protonated hydroxyl groups of the support [26]. Besides the anionic Au complex solution, there are also negatively charged  $\text{Cl}^-$  anions present due to hydrolysis of  $\text{AuCl}_4^-$ . The  $\text{Cl}^-$  anions are adsorbed on the surface of the support to an extent that depends on the surface charge [27]. Thus the seriousness of chloride contamination depends critically on the isoelectric point (IEP) of the support [12].

The types of gold precursor and support used greatly influence the activity of supported gold catalysts as well; this makes it very difficult to derive any general conclusions as to how the method of preparation affects structure and activity [10]. Other areas of keen debate that are paramount in the minds of researchers working in the field of gold catalysis include the mechanism of the CO oxidation reaction, *i.e.* the nature of the active site, the importance of both metallic ( $\text{Au}^0$ ) and ionic ( $\text{Au}^{+1}$ ) gold and the influence of  $\text{H}_2/\text{H}_2\text{O}$  in promoting the reaction. All these and other issues are comprehensively reviewed elsewhere [10]. Some of the controversies are discussed in the next section.

## **2.2.2 Controversial issues**

### **2.2.2.1 Oxidation state of active Au**

The oxidation state of the Au active site is one of the unresolved issues in the oxidation of CO by supported gold-based catalysts. Despite the tremendous amount of research into the nature of the active site, contradicting reports still appear in the literature claiming different oxidation states for the active Au-species. The electronic structure of the active species in the Au nano-clusters has been described as neutral [28], cationic [29] or anionic [30]. In the case of Au/ $\text{Fe}_2\text{O}_3$ , oxidized species such as Au(I) [31],  $\text{Au}^{\delta+}$  [32] or metal oxide support surfaces with modified reducibility by the interaction with Au nano-particles [33, 34] were all claimed to play the dominant role in the catalytic oxidation of CO.

Some researchers claim the ionic Au as the active species [35, 36]. One such proposed model containing ionic Au entails an ensemble consisting of metallic Au and Au-OH species [37-39]. However, there are counter claims that it is unlikely that oxidic Au species are major catalytically active phases because the most active supported Au catalysts are prepared by calcination in air at 573 K, where Au precursors (hydroxides or organo complexes) can be transformed mostly into metallic particles [40]. Hence some researchers attribute the catalytic activity entirely to the presence of neutral Au atoms on the Au nano-particles. This is due to the fact that generally, the only detectable species is

metallic Au on an active catalyst. The spectroscopic techniques used to arrive at this conclusion include XPS [41, 42], Au<sup>197</sup> Mössbauer spectroscopy [43] and XANES [44]. On the other hand, oxidized Au species have been considered to be active sites on the basis of relative catalytic activities after different treatments (calcination and reduction) of the samples [1, 45-47].

The positions adopted by investigators are often based on experience with only one system, although they may be claimed to have general relevance. However, it seems more realistic to seek an answer for each individual system. From the suggestions found in the literature [10 and refs. therein] one might conclude that with ceramic oxides, including titania and zirconia, the dominant active species is Au<sup>0</sup>, either alone or with some cationic species. With ferric oxide, the catalytic activity may be attributed to Au<sup>0</sup> associated with Au<sup>III</sup>, with magnesia, it may be Au<sup>0</sup> associated with Au<sup>I</sup>, and with ceria, it is not clear which combination of the three species is the dominant active phase [10].

#### **2.2.2.2 Activation of molecular oxygen (O<sub>2</sub>)**

The ability of a metal surface to form bonds with a gas is a measure of how noble it is. The nobility of a metal is well illustrated by the ability of the surface of the metal to oxidize, that is, to chemisorb dioxygen dissociatively [48]. Many important reactions that gold is currently known to catalyze involve molecular oxygen. At first sight this seems strange and unexpected, because Au is at the summit of nobility, and its refusal to corrode under any circumstance implies that it cannot react with oxygen. Au has *d*-states so low in energy that the interaction with oxygen 2*p*-states is net repulsive [48]. Hence the activity of gold-based catalysts in the oxidation of CO is somewhat surprising because dissociatively adsorbed oxygen is generally thought to be the active oxidant in related reactions on other noble metals. Molecular oxygen is known not to dissociatively adsorb on bulk Au at pressures as high as 1400 Torr and temperatures between 300 and 500 K [49].

No direct experimental evidence has yet been presented showing where oxygen is activated for reaction with CO adsorbed on Au surfaces, and whether the oxygen molecule is dissociatively or non-dissociatively adsorbed. A TAP (temporal analysis of products) study of O<sub>2</sub> with CO [50, 51], <sup>18</sup>O<sub>2</sub> isotope experiments [50-52] and ESR measurements [52, 53], indicate that molecularly adsorbed O<sub>2</sub>, most likely O<sub>2</sub><sup>-</sup> at the perimeter interface, is involved in the oxidation of CO.

Figure 3 shows the calculated oxygen chemisorption energies on a selection of transition metals [54]. It can be seen that the metals located above and to the left of Au in the periodic table have increasingly large chemisorption energies, and that the metals neighboring Au bind oxygen weakly. Au is the only metal with an endothermic chemisorption energy, which implies that it does not bind oxygen at all. This illustrates the well-known fact that Au is inert in an oxygen atmosphere [55].

<b>Cr</b>	<b>Mn</b>	<b>Fe</b>	<b>Co</b>	<b>Ni</b>	<b>Cu</b>
		-6,30	-5,07	-3,90	-2,51
<b>Mo</b>	<b>Tc</b>	<b>Ru</b>	<b>Rh</b>	<b>Pd</b>	<b>Ag</b>
-7,48		-4,62	-4,03	-1,20	-0,65
<b>W</b>	<b>Re</b>	<b>Os</b>	<b>Ir</b>	<b>Pt</b>	<b>Au</b>
-8,62			-4,65	-2,17	+0,54

**Figure 3:** The dissociative chemisorption energies for oxygen on transition metal surfaces with respect to a molecule in vacuum calculated by density functional theory (DFT) [48, 56].

There has been many attempts over the years to establish under what conditions if any molecular oxygen is chemisorbed by Au. The consensus is that under ambient conditions

of temperature and pressure it does not take place on massive gold, as supported by DFT calculations (Figure 3). In addition, further DFT studies have shown that small coordinatively unsaturated Au nano-particles are capable of chemisorbing  $O_2$ , O, and CO [48, 56], as illustrated by Figure 4. Small particles have a relatively large number of low-coordinated Au atoms, which are located at the edges and, in particular, at the corner particles. DFT studies [10, 48, 56] have indicated that these atoms are able to bind CO and oxygen, which is a prerequisite for a catalytic reaction. It is therefore conceivable that at these sites the CO oxidation reaction is possible at room temperature – the barriers are small and, importantly, the intermediates and  $CO_2$  that are formed are only weakly bound, so it is not necessary to have a high temperature to keep part of the surface free [48].

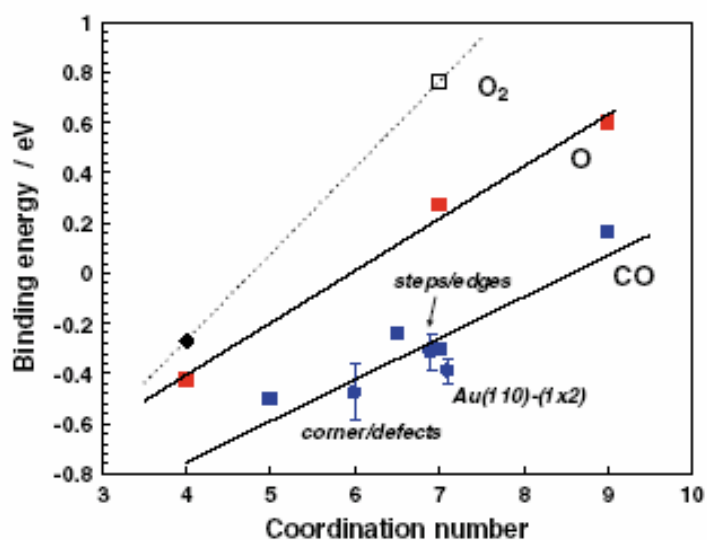


**Figure 4:** The correlation between the binding energies for  $O_2$ , O and CO on Au and the coordination number of the Au atoms in different surfaces and clusters [56].

In summary, molecular oxygen may interact with gold in one of four ways [10]: (i) by becoming adsorbed on the support in an activated form adjacent to a gold particle to which the other reactant is attached; or (ii) by directly reacting with that reactant in a kind of Rideal-Eley mechanism, without prior chemisorption; or (iii) by extracting charge from gold atoms, most probably on very small gold particles, having a high concentration

of low CN surface atoms, with the possible formation of an ionic bond such as  $\text{Au}^+-\text{O}_2^-$ ; or (iv) by dissociative chemisorption in atoms on the same kind of surface site. The first possibility is often mentioned and there is much evidence in its favour [50-52], but the extreme dependence of CO oxidation rate on particle size (Figure 1) is strong support for the last two possibilities.

Recent theoretical and experimental studies have focused on the effect of water vapour on the adsorption of  $\text{O}_2$  on small Au clusters [57]. It was found that the presence of a hydroxide group ( $\text{OH}^-$ ) on  $\text{Au}_N$  clusters causes previously inactive clusters to become highly active for  $\text{O}_2$  adsorption. For instance,  $\text{Au}_3^-$  is normally inactive for  $\text{O}_2$  adsorption due to its complete pairing of electrons. However, by introducing water vapour into the cluster source, a cluster with the composition  $\text{Au}_3\text{OH}^-$  can be produced, which shows a large amount of  $\text{O}_2$  adsorption [58].

### 2.2.2.3 Role of moisture

Gold nano-particles supported on metal oxides such as  $\text{Fe}_2\text{O}_3$ ,  $\text{NiO}$  and  $\text{TiO}_2$  have been shown to have high catalytic activity for CO oxidation, even at  $-70$  oC [1]. Unfortunately, these gold-based catalysts have not yet been put to use in practical conditions due to certain disadvantages, such as rapid deactivation. Some gold catalysts, such as  $\text{Au}/\text{MnO}_x$  [59] and  $\text{Au}/\text{ZrO}_2$  [35] are very sensitive to water and rapidly deactivate under moist conditions. Clearly these catalyst systems cannot be applied in practical conditions where moisture is always present, at least in ppm levels.

Bollinger and Vannice reported that water inhibits CO oxidation over  $\text{Au}/\text{TiO}_2$  [60]. However, Haruta *et al* later reported that small amounts of water were beneficial for CO oxidation on the same catalyst system [61]. These contrasting findings have led to the proposal of different mechanisms of CO oxidation involving  $\text{H}_2\text{O}$  or  $\text{H}_2\text{O}$  derived species (e.g.  $\text{OH}^-$  groups) in the literature. One such possible explanation given for the enhancement of activity upon addition of water is that surface OH groups, originating from  $\text{H}_2\text{O}$ , are either reactive towards CO or assist in the activation of  $\text{O}_2$  [57, 58, 62].

Based on *in situ* IR spectroscopy data, it was reported that the intrinsic gradual deactivation of gold-based catalysts is mainly related to the build-up and accumulation of carbonate species on the catalyst surface [63]. It was suggested that in the presence of water, these carbonate species could be transformed into less thermally stable bicarbonate species, which reduced the tendency for deactivation. In addition, the decomposition of these carbonate ad-species has been postulated as the rate limiting step [44].

Hu *et al* [64] carried out a detailed DFT study on the possible role that water plays in promoting CO oxidation on Pt (111). From the study, they concluded that in the presence of H<sub>2</sub>O the CO oxidation energy barrier can be substantially reduced. The barrier for CO<sub>2</sub> formation from the reaction of CO + O + H<sub>2</sub>O → CO<sub>2</sub> + H<sub>2</sub>O is 0.33 eV, significantly lower than that without H<sub>2</sub>O (0.80 eV). The hydrogen bonding in the transition state (TS) in the presence of H<sub>2</sub>O was attributed as the main source for the barrier reduction of CO oxidation.

The debate of how exactly water promotes CO oxidation on gold-based catalysts will continue well into the foreseeable future [10, 57, 58]. New findings on the possible role played by moisture in promoting CO oxidation are presented in Chapter 4 of this thesis. It is worth mentioning here that, based on literature reports [65], it is not totally unthinkable that the mechanism of water promotion differs from one type of support to another. Careful studies [61, 65] have shown that the effect that water has on catalytic activity depends primarily on the support and on its concentration (Figure 5). Activation energies shown for Au/TiO<sub>2</sub> and Au/Al<sub>2</sub>O<sub>3</sub> were almost independent of water concentration; however, for Au/SiO<sub>2</sub> the conversion-temperature curves were changed markedly by the presence of water [65].

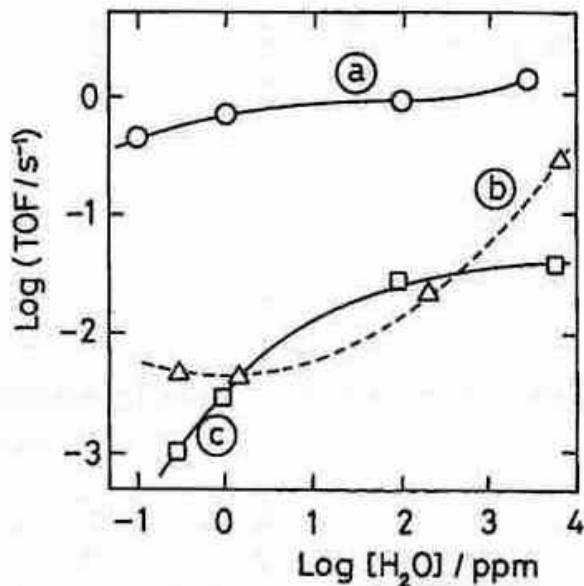


**Figure 5:** Turnover frequencies per surface gold atom at 273 K for CO oxidation over: (a) Au/TiO<sub>2</sub>, (b) Au/Al<sub>2</sub>O<sub>3</sub> and (c) Au/SiO<sub>2</sub> as a function of moisture concentration [10, 65].

#### 2.2.2.4 The active site

There has been much debate concerning the nature of the active site for CO oxidation over gold-based catalysts [10 and refs. therein]. Costello *et al* [66] proposed a mechanism thought to occur only on a gold particle for Au/Al<sub>2</sub>O<sub>3</sub> as shown in Figure 6. This mechanism requires an Au<sup>+</sup> cation carrying an OH<sup>-</sup> group to be present at the edge of the Au particle. An oxygen molecule then adsorbs dissociatively on steps or defects sites of metallic gold atoms. A CO molecule then arrives and reacts with *via* a hydroxycarbonyl ion as shown, liberating CO<sub>2</sub> and restoring the initial centre. However, no kinetic evidence has been advanced to support this mechanism.

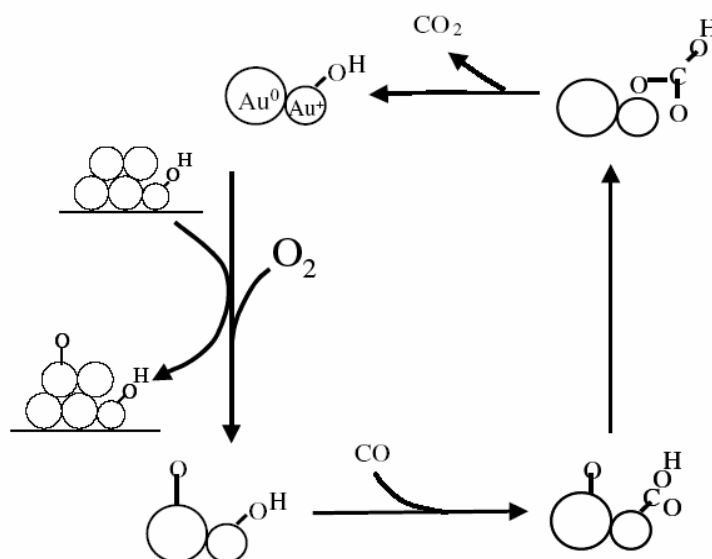


**Figure 6:** Mechanism of low temperature CO oxidation on Au catalysts [66].

The main issue with ‘metal only’ mechanisms is to find a plausible way of activating the oxygen molecule. However, since more data has been reported supporting the ability of small Au nano-clusters to adsorb molecular O<sub>2</sub> [48, 50-52, 56], it appears that this mechanism might be possible after all, although more detailed kinetic data remains to be provided in its support.

Bond and Thompson [37] proposed a mechanism for the reaction on gold-based catalysts where the support is assigned an active role (Figure 7). The presence of the support provides an escape route from the problem of oxygen chemisorption and subsequent ‘activation’ [10]. In this mechanism a CO molecule is chemisorbed on a low coordination number (CN) gold atom, and an hydroxyl ion moves from the support to an Au(III) ion, creating an anion vacancy. The hydroxyl ion and the OH<sup>-</sup> group react and form a carboxylate group, and an O<sub>2</sub> molecule occupies the anion vacancy as O<sub>2</sub><sup>-</sup>. This superoxide ion then oxidizes the carboxylate group by abstracting a hydrogen atom and forming CO<sub>2</sub>. The resulting HO<sub>2</sub><sup>-</sup> ion then oxidizes a further carboxylate species forming another CO<sub>2</sub> molecule and restoring two OH<sup>-</sup> ions to the support surface. This latter step

completes the catalytic cycle. In addition to the fact that no attempt was made to suggest the charges carried by the reacting species, no kinetic data was provided to support the mechanism.

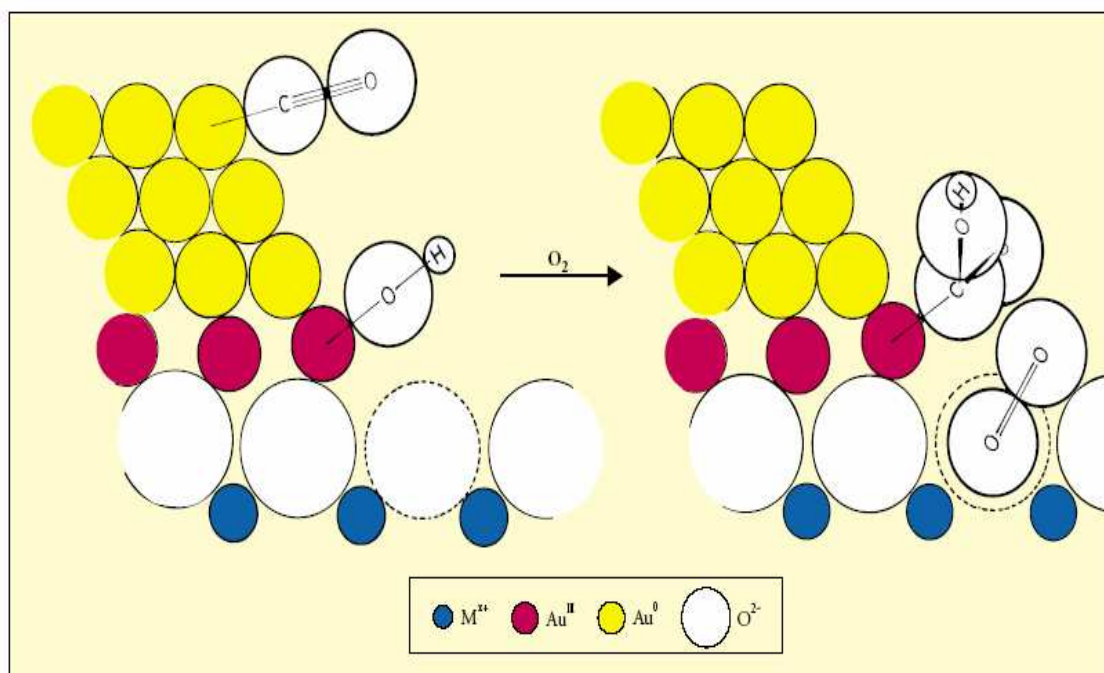


**Figure 7:** The mechanism proposed by Bond and Thompson [37].

From the mechanism proposed by Bond and Thompson [37], it remains unclear whether  $\text{Au}^{3+}$  or  $\text{Au}^0$  is the active form of gold. However, some researchers consider that the active phase of gold is the fully metallic gold particle [67]. Haruta *et al* [68] proposed a mechanism which involves both the Au metal particle and the support (Figure 8). In this mechanism it is assumed that adsorbed CO reacts with molecular  $\text{O}_2$  and that this is the rate limiting step. The manner in which the support ‘activates’ the oxygen molecule was not made clear.

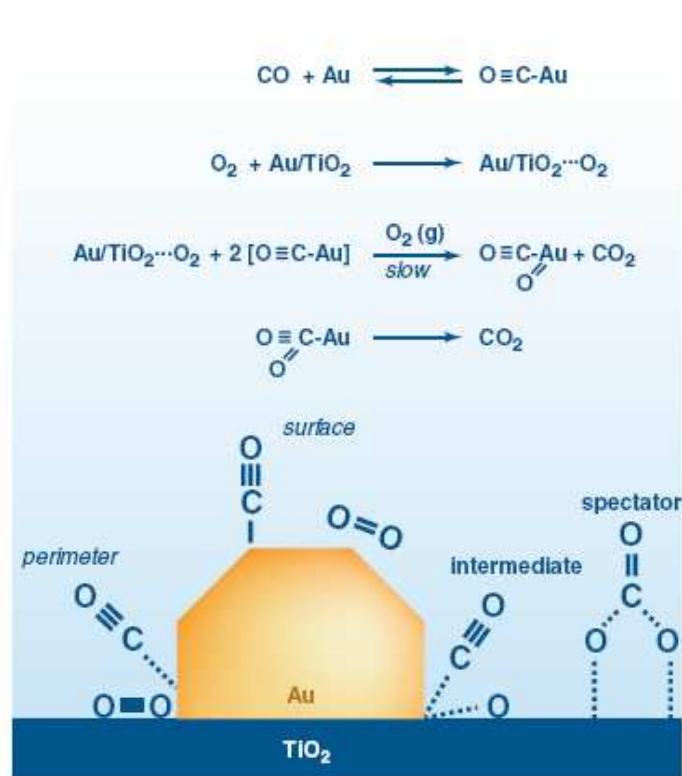


**Figure 8:** Reaction mechanisms proposed for CO oxidation over Au/TiO<sub>2</sub> [68].

## *2.3 Direct synthesis of dimethyl ether from syngas*

### **2.3.1 What is DME?**

Dimethyl ether (DME) is the simplest ether known. It has the chemical formula  $\text{CH}_3\text{OCH}_3$ . DME is colorless, its boiling point is  $-25.1\text{ }^\circ\text{C}$  and it has properties similar to propane and butane, the principal constituents of LPG. As it is easily liquefied, it can be distributed and stored employing the same technology as used for LPG. Many other potential markets for DME are highlighted in Figure 9.

Future energy demands as well as environmental issues require a 'clean' fuel and DME has been identified as a potential substitute for fuels derived from oil. Recently, DME has come to the attention of various companies, research centers and universities in leading countries, due to its potential use as a fuel [69]. This substance has been shown to be capable of powering diesel engines, thermoelectric power plants, as well as fuel cells. The fact that DME can be obtained from natural gas should be highlighted because that allows production costs to be independent of the swing in the price of oil. Also the world reserves of the raw material, natural gas, are still immense.

In order to use DME as a fuel, it must be produced at a low cost in large quantities. As shown in Figure 9, DME can be produced directly from syngas. The raw materials used to make the syngas, like natural gas, are abundant in nature. Although synthesis from methanol is simpler, direct synthesis is more interesting in as far as catalysis is concerned. The latter route may also be economically more interesting.

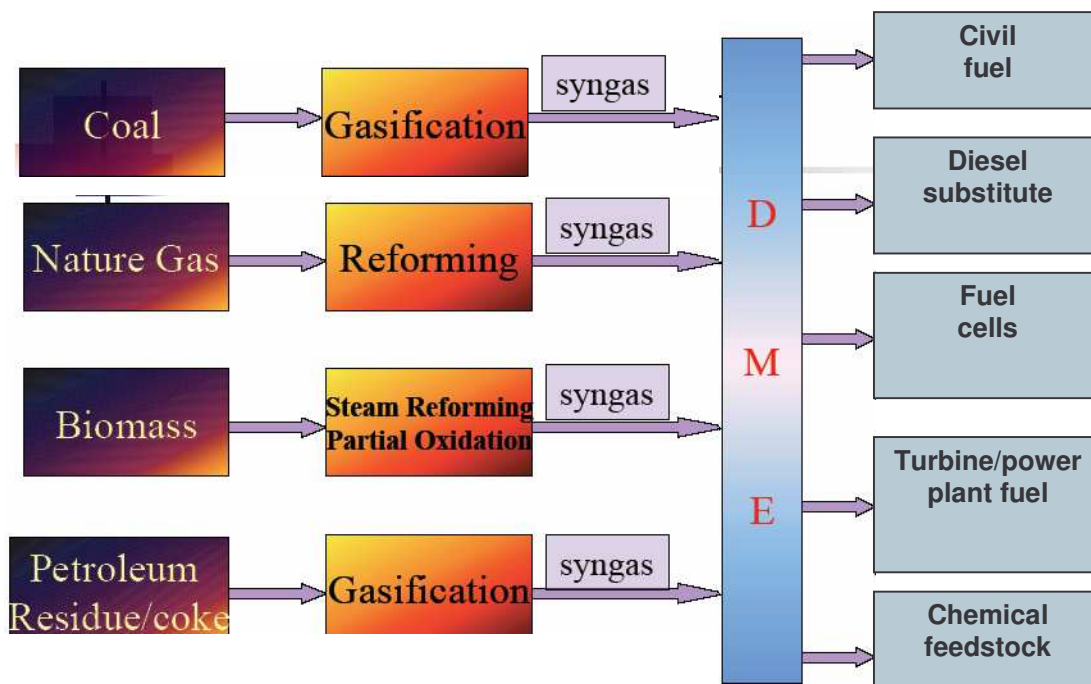


**Figure 9:** Potential raw materials which can be used to synthesize DME and its potential markets.

### 2.3.2 Process thermodynamics

The direct synthesis of DME basically proceeds through three reaction steps, namely: methanol synthesis, methanol dehydration and the water gas shift (WGS) reaction. Table 4 shows the reactions involved in the direct synthesis of DME together with their corresponding heats of reaction.

There are two possible overall reaction routes used for the synthesis of DME from syngas ( $H_2 + CO$ ); these are represented by Reactions 1 and 2 (Table 4). The overall reaction route depends on both the nature of the catalyst and/or reaction conditions. Reaction 1 yields DME as a culmination of three steps, which are the methanol synthesis reaction (3), the dehydration reaction (4) and the water gas shift reaction (5). When the shift reaction does not take place, Reactions 3 and 4 combine to give Reaction 2, which is the other DME synthesis route.

**Table 4:** Reaction formulae involved in the direct synthesis of DME from syngas.

Reaction	Reaction heat (kJ/mol)	Reaction number
$3\text{CO} + 3\text{H}_2 \rightarrow \text{CH}_3\text{OCH}_3 + \text{CO}_2$	-246	1
$2\text{CO} + 4\text{H}_2 \rightarrow \text{CH}_3\text{OCH}_3 + \text{H}_2\text{O}$	-205	2
$2\text{CO} + 4\text{H}_2 \rightarrow 2\text{CH}_3\text{OH}$	-182	3
$2\text{CH}_3\text{OH} \rightarrow \text{CH}_3\text{OCH}_3 + \text{H}_2\text{O}$	-23	4
$\text{CO} + \text{H}_2\text{O} \rightarrow \text{CO}_2 + \text{H}_2$	-41	5

High pressures are desirable to synthesize DME directly since both Reactions 1 and 2 involve a huge volume contraction. Hence high reaction pressures result in high syngas conversion.

The methanol synthesis reaction (Reaction 3) is limited by thermodynamics; however, the presence of an acid catalyst removes the methanol formed, shifting the overall reaction towards the right hand side (Reaction 4). The presence of such an acid catalyst strongly shifts the methanol synthesis reaction, increasing significantly the pass conversion of CO. Hence, a strong acidic material will result in a high rate of DME formation [70].

### 2.3.3 Choice of reactor

Generally, the aim of work done in this area of research is to develop a catalytic process in which 90% CO conversion to DME and CO<sub>2</sub> of syngas (Reaction 1) is attained at as low a temperature and pressure as possible. In such a process, both a recycling loop and compression of syngas can be omitted resulting in an economic process based on unused, dispersed and small-scale carbon resources [71]. To overcome the thermodynamic equilibrium conversion limit many researchers have used different reactor designs.

Two kinds of reactor technologies for DME synthesis have been proposed and extensively researched by previous workers: the fixed bed reactor and the slurry reactor. Ng et al. [72] comprehensively compared the differences between the two kinds of

reactors and discussed the complexity of reaction variables that influence DME formation. As the reactions involved in the process are highly exothermic and the temperature window of the catalyst is very narrow, the fixed bed reactor provides a limited heat removal capability and a low conversion of the syngas. The slurry reactor can provide an effective temperature control but a very high inter-phase mass transfer resistance is added by the liquid medium. The fluidized bed reactor can be an ideal reactor for DME synthesis as it possesses both high heat and mass transfer efficiencies [72].

In this work we report the hydrogenation of carbon monoxide over gold-containing copper based methanol synthesis catalysts. The incorporation of gold altered the product spectrum but had no net effect on the DME yield.

## 2.4 References

1. G. Bond and D. Thompson, *Cat. Rev.*, **1999**, 41, 319; M. Haruta, *CATTECH*, **2002**, 6, 102; A. S. K. Hashmi and G. J. Hutchings, *Angew. Chem. Int. Ed.*, **2006**, 45, 7896.
2. B. Zhou, S. Hermanans and G. A. Sormojai, *Nanotechnology in Catalysis, Volumes 1-2*, Kluwer Academic press, **2004**.
3. D. Thompson, *Gold Bull*, **1999**, 32, 12.
4. C. W. Corti, R. J. Holliday and D. T. Thompson, *Appl. Catal. A*, **2005**, 291, 253.
5. P. Claus, *Appl. Catal. A*, **2005**, 291, 222.
6. M-C. Daniel and D. Astruc, *Chem. Rev.*, **2004**, 104(1), 293.
7. N. Russo, D. Fino, G. Saracco and V. Specchia, *Catal. Today*, **2006**, 117, 214.
8. A. I. Kozlow, A. P. Kozlova, H. Liu and Y. Iwasawa, *Appl. Catal. A*, **1999**, 182, 9.
9. M. M. Schubert, S. Hackenberg, A. C. Van Veen, M. Muhler, V. Plazk, and R. J. Bhém, *J. Catal.*, **2001**, 197, 113.
10. G. C. Bond, C. Louis and D. T. Thompson, *Catalysis by Gold*, Imperial College Press London, **2006**.
11. P. A. Cox and V. E. Henrich, *The Surface Science of Metal Oxides*, Cambridge University Press, **1994**.
12. J. J. Spivey, *Catalysis*, Volume 17, Royal Society of Chemistry, **2004**.
13. M. Comotti, W. Li, B. Spliethoff and F. Schuth, *J. Am. Chem. Soc.*, **2006**, 128, 917.
14. T. V. W. Janssens, A. Carlsson, A. Puig-Molina and B. S. Clausen, *J. Catal.*, **2006**, 240, 108.
15. S. Aarii, F. Mortin, A. J. Renouprez and J. L. Rousset, *J. Am. Chem. Soc.*, **2004**, 126, 1199.
16. R. A. Van Santen and M. Neurock, *Molecular Heterogeneous Catalysis: A Conceptual and Computational Approach*, Wiley-VCH, **2006**.
17. M. Valden, X. Lai and D. W. Goodman, *Science*, **1998**, 281, 1647.

18. S. Tsubota, T. Nakaruma, K. Tanaka, M. Haruta, *Catal. Lett.*, **1998**, 56, 131.
19. G. R. Bamwenda, S. Tsubota, T. Nakamura, M. Haruta, *Catal. Lett.*, **1997**, 44, 83.
20. H. H. Kung, M. C. Kung, C. K. Castello, *J. Catal.* **2003**, 216, 425.
21. M. Okumura, S. Nakamura, S. Tsubota, T. Nakamura, M. Azuma, M. Haruta, *Catal. Lett.*, **1998**, 51, 53.
22. A. I. Koflova, A. P. Kaflova, H. Lui, Y. Iwasawa, *Appl. Catal. A: Gen.*, **1999**, 182, 9.
23. D. Horath, M. Polisset-Thfein, J. Frissard, L. Gucci, *Solid State Ionics*, **2001**, 141, 153.
24. S. D. Lin, M. Bollinger, M. A. Vannice, *Catal. Lett.*, **1993**, 17, 245.
25. H. S. Oh, J.H. Yang, C. K. Castello, Y. Wang, S. R. Bare, H. H. Kung, *J. Catal.*, **2002**, 210, 375.
26. M. Che, *Stud. Surf. Sci. Catal.*, **1993**, 75, 32.
27. C. F. Bates Jr. and R. E. Mesmer, *The Hydrolysis of Cations*, Wiley and sons, New York, **1976**, pp 282.
28. M. Okumura, S. Tsubota and M. Haruta, *J. Mol. Catal. A: Chem.*, **2003**, 199, 73.
29. J. Guzman and B. C. Gates, *J. Am. Chem. Soc.*, **2004**, 126, 2672.
30. B. Yoon, H. Häkkinen, U. Landman, A. S. Wörz, J. M. Antonietti, S. Abbet, K. Judai and U. Heiz, *Science*, **2005**, 307, 403.
31. S. Minic, S. Scir, C. Crisafulli, A. M. Visco and S. Galvagno, *Catal. Lett.*, **1997**, 47, 273.
32. Z. Hao, L. An, H. Wang and T. Hu, *React. Kinet. Catal. Lett.*, **2000**, 70 (1), 153.
33. D. Horvath, L. Toth and L. Gucci, *Catal. Lett.*, **2000**, 67, 117.
34. F. E. Wagner, S. Galvagno, C. Milone, A. M. Visco, L. Stievano and S. Calogero, *J. Chem. Soc., Faraday Trans.*, **1997**, 93, 3403.
35. E. D. Park and J. S. Lee, *J. Catal.*, **1999**, 186, 1.
36. R. M. Finch, N. A. Hodge, G. J. Hutchings, A. Meagher, Q. A. Pankhurst, M. R. H. Siddiqui, F. E. Wagner and R. Whyman, *Phys. Chem. Chem. Phys.*, **1999**, 1, 485.
37. G. C. Bond and D. T. Thompson, *Gold Bull.*, **2000**, 41, 33.

38. C. K. Costello, M.C. Kung, H. S. Oh, Y. Wang and H. H. Kung, *Appl. Catal. A: Gen.*, **2002**, 232, 159.
39. L. Fu, N. Q. Wu, J. H. Yang, F. Qu, D. L. Johnson, M. C. Kung, H. H. Kung and V. P. Dravid, *J. Phys. Chem. B*, **2005**, 109, 3704.
40. M. Haruta, *CATTECH*, **2002**, 6, 102.
41. S. J. Lee, A. Gavriilidis, Q. A. Pankhurst, A. Kyek, F. E. Waner, P. C. L. Won and L. Yeun, *J. Catal.*, **2001**, 200, 298.
42. L. Ucsi, D. Horvath, Z. Paszti, L. Toth, Z. E. Horvath, A. Karacs and G. Peto, *J. Phys. Chem. B*, **2000**, 104, 3183.
43. A. Goossens, M. W. J. Craje, A. M. Van der Kraan, A. Zwijnenbur, M. Makkee, J. A. Moulijn and L. J. DeJohn, *Catal. Today*, **2002**, 72, 95.
44. M. Haruta, S. Tsubota, T. Kobayashi, H. Kageyama and B. Delmon, *J. Catal.*, **1993**, 144, 175.
45. Y. M. Kang and B. Z. Wan, *Catal. Today*, **1995**, 26, 59.
46. S. D. Gardner, G. B. Hoflund, D. R. Schryrer, J. Schyer, B. T. Upchurch and E. J. Kirlin, *Langmuir*, **1991**, 7, 2135.
47. A. M. Visco, F. Neri, G. Neri, A. Donato, C. Milone and S. Galvagno, *Phys. Chem. Chem. Phys.*, **1999**, 1, 2869.
48. B. Hvolbaek, T. V. W. Janssens, B. S. Clausen, H. Falsig, C. H. Christensen and J. K. Nørskov, *Nanotoday*, **2007**, 2 (4), 14.
49. A. G. Sault, R. J. Madix and C. T. Campbell, *Surf. Sci.*, **1986**, 169, 347.
50. M. Olea, M. Kunitake, T. Shido and Y. Iwasawa, *Phys. Chem. Chem. Phys.*, **2001**, 3, 627.
51. M. M. Schubert, S. Hackenberg, A. C. van Veen, M. Muhler, V. Plazk and R. J. Bhem, *J. Catal.*, **2001**, 197, 113.
52. H. Liu, A. I. Kozlov, A. P. Kozlova, T. Shido, K. L. Asakura and Y. Iwasawa, *J. Catal.*, **1999**, 185, 252.
53. M. Okumura, J. M. Coronado, J. Soria, M. Haruta and J. C. Conesa, *J. Catal.*, **2001**, 203, 168.
54. T. Bligaard, J. K. Nørskov, S. Dahl, J. Matthiesen, C. H. Christensen and J. Sehested, *J. Catal.*, **2004**, 224, 206.

55. J. Kim, E. Samano and B. E. Koel, *Surf. Sci.*, **2006**, 600, 4622.
56. T. V. W. Janssens, B. S. Clausen, B. Hyolbæk, H. Falsig, H. Christensen and T. Bligaard, *Top. Catal.*, **2007**, 44, 15.
57. W. T. Wallace, R. B. Wyrwas, R. L. Whetten, R. Mitric and V. Bonacic-Koutecky, *J. Am. Chem. Soc.*, **2003**, 125, 8408.
58. W. T. Wallace, R. B. Wyrwas, A. J. Leavitt and R. L. Whetten, *Phys. Chem. Chem. Phys.*, **2005**, 7, 930.
59. G. B. Hoflund, S. D. Gardner, and D. R. Schryer, *Appl. Catal. B*, **1995**, 6, 117.
60. M. A. Bollinger and M. A. Vannice, *Appl. Catal. B*, **1996**, 8, 417.
61. M. Dáte and M. Haruta, *J. Catal.*, **2001**, 201, 221.
62. R. H. Grisel and B. E. Nieuwenhuys, *J. Catal.*, **2001**, 199, 48.
63. M. M. Schubert, A. Venugopal, M. J. Kahlich, V. Plazk and R. H. Bhem, *J. Catal.*, **2004**, 222, 32.
64. X-Q Gong and P. Hu, *J. Chem. Phys.*, **2003**, 119, 6324.
65. M. Dáte, M. Okumura, S. Tsubota and M. Haruta, *Angew. Chem. Int. Ed.*, **2004**, 43, 2129.
66. C. K. Costello, J. H. Yang, H. Y. Law, Y. Wang, J. N. Lin, L. D. Marks, M. C. Kung and H. H. Kung, *Appl. Catal. A: Gen.*, **2003**, 243, 15.
67. M. Haruta and M. Dáte, *Appl. Catal. A: Gen.*, **2001**, 222, 427.
68. M. Haruta, *J. New. Mater. Electrochem Systems*, **2004**, 7, 163.
69. T. Ogana, N. Inove, and Y. Ohno, *Journal of Natural Gas Chem.*, **2003**, 12, 219.
70. F.S. Ramos, A. M. Duarte de Farias, L. E. P. Borges, J. L. Monterio, M. A. Fraga, E. F. Sausa-Aguiar and L.G. Appel, *Catal Today*, **2005**, 101, 39.
71. K. Omata, Y. Watanabe, T. Umegaki, G. Ishiguro and M. Yamada, *Fuel*, **2002**, 81, 1605.
72. K. L. Ng, D. Chadwick, B. A. Toseland, *Chem. Eng. Sci.*, **1999**, 54, 3587.
73. W-Z. Lu, L. Teng and W. Xiao, *Int. J. Chem. Reactor Eng.*, **2003**, 1, S2.

# Chapter 3

## Experimental procedures

### *3.1 Catalyst preparation*

#### **3.1.1 Synthesis of titanate nanotube support**

The synthesis procedure followed to generate the titanate material has been reported before [1]. Commercial TiO<sub>2</sub> (P25) powder (25 g) was added to a 200 ml solution of  $2.8 \times 10^{-1}$  M KOH in a 1 L stainless steel autoclave. The mixture was heated for 24 h at 120 °C (stirring at 500 rpm). The resulting material was cooled down to room temperature, then allowed to age for 2 days in the base solution. It was then repeatedly centrifuged with deionized water until the conductivity was below  $100 \mu\text{S cm}^{-1}$ . The material was finally dried in air at 120 °C for at least 12 h. From here onwards the resultant material shall be referred to simply as the titanate nanotube (TN).

#### **3.1.2 Preparation of titanate nanotube-supported Au catalyst**

Deposition-precipitation was the method used to load gold onto the titanate nanotube support [2]. The support was slurred in distilled water (600 ml) under vigorous stirring. A required amount of diluted HAuCl<sub>4</sub> solution ( $10^{-2}$  M) was added slowly to the support slurry with continuous stirring. Due to the basicity of the titanate support, the pH was already at  $\sim 9$ ; so the addition of base was not necessary. The precipitated solution was aged for 15 h. A solution of NaBH<sub>4</sub> was prepared in ice water and added in the required amount to ensure the reduction of Au (III) to Au (0). The resulting catalyst powder of Au/TN contained 0.48 wt% Au, as determined by flame assay with atomic absorption finish.

### **3.1.3 Synthesis of nitrogen-doped anatase TiO<sub>2</sub>: TiO<sub>2-x</sub>N<sub>x</sub> [3]**

To prepare nitrogen doped anatase TiO<sub>2</sub>, a solution (150 mL) of 15 % NH<sub>4</sub>OH (Analytical reagent grade) was added drop-wise to 100 mL of Titanium (IV) butoxide (sigma-Aldrich, reagent grade 97%) with vigorous stirring at room temperature. The formed gel was aged for 24 h under continuous stirring. Then, it was centrifuged to remove the solvent and dried at 120 °C for 4 h and finally calcined at 450 °C for 3 h. The procedure was followed according to an earlier report [3]. The pure anatase TiO<sub>2</sub> was prepared following the same procedure; however, distilled water was used as the hydrolysing agent instead of NH<sub>4</sub>OH.

### **3.1.4 Preparation of the Au/TiO<sub>2-x</sub>N<sub>x</sub> and Au/TiO<sub>2</sub> catalysts**

Au/TiO<sub>2-x</sub>N<sub>x</sub> and Au/TiO<sub>2</sub> were prepared by drop-wise addition of a required amount of dilute aqueous solution of HAuCl<sub>4</sub> · xH<sub>2</sub>O to the water suspended TiO<sub>2-x</sub>N<sub>x</sub> or TiO<sub>2</sub>. After 1 h of stirring, the pH of the slurry was adjusted to 8.5 with 15 % NH<sub>4</sub>OH. Then, the slurry was aged for 2 h, with stirring, after which it was filtered and washed with 10 L of hot distilled water to remove chloride ions. Then, the resulting catalyst powders were kept in the dark in a cupboard for 24 h and subsequently transferred to a sample vial.

### **3.1.5 Methanol synthesis catalysts**

#### **3.1.5.1 Preparation of the CuO-ZnO-Al<sub>2</sub>O<sub>3</sub> catalyst**

The catalyst was prepared by following the method reported by Fujimoto et al. [4]. A mixed aqueous solution of Cu(NO<sub>3</sub>)<sub>2</sub>·3H<sub>2</sub>O (95 g), Zn(NO<sub>3</sub>)<sub>2</sub>·6H<sub>2</sub>O (69 g), and Al(NO<sub>3</sub>)<sub>3</sub>·H<sub>2</sub>O (140 g) was precipitated with an aqueous solution of Na<sub>2</sub>CO<sub>3</sub> (1.0 M). The precipitate was washed repeatedly with hot water and then dried at 120 °C over-night. Finally it was calcined in air at 300 °C for 12 h. Au was deposited on this catalyst as outlined above (section 3.1.4). The approximate composition of the resultant catalyst was Cu/Zn/Al = 40/23/37 (atom %). From here onwards, the catalyst will be abbreviated as Cu-Zn-Al.

### 3.1.5.2 Preparation of CuO-ZnO-Al<sub>2</sub>O<sub>3</sub>-Cr<sub>2</sub>O<sub>3</sub>-ZrO<sub>2</sub>-CeO<sub>2</sub>

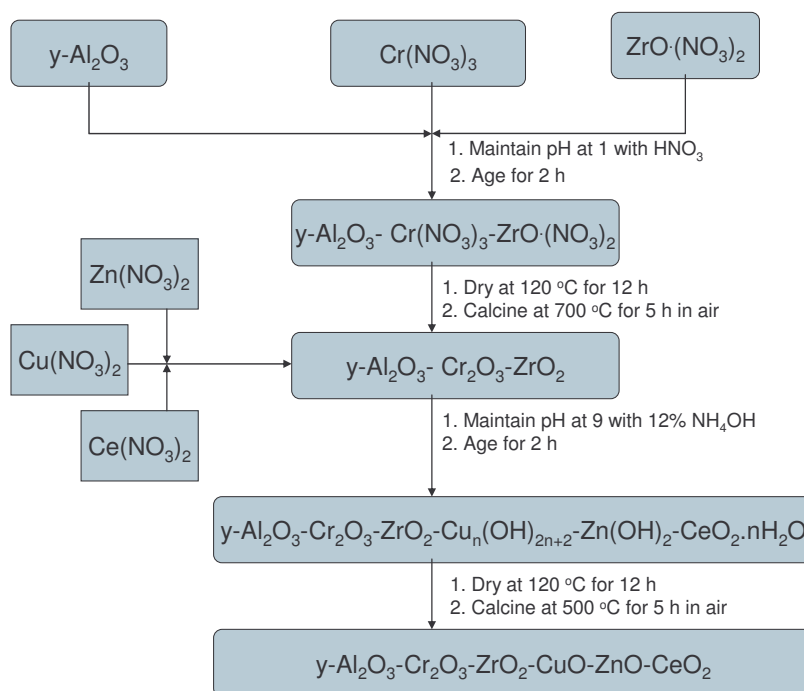


**Figure 1:** Flowchart depicting the preparation of CuO-ZnO-Al<sub>2</sub>O<sub>3</sub>-Cr<sub>2</sub>O<sub>3</sub>-ZrO<sub>2</sub>-CeO<sub>2</sub> methanol synthesis catalyst (abbreviated Cu-S5).

Figure 1 illustrates the flowchart of how the six part mixed oxide CuO-ZnO-Al<sub>2</sub>O<sub>3</sub>-Cr<sub>2</sub>O<sub>3</sub>-ZrO<sub>2</sub>-CeO<sub>2</sub> catalyst was prepared. Au was deposited on this catalyst following the procedure outlined above in section 3.1.4.

The composition of the resultant catalyst is outlined in table 1.

Table 1: Composition of the Cu-S5 catalyst.

Compound formula	Concentration (%) <sup>a</sup>
Al <sub>2</sub> O <sub>3</sub>	33.0
Cr <sub>2</sub> O <sub>3</sub>	2.9
CuO	25.0
ZnO	25.0
ZrO <sub>2</sub>	6.2
CeO <sub>2</sub>	7.9

a: determined by XRF spectroscopy.

### ***3.2 Catalyst characterization***

#### **3.2.1 Surface area determination: BET**

Nitrogen adsorption-desorption isotherms were measured on a Micromeritics TRISTAR 3000 analyzer. The samples were degassed under vacuum for several hours before the nitrogen adsorption measurements. The specific surface areas were determined by the Brunauer-Emmett-Teller (BET) method.

#### **3.2.2 Diffuse Reflectance Infrared Fourier Transform (DRIFT) Spectroscopy**

Samples (50 mg) were loaded into a DRIFTS cell with CaF<sub>2</sub> windows; the cell was equipped with a heating system that allowed operation under different atmospheres up to 600 °C. Spectra were collected at a resolution of 4 cm<sup>-1</sup> on a Perkin-Elmer 1720 FTIR spectrometer. Gases were led into the cell via a computer-controlled gas blender and exit gases were analysed by a Baltzers Prisma QMS. All samples were heat treated at 300 °C in air (20 ml/min) for 30 minutes prior to DRIFTS studies. A typical gas blend was 2 % CO + 10 % air, balanced in N<sub>2</sub>. Water (100 µL) was injected with a syringe when it was used.

### **3.2.3 Temperature Programmed Desorption (TPD)**

All TPD experiments were carried out in a flow apparatus with helium as carrier gas (50 ml/min) using a quartz U-tube reactor (6 mm i.d.). For detection of desorbed CO<sub>2</sub> a Baltzers Prisma QMS was used. Prior to adsorption, samples (220 mg) were heat treated at 300 °C in a flow of 5 % O<sub>2</sub> balanced in He. In a typical TPD experiment, adsorbents (e.g. 2 % CO + 5 % O<sub>2</sub> balanced in He) were passed over the catalyst bed at 70 °C at a flow rate of 100 ml/min for 30 minutes. Then the reactor was cooled down to room temperature for the start of CO<sub>2</sub>-TPD reaction. All samples were heated up to 600 °C at the rate of 8 °C /min. A water bubbler saturator was used when water was co-fed.

### **3.2.4 Temperature Programmed Oxidation (TPO)**

Pure support (200 mg) was placed in a U shaped quartz reactor and pre-treated in He (60 ml/min) at 150 °C for 30 minutes. After cooling down to room temperature, a TPO run was carried out up to 800 °C at a heating rate of 7.5 °C/min under 5 % O<sub>2</sub> (balance He) flow. The flow rate was maintained at 30 ml/min.

### **3.2.5 High Resolution Transmission Electron Microscope (HR-TEM)**

A JEM-100S Transmission Electron Microscope operating at 80 kV was used to establish the dispersion and the particle size of the metal on the catalyst surfaces. The catalysts were ground and slurred in methanol. A droplet of the slurry was placed on a carbon-film-coated copper grid. After leaving the grid to dry, it was then mounted onto the microscope.

### **3.2.6 X-ray Diffraction (XRD) measurements**

Powder samples were loaded on a sample holder and their diffraction patterns were recorded from 5 to 90° 2θ on a Bruker x-ray diffractometer using Cu as a target.

### **3.2.7 Diffuse Reflectance spectroscopy (DRS-UV-Vis) and Raman**

Diffuse reflectance spectra were recorded for powder samples on a UV-Visible spectrophotometer (Varian Cary 500 Scan) equipped with a diffuse reflectance attachment. The spectra were collected in the UV-Vis region from 800-200 nm at a scanning at a rate of 120 nm/min. Raman spectra were recorded on a micro Raman spectrometer (J-Y T 64000) with an Ar green laser beam (514 nm) as an excitation source.

### **3.2.8 X-ray Florescence (XRF) spectroscopy**

The XRF measurements were carried out on a PW 12404 Panalytical model instrument. Powder samples were mixed with 2 % Mowiol binder before being pressed. The X-ray source used was a Rh tube.

### **3.3 Catalytic evaluation**

#### **3.3.1 CO Oxidation**

##### **3.3.1.1 Activity measurement of Au/TN**

The catalyst sample (Au/TN) was calcined at 300 °C in 10 % O<sub>2</sub> (balance He) for 30 minutes prior to testing. The catalytic performance of the catalyst for CO oxidation was tested in a continuous flow quartz fixed-bed reactor (6 mm i.d). Solid catalyst (100 mg, powder particle size about 150 μm) was loaded into the reactor. The gas mixtures consisted of 5 % CO and 10 % O<sub>2</sub> balanced in He and the total flow was generally 40 ml/min. The course of the reaction was monitored quantitatively by use of a gas chromatograph facility equipped with a thermal conductivity detector. All measurements were carried out at 70 °C and atmospheric pressure.

##### **3.3.1.2 Activity measurement of Au/TiO<sub>2</sub> and Au/TiO<sub>2-x</sub>N<sub>x</sub>**

Catalysts (20 mg) were diluted with 100 mg of SiC before being charged into a U shaped quartz reactor (6 mm i.d.). Then they were pre-treated at 300 °C under 5 % O<sub>2</sub> flow (balance He). The CO oxidation reaction was carried out at different temperatures (30 to 250 °C) by passing 10 % CO (balance He, 100 ml/min) and 5% O<sub>2</sub> (balanced He, 100 ml/min). The total flow rate of the mixed gas was 200 ml/min. Outlet gases from the reactor were analysed by GC (equipped with a *Carboseive SII* column and a TCD detector). All experiments were carried out at atmospheric pressure.

### 3.3.2 Direct DME synthesis

The reactor used and rig design are shown below in Figures 2 and 3. All the experimental runs were carried out at temperatures between 250 and 300 °C. Catalyst samples (1 g of 1:1 bifunctional catalysts) were pressed at 10 MPa for 90 s before being loaded into the reactor. All samples were pre-reduced for 3 h at 300 °C in H<sub>2</sub> flow. The reactor outlet flow rate was maintained at 8 ml/min. A total pressure of 5 MPa was applied in all runs. On average, steady conversion levels were reached after 3 h. The dehydration catalyst used was  $\gamma$ -Al<sub>2</sub>O<sub>3</sub>.

In this work a fixed bed reactor was used, and it is schematically represented in Figure 2. The reactor was basically a ¼ inch stainless steel tube in which the catalyst bed was supported on quartz wool resting on a ⅛ inch stainless steel tube. For better temperature control a brass sleeve was used to cover the reactor.

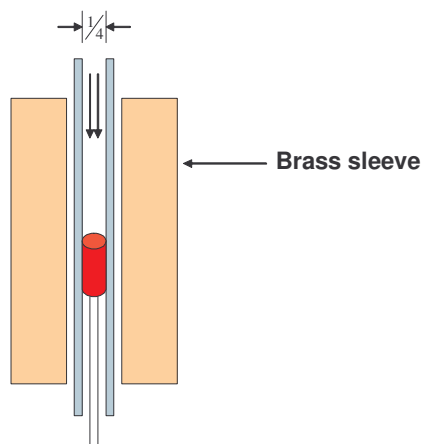


**Figure 2:** Schematic representation of the reactor used in the direct DME synthesis.

### 3.3.2.1 Product analysis: the rig

Figure 3 shows the schematic representation of the reactor system used in the direct DME synthesis process. The DME synthesis was carried out over physical mixtures (1:1) composed of the methanol synthesis catalyst and the dehydration solid in a continuous unit composed basically of the reactor described above (Figure 2). Product analyses were performed by the use of both a thermal conductivity detector (TCD) and a flame ionization detector (FID) equipped gas chromatographs, all connected in series.

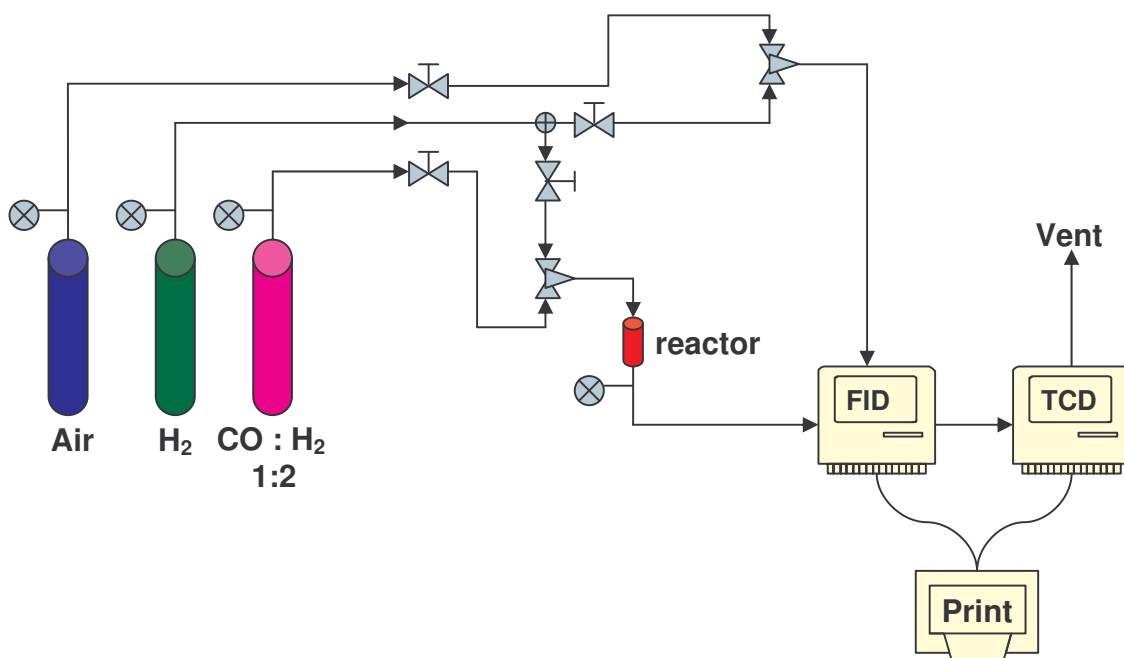


**Figure 3:** Schematic representation of the rig used in the direct DME synthesis process.

The reactor outlet gas flow was controlled by a needle valve. In order to prevent methanol and water condensation, the line between the reactor outlet and the chromatograph injection valves was electrically heated and kept at around 120 °C during tests.

### 3.3.2.2 Quantification of products

The catalyst activities were evaluated based on the overall reaction rate and the product selectivities were calculated at the same CO conversion level. The analysis of both reactants and products in the two gas chromatographs was recorded and printed out as area counts with the aid of a computerized integrator. The area counts of each individual component were converted to molar quantities by calculation. The derivation of the equations used to calculate the molar quantities of both reactants and products is given below.

One of the most important variables, in any reactor work, is the total molar flow-rate of reactants into the reactor ( $F_{in}$ ). This parameter can easily be measured using a mass-flow controller placed at the reactor inlet. However, in this work, what was measured was the total molar flow-rate at the reactor exit ( $F_{out}$ ) by the use of a bubble meter. In order to relate  $F_{out}$  to  $F_{in}$ , taking into account the huge pressure drop, an (inert) internal standard contained in the syngas was used. The internal standard used was argon (Ar) and the syngas was mixed in the ratio  $H_2 : CO : Ar$  (60:30:10).

The inlet total molar flow-rate ( $F_{in}$ ) is related to the outlet molar flow-rate ( $F_{out}$ ) by a contraction factor:

$$F_{in} = F_{out} \times \left\{ \frac{X_{in,Ar}}{X_{out,Ar}} \right\} \quad (6)$$

where the last term is referred to as the gas contraction factor.  $X_{in,Ar}$  and  $X_{out,Ar}$  refer to the inlet and outlet molar fractions of the internal standard, Ar, respectively.

Let the total number of moles of carbon fed into the reactor be  $X_{in,CO}$ , i.e. the molar fraction of CO in the syngas feed. Then the total molar flow-rate of carbon into the reactor ( $F_{in,CO}$ ) is given by:

$$(7) \quad F_{in,CO} = F_{in} \times X_{in,CO}$$

The % CO conversion was defined as:

$$\% CO_{conv} = \left\{ \frac{CO_{in} - CO_{out} \times \frac{Ar_{in}}{Ar_{out}}}{CO_{in}} \right\} \times 100 \quad (8)$$

where  $Ar_{in}/Ar_{out}$  is the contraction factor. The rate of consumption of CO,  $r_{CO}$ , was defined as :

$$r_{CO} = F_{in,CO} \times \% CO_{conv} \quad (9)$$

The rate of formation of product  $i$  was defined as:

$$r_i = F_{out} \times X_{out,i} \quad (10)$$

where  $X_{out,i}$  is the molar fraction of product  $i$  in the reactor exit stream and  $F_{out}$  represents the total molar flow of CO out . The % selectivity of product  $i$  was defined as:

$$\% S_i = \frac{r_i}{\sum_i r_i} \times 100 \quad (11)$$

Finally the yield of DME in mole percentage of carbon ( $c-mol$  %) units was defined as:

$$\% DME Yield = S_{DME} \times CO_{conv} \times 100 \quad (12)$$

### 3.4 References

1. D. V. Bavykin, A. A. Lapkin, P. K. Plucinski, L. Torrente-Murciano and J. M. Friedrich, F. C. Walsh, *Topics in Catalysis*, **2006**, 39, 151.
2. G. C Bond and C. Louis, D.T. Thompson., *Catalysis by Gold*, Imperial College Press, London, **2006**.
3. Y. Kuroda, T. Mori, K. Yagi, N. Makihata, Y. Kawahara, M. Nagao and S. Kittaka, *Langmuir*, **2005**, 21, 8026.
4. K. Fujimoto, K. Asami, H. Saima, T. Shikada and H. Tominaga, *Ind. Eng. Chem. Prod. Res. Dev.*, **1986**, 25, 262.

## Chapter 4

### CO oxidation over titanate nanotube supported gold: Deactivation due to bicarbonate species.

#### *4.1. Introduction*

Much of the interest in gold catalysis in the last decade stems from the pioneering work by Haruta et al. [1]. In particular, extensive work has been done on low temperature CO oxidation over metal oxide supported gold catalysts [2-7]. Despite a high initial activity for CO oxidation, gold catalysts suffer rapid deactivation within the first few hours of time-on-line. Although catalyst deactivation is an important phenomenon in industrial applications, the deactivation of gold catalysts has not always received the attention it deserves as evidenced by the lack of deactivation kinetic data.

The problem of the lack of kinetic data for the deactivation process is closely related to the fact that there is still no consensus on the mechanism of CO oxidation over gold catalysts. There is much confusion in the literature regarding the mechanism of CO oxidation catalysed by supported gold. The most popular mechanistic models reported involve: (i) the importance of the gold-support interface, which is governed by the metal-support interaction [8-12], (ii) the importance of catalyst particle geometry which dictates the presence of low coordinated atoms on the nanoparticles [13, 14] and (iii) quantum size effects due to the low dimensionality of the gold particles [15, 16].

Generally, there is discord in the results that are reported in the literature regarding the rate of (de)activation and means of reactivation [17]. Some of the possible reasons cited in the literature for deactivation include growth of metal particles, blockage of support (e.g. TiO<sub>2</sub>) interfacial sites by water, build up of 'carbon species', and the depletion of surface hydroxyl groups [17 and refs. therein]. Deactivation due to the reduction of Au<sup>x+</sup> ions by carbon monoxide has also been reported [18].

Adsorbed carbonate species are formed on most metal oxide surfaces because of chemisorption of carbon dioxide [19]. The exact speciation and coordination of these species is crucial to be fully understood, due to the important role they supposedly play in CO oxidation. Originally, Haruta et al. [2] proposed a mechanism involving the formation and decomposition of carbonates as the rate-limiting step in CO oxidation catalysed by gold. Daniells et al. [20] later proposed that the active site was an ensemble of  $\text{Au}^{3+}$  and  $\text{Au}^0$ , with hydroxyls from the cationic gold and the support promoting bicarbonate formation and their subsequent decomposition to produce  $\text{CO}_2$ . However, Tripathi et al. [21] argued that both carbonates and bicarbonates were not possible intermediates in the mechanism. Formates [8] and bicarbonates [10] have also been reported as possible reaction intermediates during CO oxidation.

In this investigation, new experimental findings, which offer further information concerning the deactivation mechanism of CO oxidation over titania nanotube (TN) supported gold, are reported. Contrary to earlier reports [22], we have observed that the formation of bicarbonate species during CO oxidation on the Au/TN catalyst is a competing reaction (for gold sites) that leads to catalyst deactivation. All measurements were carried out at 70 °C and atmospheric pressure, unless specified otherwise.

## ***4.2. Results***

### **4.2.1 Characterization of the support and catalyst**

The BET surface areas of both the support (TN) and catalyst (Au/TN) were approximately 148  $\text{m}^2/\text{g}$  with a pore volume of 0.26  $\text{cm}^3/\text{g}$ . The gold loading on the support was 0.48 wt%, (intended loading was 1 wt%). Titanate nanotubes in aqueous suspension have a relatively high negative zeta-potential over a wide range of pH [23]. The fact that a negatively charged gold precursor ( $\text{HAuCl}_4$ ) was used explains why the resultant gold loading was relatively low. The morphologies of the titanate nanotube (TN) and the catalyst Au/TN were studied by the use of HRTEM and corresponding

images shown in Figure 1 reveal the presence of the catalyst on the support. The average particle size of gold on the catalyst Au/TN was found to be  $4.5 \pm 1$  nm. Careful analysis of the TN material suggested that it was in the form of very thin sheets, which rolled up into two or more layered sheets of titanate material [23]. The chemical composition of the TN sample was examined by EDS (Figure 2), which revealed the presence of potassium in the sample.

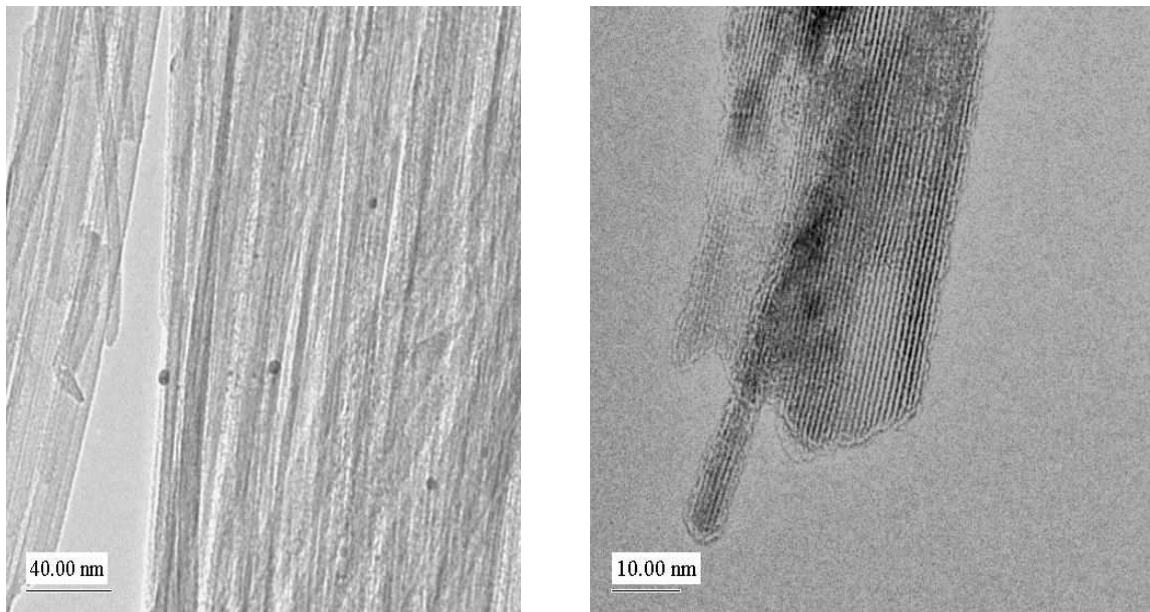


**Figure 1:** The TEM images of the titanate nanotube support (right) and the catalyst Au/TN (left).

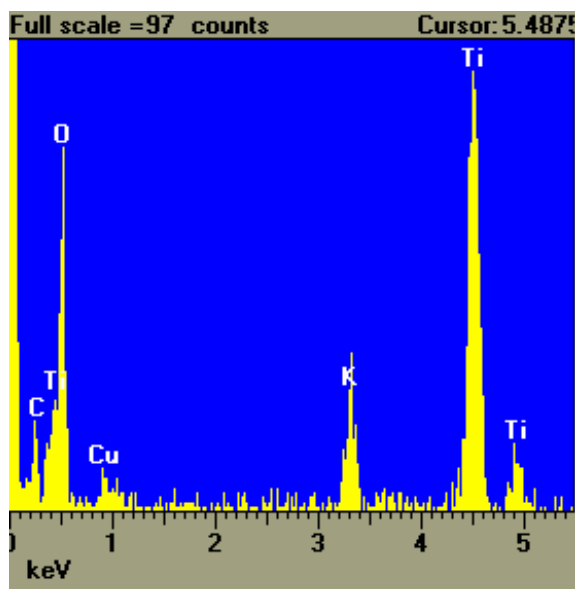


**Figure 2:** EDS spectrum of the titanate nanotube support confirming the presence of potassium in the material.

#### 4.2.2 CO oxidation

The primary aim of this work was to interrogate the reasons as to why the Au/TN catalyst system deactivated during CO oxidation. In order to study deactivation properly, diffusion/mass transfer limitations must be avoided. This is best done by keeping catalytic conversions low where the rate of the reaction proceeds under kinetic control. Figure 3 illustrates the deactivation observed during a typical CO oxidation run over the Au/TN catalyst. The catalyst deactivated rapidly within the first few hours of time-on-line.

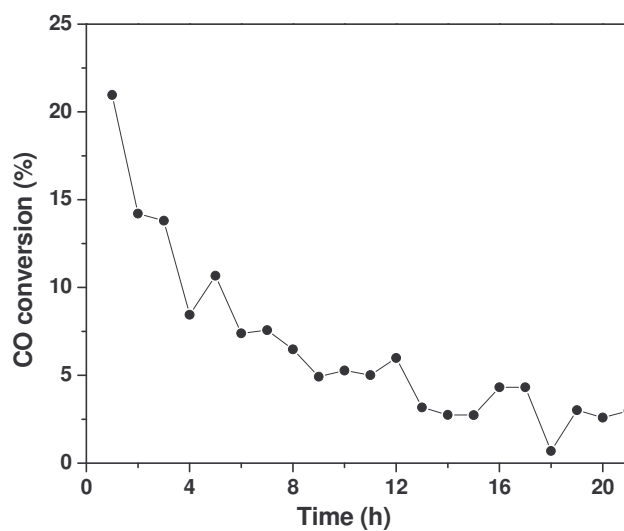


**Figure 3:** Deactivation of the Au/TN catalyst during time-on-line of the oxidation of CO at 70 °C.

Figure 4 illustrates the effect of introducing water into the feed stream during CO oxidation. In this experiment, a DRIFTS cell was used as a reactor and the exit gases were analysed using a quadruple mass spectrometer. Water promoted the reaction and the corresponding DRIFTS spectra for these particular experiments are shown in Figure 8.

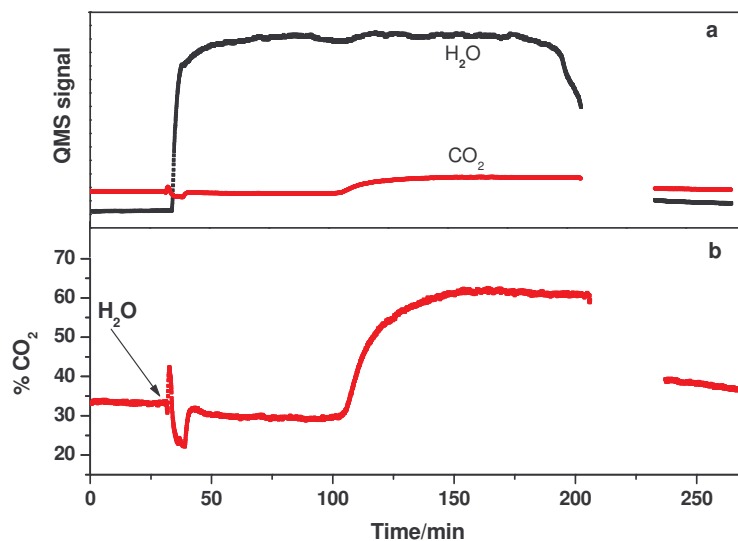
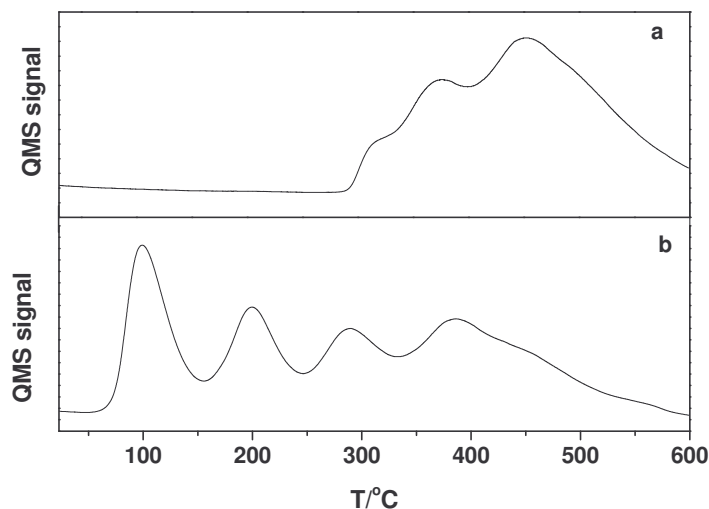


**Figure 4:** Effect of water (100  $\mu\text{L}$ ) on the catalytic activity of the Au/TN catalyst measured in a DRIFTS cell: (a) promotion of the oxidation of CO reaction by added water, (b) graph showing the quantification of the CO<sub>2</sub> produced.

### 4.2.3 CO<sub>2</sub>-TPD

#### 4.2.3.1 Titanate nanotube (TN)

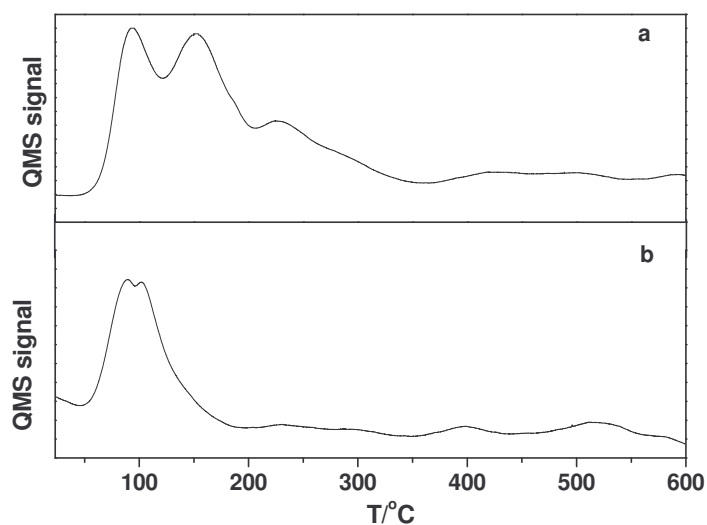
The CO<sub>2</sub>-TPD profiles illustrated in Figure 5 show the desorption of carbon dioxide from the pure support material (TN); after a mixture of CO + O<sub>2</sub> (Figure 5a) and CO<sub>2</sub> (Figure 5b) were flowed over it for 30 minutes at 70 °C. Under both desorption conditions (CO + O<sub>2</sub> and CO<sub>2</sub>) the support material (TN) showed similar basic surface sites at temperatures above 300 °C. However, below 300 °C there was no CO<sub>2</sub> desorbed for the case where CO + O<sub>2</sub> mixture was passed over the TN support. In the case where CO<sub>2</sub> was adsorbed, two low temperature desorption peaks were observed at 99 °C and 199 °C.



**Figure 5:** CO<sub>2</sub>-TPD spectra for the titanate nanotube (TN) support: (a) CO + O<sub>2</sub> co-adsorbed, (b) CO<sub>2</sub> adsorbed.

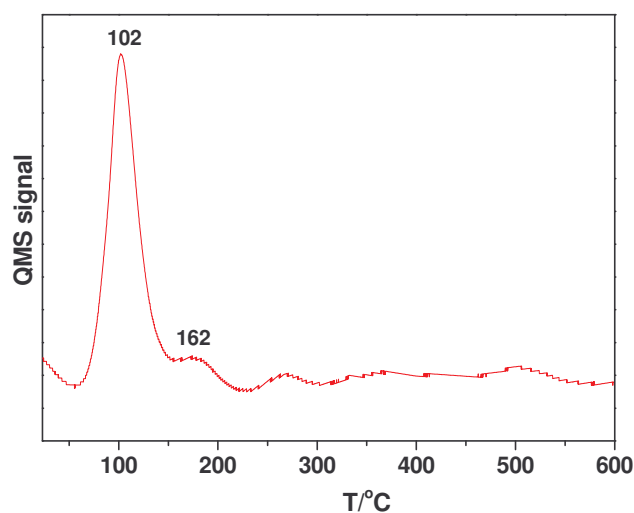
#### 4.2.3.2 Au/TN catalyst

Figure 6 shows the desorption profiles of CO<sub>2</sub> from the catalyst Au/TN. The desorption profiles were obtained after a mixture of CO + O<sub>2</sub> had been passed over the catalyst for 30 minutes at 70 °C under dry and wet conditions. Under dry conditions, there were CO<sub>2</sub> desorption peak species at 94, 153, and 229 °C. The latter two peaks were absent when the adsorption was done under wet conditions. Similarly, there were CO<sub>2</sub> desorption peaks at 89 and 102 °C under the wet adsorption/desorption experiment.



**Figure 6:** CO<sub>2</sub>-TPD spectra for the catalyst (Au/TN): (a) CO + O<sub>2</sub> co-adsorbed under dry conditions, (b) CO + O<sub>2</sub> co-adsorbed under wet conditions (~ 2 % vol/vol H<sub>2</sub>O).

Figure 7 shows a typical CO<sub>2</sub>-TPD spectrum of CO<sub>2</sub> after a 1 % CO<sub>2</sub> (balance N<sub>2</sub>) gas was passed over the catalyst for 30 minutes at 70 °C. The distinct feature from this figure was the CO<sub>2</sub> desorption peak at 162 °C, which within experimental errors, was due to the same CO<sub>2</sub> species that desorbed at 153 °C when CO + O<sub>2</sub> mixture was passed over the dry catalyst. This species of CO<sub>2</sub> seemed to be associated with the presence of Au on the support as it was not observed on the pure support when either CO + O<sub>2</sub> or CO<sub>2</sub> were adsorbed on the pure support.



**Figure 7:** CO<sub>2</sub>-TPD for the Au/TN catalyst after adsorption of CO<sub>2</sub> at 70 °C.

#### 4.2.4 DRIFT spectroscopic measurements

In order to characterize the adsorption state of carbon dioxide on both the pure support (TN) and the catalyst (Au/TN), DRIFT spectroscopic studies were carried out.

In principle, IR-active vibration frequencies are highly sensitive to the structure, protonation states, and speciation of carbonate (adsorbed CO<sub>2</sub>) [24]. However, in practice, there are many inherent difficulties in assigning the molecular structure of carbonate from its vibrational frequencies. Accurate definition of the important carbonate asymmetric C-O stretching region ( $\sim 1450\text{--}1600\text{ cm}^{-1}$ ) is difficult when DRIFTS measurements are carried out on samples where H<sub>2</sub>O is one of the co-reactants/adsorbents. Adsorbed water might contribute H-O-H bending intensity at locations different from that of bulk water [24].

Figure 8 shows the DRIFT spectra collected over the catalyst Au/TN during a typical CO + O<sub>2</sub> + H<sub>2</sub>O co-adsorption experiment. The experiment was conducted under the flow of the

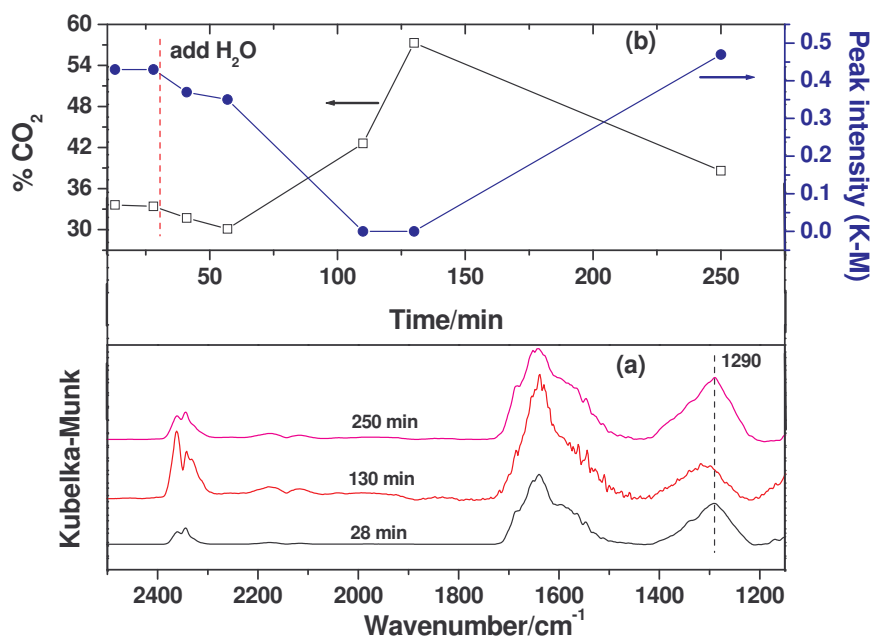


**Figure 8:** FTIR spectra scanned before and after the addition of water (100  $\mu\text{L}$ ) into the feed stream: (a) Spectra showing the growth of the peak at  $1290\text{ cm}^{-1}$  in the absence of water in the feed, (b) Plot of  $\text{CO}_2$  yield vs. the intensity of the peak at  $1290\text{ cm}^{-1}$ .

adsorbates ( $\text{CO} + \text{O}_2$ ) at  $70\text{ }^\circ\text{C}$ . All the spectra were recorded at  $70\text{ }^\circ\text{C}$ . Spectra were recorded nominally at 13 and 28 minutes during time-on-line, after which  $100\text{ }\mu\text{L}$  of water was introduced into the feed and subsequently spectra were recorded as a function of time. The quantification of the  $\text{CO}_2$  produced in this particular experiment is shown in Figure 4.

What can be concluded from Figures 4 and 8 was that as previously reported [17], water had a similar promoting effect on the Au/TN catalyst system as on other common gold catalysts. Figure 4 showed a double increase in the amount of  $\text{CO}_2$  produced when  $\text{H}_2\text{O}$  was introduced and the same promoting effect was shown in Figure 8, characterized by the increased intensity of the  $\text{V}_3$  vibration of linearly adsorbed  $\text{CO}_2$  at  $2361\text{ cm}^{-1}$ .

In addition, in Figures 4 and 8, it is observed that as soon as the amount of water decreases in the feed/surface the catalysts suffered rapid deactivation. Figure 8(b) illustrates that the deactivation coincided with a build up (characterized by the increasing peak intensity with time) of some carbonate species with a vibration band at  $1290\text{ cm}^{-1}$ . This carbonate species has previously been assigned as an OH deformation of bicarbonate species [25]. To confirm whether these bicarbonate species needed the presence of gold to form or they could form on the support under reaction conditions without gold, a control experiment was performed and the result is shown in Figure 9.

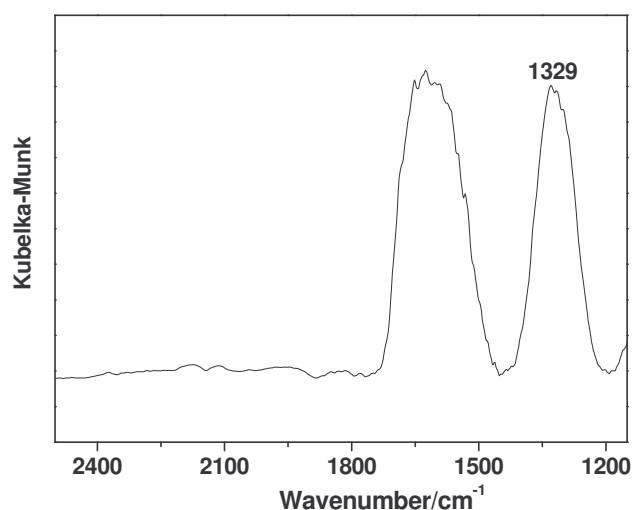


**Figure 9:** FT-IR spectrum scanned on the titanate nanotube (TN) support under 2 % CO + 5 % O<sub>2</sub> (balance He) flow at 70 °C.

The absence of the peak at  $1290\text{ cm}^{-1}$  on the support alone (Figure 9) confirmed that gold was a necessary ingredient to form the bicarbonate species. Indeed Figure 10(b) confirms that gold was a necessary ingredient to form the bicarbonate species. The vibration bands at  $1316\text{ cm}^{-1}$  and  $1329\text{ cm}^{-1}$  in Figures 9 and 10, due to unidentate carbonate species on the support [25], were not affected by the presence of water; while that of the bicarbonate ( $1290\text{ cm}^{-1}$ ) was completely removed by water (Figure 10a).

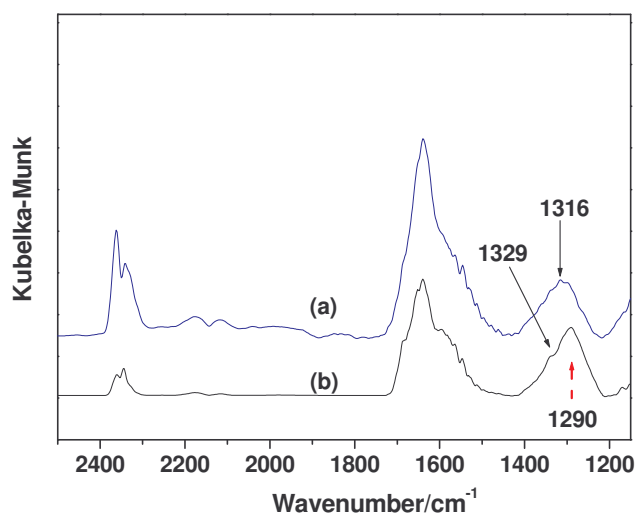


**Figure 10:** FT-IR spectrum scanned on the Au/TN catalyst under 2 % CO + 5 % O<sub>2</sub> (balance He) flow at 70 °C: (a) 100 min. after addition of water (100 μL), (b) 28 min. of reaction under dry conditions.

### 4.3. Discussion

The high activity of gold catalysts for the oxidation of CO is well documented [17]. However, activity alone is not the only criterion that must be fulfilled for a suitable catalyst for CO oxidation [26]. Long term stability is also a crucial feature.

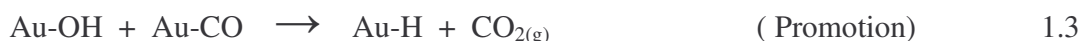
Figure 3 illustrates the deactivation of the Au/TN catalyst with time-on-line while Figure 4 shows the beneficial effect of water in the oxidation of CO. Also in Figure 4 it is shown that as long as there was moisture in the feed, deactivation was inhibited. The observed gradual deactivation in Figure 3 can be correlated to the growth of the bicarbonate band [OH deformation,  $1290\text{ cm}^{-1}$ ] that is illustrated in Figures 8 and 10b. As shown in Figure 4, it took about one hour for water to effect the promotion of CO oxidation and that could be related to how long water takes to decompose these bicarbonate species (Scheme 1).

Also the CO<sub>2</sub>-TPD data (Figures 6 and 7) showed desorption peaks (152 °C and 162 °C respectively) due to some CO<sub>2</sub> species whose formation/desorption was directly linked to the presence of Au, as they were not formed on the pure support (Figure 5) under reaction conditions. We deduce that the carbonate species seen in the DRIFTS data ( $1290\text{ cm}^{-1}$ ) and the CO peak from CO<sub>2</sub>-TPD data (152 °C) are the same species which lead to the deactivation of the catalysts. This conclusion was reached because the formation of these CO<sub>2</sub>-based species coincided with the presence of Au on the support. The gradual accumulation of the CO<sub>2</sub>-based species (bicarbonate) leads to the blockage/occupation of active sites on the catalysts.

To understand the mechanism of deactivation one needs to first look at the proposed reaction mechanisms. There has been much debate concerning the nature of the active site for gold catalysts [17]. More than a decade ago, a reaction mechanism was proposed for Au-TiO<sub>2</sub> involving the effect of water in the CO oxidation reaction [27]. The mechanism involved the dissociative adsorption of water on the TiO<sub>2</sub> surface, followed by the formation of formate species (Au-COOH); which subsequently decomposes to CO<sub>2</sub> and H<sub>2</sub>. However, this mechanism has recently been disputed [28]. Schubert *et al*

[22] proposed that water transforms the carbonate species formed during the oxidation of CO into less thermally stable bicarbonate species. They suggested that in the presence of water these bicarbonate species are possibly reaction intermediates.

From our work, we noted that the formation of bicarbonate species is not an intermediate step but rather a product of the CO<sub>2</sub> produced during CO oxidation. The bicarbonate species detected at 1290 cm<sup>-1</sup> (Figures 8 and 10b) was very stable and only desorbed at 152 °C (Figure 6). The thermal stability of bicarbonate type species has been also reported elsewhere [29]. In the presence of water the bicarbonate species (1290 cm<sup>-1</sup>) did not form (Figure 10a) under the reaction conditions. Our CO<sub>2</sub>-TPD results implied that water possibly reacted with and removed the already formed bicarbonate species and prevented its further formation and in the process promoted the reaction and prevented deactivation. The possible reactions of how water (OH) might remove the gold associated bicarbonate and hence reactivate and promote the oxidation of CO are outlined in Scheme 1. Schumacher *et al* [30] have also proposed that water reacts with the carbonate-like poison species (possibly via CO<sub>3</sub><sup>2-</sup> + H<sub>2</sub>O → CO<sub>2</sub> + 2OH<sup>-</sup>) preventing catalyst deactivation.



**Scheme 1.** Possible reactions showing how water might reactivate and promote the oxidation of CO on Au/TN catalyst system.

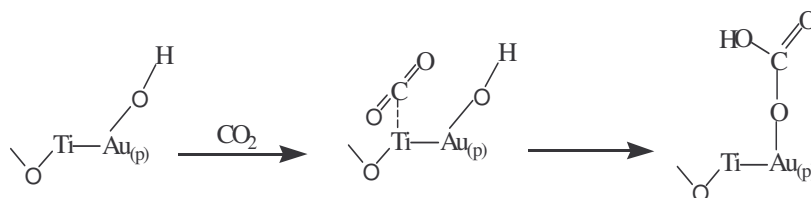
Figure 7 shows a very interesting result in that it shows the formation of the gold-associated CO<sub>2</sub> species (bicarbonate) by simply passing 1 % CO<sub>2</sub> (balance N<sub>2</sub>) over the catalyst. These species did not form on the pure support (Figure 5). This result suggested

that the formation of  $\text{CO}_2$  did not go through the bicarbonate as an intermediate during the oxidation of CO but rather,  $\text{CO}_2$  was a reactant in the formation of the bicarbonate. There are two obvious pathways by which  $\text{CO}_2$  can react with gold (Au-OH) to form the gold-associated bicarbonate species (responsible for deactivation):

(i) The first possibility is the reaction of  $\text{CO}_2$  (g) with Au-OH in a Rideal-Eley type mechanism,



(ii) The second possibility could be the reaction of  $\text{CO}_2$  adsorbed on Lewis acid sites ( $\text{Ti}^{4+}$ ) surrounding the gold particles  $[\text{Au}_{(p)}]$ ,



The above mechanisms for the formation of the observed bicarbonate may account for the deactivation of the Au/TN catalyst during CO oxidation; this reaction would consume the OH groups on Au which have been reported as essential in the mechanism of CO oxidation [17]. The above hypothesis of  $\text{CO}_2$  being able to chemisorb on gold nanoparticles is not unique. Based on IR studies [22, 31], evidence was provided which pointed to the fact that CO and  $\text{CO}_2$  competed for adsorption on the same site on Au surfaces. To the best of our knowledge, this is the first time that DRIFTS and  $\text{CO}_2$ -TPD have been combined to show that  $\text{CO}_2$  is adsorbed on the gold-nanoparticle sites in the form of bicarbonate to the detriment of the oxidation of CO.

#### ***4.4. Conclusions***

- (1) The Au/TN catalyst deactivates due to the formation of bicarbonate species on gold sites.
- (2) The bicarbonate is formed from the CO<sub>2</sub> produced from CO oxidation.
- (3) Water removes and inhibits further formation of these bicarbonate species.

#### 4.5. References

1. M. Haruta, T. Kobayashi, H. Sano and N. Yamanda, *Chem. Lett.*, **1987**, 2, 405.
2. M. Haruta, S. Tsubota, T. Kobayashi, H. Kayeyama, M.J. Genet and B. Delmon, *J. Catal.*, **1993**, 144, 175.
3. F. Boccuzzi, A. Chiorino, S. Tsubota and M. Haruta, *J. Phys. Chem.*, **1996**, 100, 3625.
4. M. Daté, M. Okumora, S. Tsubota and M. Haruta, *Angew. Chem. Int. Ed.*, **2004**, 43, 2129.
5. M. Haruta, *Cattech*, **2002**, 6, 102.
6. P. Konova, A. Naydenov, C. Venkov, D. Mehandjiev, D. Andreeva, T. Tabakova, *J. Mol. Catal. A*, **2004**, 213, 235; M. Manzoli, A. Chiorino and F. Boccuzzi, *Appl. Catal. B.*, **2004**, 52, 259.
7. M. A. Saez-Castillo, C. Couto, W.B Kim and J.A Dumesic, *Angew. Chem. Int. Ed.*, **2004**, 43, 1140.
8. G. C. Bond and D.T Thompson, *Gold Bull.*, **2000**, 33, 41.
9. M. Haruta, *Gold Bull*, **2004**, 37, 27.
10. C. K. Castello, M.C. Kung, H.S Oh, Y. Wang and H.H. Kung, *Appl. Catal. A.*, **2002**, 232, 159.
11. L. M. Molina, B. Hammer, *Appl. Catal. A.*, **2005**, 291, 21.
12. Z. P. Lin, X.Q. Gong, J. Kohanoff, C. Sanchez and P. Hu, *Phys. Rev. Lett.*, **2003**, 91, 266102.
13. N. Lopez, T. V. W. Janssens, B. S Clausen, Y. Xu, M. Mavrikakis. T. Bligaard and J.K Narskow, *J. Catal.*, **2004**, 223, 232.
14. C. Lemise, R. Meyer, S. Shaikhutdinov and H. J. Freund, *Angew. Chem. Ed.*, **2004**, 43, 118.
15. M. S Chen and D. W Goodman, *Science*, **2004**, 306, 252.
16. B. Yoon, H. Hakkinen, U. Landman, A. S. Worz, J.M Antonetti, S Abbet and K. Judai, *Science*, **2005**, 307, 403.
17. G. C Bond, C. Louis, D.T. Thompson., *Catalysis by Gold*, Imperial College Press, London (**2006**).

18. A. M. Visco, F. Neri, G. Neri, A. Donato, C. Milone and S. Galvagno, *Chem. Phys.*, **1999**, 1, 2869.
19. J. C. Lavalley, *Catal Today*, **1996**, 27, 377.
20. S. T. Daniells, M. Makkee and J. A. Moulijn, *Catal. Lett.*, **2005**, 100, 39.
21. N. M. Gupta and A. K. Tripathi, *Gold Bulletin*, **2001**, 34(4), 120.
22. N. M. Schubert, A. Venugopal, M. J. Kalich, V. Plazk and R. J. Behm, *J. Catal.*, **2004**, 222, 32.
23. T. Kasuga, M. Hiramatsu, A. Hoson, T. Sekino and K. Niihara, *Langmuir*, **1998**, 14(12), 3160.
24. J. R. Bargar, J. D. Kubicki, R. Reitmeyer and J. A. Davis, *Geochim. Cosmochim. Acta*, **2005**, 69, 1527.
25. H. Knozinger, *Advances in Catalysis*, **1976**, 25, 235.
26. F. Moreau and G. C. Bond, *Catal. Today*, **2006**, 114, 362.
27. D. Andreeva, V. Idakiev, T. Tabakova, A. Andreev and R. Giovanoli, *Appl. Catal.*, **1996**, 134, 275.
28. M. A. Debeila, R. P. K. Wells and J. A. Anderson, *J. Catal.*, **2006**, 239, 162.
29. M. Maciejewski, P. Fabrizioli, J. Grunwaldt, O. S. Becker and A. Baiker, *Phys. Chem. Chem. Phys.*, **2001**, 3, 3846.
30. B. Schumacher, Y. Denkwitz, V. Plzak, M. Kinne and R. J. Behm, *J. Catal.*, **2004**, 224, 449.
31. M. A. Bollinger and M. A. Vannice, *Appl. Catal. B*, **1996**, 8, 417.

## Chapter 5

CO oxidation over anatase TiO<sub>2</sub> supported Au: Effect of nitrogen doping.

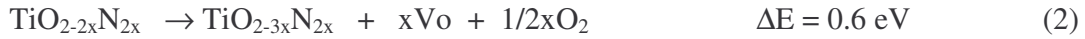
### *5.1. Introduction*

The bulk form of gold is chemically inert; however, it has been shown that in nanoparticle form (<10 nm) gold has exceptional high activity for CO oxidation at low temperatures [1-6]. The activity of a supported Au catalyst for CO oxidation chiefly depends on the particle size of gold and both the chemical and physical characteristics of the support. Recently, work has been reported on Au/TiO<sub>2</sub> that focused on studying the effects of phase structure, crystal size, surface and textural properties of the TiO<sub>2</sub> support on the catalytic activity for CO oxidation [7]. Little is known about the effects of electro-optical properties of anatase TiO<sub>2</sub> support on Au/TiO<sub>2</sub> catalysts used for CO oxidation. This work attempts to understand the effects of nitrogen doping on the electronic properties of TiO<sub>2</sub> as reflected by optical properties anatase TiO<sub>2</sub> support used to support Au. The electronic properties of TiO<sub>2</sub> were altered by doping it with nitrogen; this also brought about change in its oxygen vacancy density.

It is believed that a metal-support interaction creates the active sites for adsorption of reacting gases to facilitate the CO oxidation reaction [8]. It has also been reported that Au is anchored on/or close to oxygen vacancy sites of the oxide support, which is relevant for the CO oxidation reaction [9, 10, 11]. Therefore, metal oxide supports with high oxygen vacancy densities would be desirable to anchor more particles of Au, i.e. to have a highly dispersed Au catalyst.

Nitrogen doped titania (TiO<sub>2-x</sub>N<sub>x</sub>), a photocatalyst that has been studied for degradation of various toxic organic compounds, has been reported to have more oxygen vacancies than pure TiO<sub>2</sub> [12]. According to density functional theory (DFT) calculations [12], N doping of TiO<sub>2</sub> favours the formation of oxygen vacancies and this finding was

confirmed by real-time transmission electron microscopy (TEM) [13] studies. The computed energy cost to create oxygen vacancies is drastically reduced from 4.2 eV in pure TiO<sub>2</sub> to 0.6 eV in N-doped TiO<sub>2</sub> [13].



These findings stimulated us to prepare TiO<sub>2-x</sub>N<sub>x</sub> as a support for gold to study its catalytic behaviour in the CO oxidation reaction. Our aim was to study the effects of the increased oxygen vacancies on the support, as well as the change in the optical properties, on the catalytic behaviour of Au/ TiO<sub>2-x</sub>N<sub>x</sub>. The catalytic behaviour of Au/ TiO<sub>2-x</sub>N<sub>x</sub> was compared to that of Au/TiO<sub>2</sub>.

## 5.2. Results

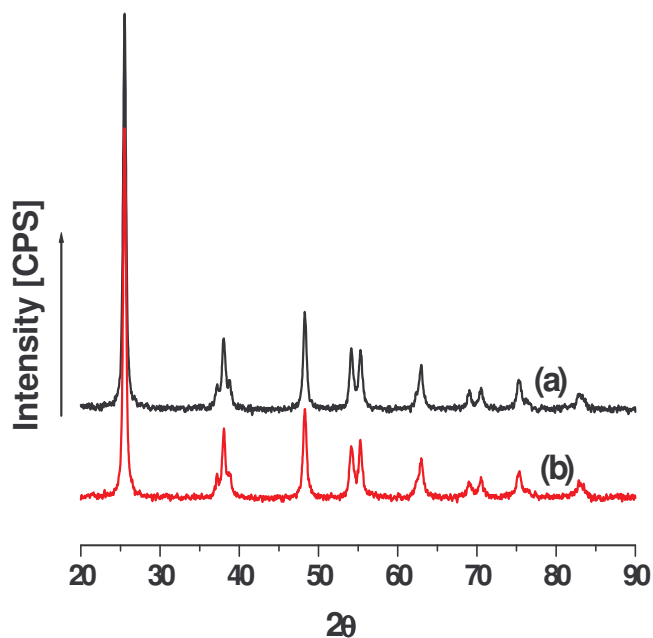
### 5.2.1 Phase characterization, surface properties and HRTEM studies

The BET surface areas and Au contents of the studied catalysts are given in Table.1. The results show that the as-prepared pure anatase TiO<sub>2</sub> had a surface area of 32 m<sup>2</sup>/g whereas TiO<sub>2-x</sub>N<sub>x</sub> has a surface area of 7 m<sup>2</sup>/g; this indicates that nitrogen doping lowers the surface area. Similarly the pore volume was reduced from 0.077 to 0.031 cm<sup>3</sup>/g. The reported surface area for Ti-O-N is 11 m<sup>2</sup>/g [14]. Both TiO<sub>2</sub> and TiO<sub>2-x</sub>N<sub>x</sub> were loaded with the same amount of Au content (1 wt %) and Au loading did not bring any change to the surface area. The nitrogen content of TiO<sub>2-x</sub>N<sub>x</sub> was analysed by ICP-AES techniques and the results reveal that it had 0.2 wt% of lattice nitrogen.

Table 1: Physical properties of the catalysts studied.

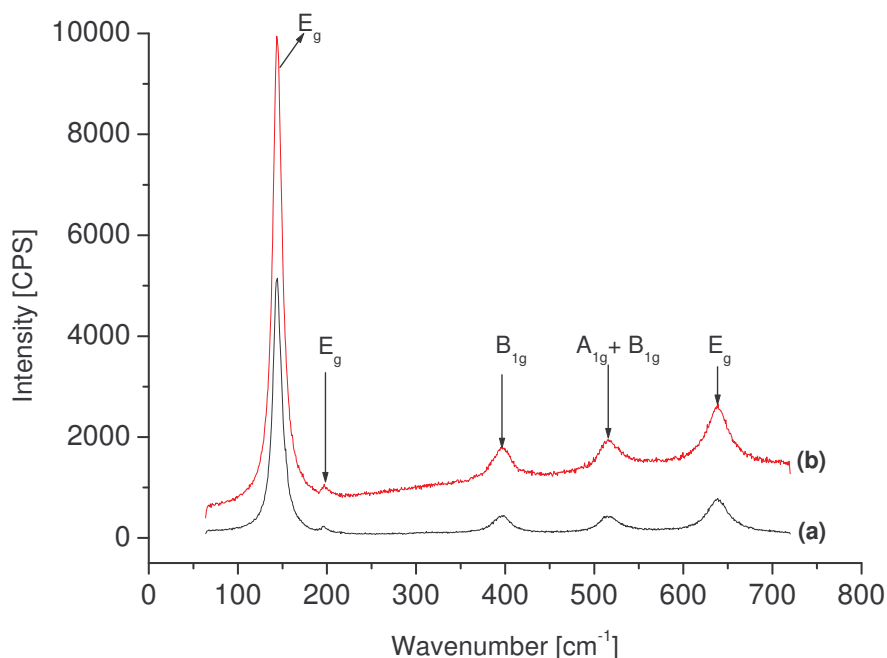
	BET surface area, m <sup>2</sup> /g	Pore volume, cm <sup>3</sup> /g	Au content, wt. %
TiO <sub>2</sub>	31.79	0.0777	-
TiO <sub>2-x</sub> N <sub>x</sub>	07.81	0.0311	-
Au/TiO <sub>2</sub>	32.03	0.0737	1.0
Au/TiO <sub>2-x</sub> N <sub>x</sub>	07.67	0.0278	1.0

Figure 1 shows XRD patterns of Au/TiO<sub>2-x</sub>N<sub>x</sub> and Au/TiO<sub>2</sub>. It indicates the diffraction lines pertaining to the anatase phase of TiO<sub>2</sub> for both samples, according to JCPDS file no: 01-089-4921. Since the Au loading was very low (1 wt. %), diffraction lines due to Au could also not be detected. The implication from the figure is that nitrogen doping does not alter the crystal structure of anatase TiO<sub>2</sub>.



**Figure 1:** XRD patterns of (a) Au/TiO<sub>2</sub> and (b) Au/TiO<sub>2-x</sub>N<sub>x</sub>.

Raman spectra of Au/TiO<sub>2-x</sub>N<sub>x</sub> and Au/TiO<sub>2</sub> are shown in Figure 2. The results show the presence of bands at 143, 197, and 638 cm<sup>-1</sup> due to the E<sub>g</sub> mode of TiO<sub>2</sub>. The bands observed at 396, and 514 cm<sup>-1</sup> are assigned to B<sub>1g</sub> and B<sub>1g</sub>+ A<sub>1g</sub> modes [15]. The B<sub>1g</sub> mode corresponds to O-Ti-O bending type vibrations while others are related to Ti-O stretching type vibrations [16]. The Raman results further confirmed that neither nitrogen doping nor Au loading changed or affected the phase structure of the TiO<sub>2</sub> support.



**Figure 2:** Raman spectra of (a) Au/TiO<sub>2</sub> and (b) Au/TiO<sub>2-x</sub>N<sub>x</sub>.

High resolution transmission electron microscope pictures of Au/TiO<sub>2</sub> and Au/TiO<sub>2-x</sub>N<sub>x</sub> are given in Figure 3. In Au/TiO<sub>2</sub>, most of the gold particles were about 5 nm in diameter and well distributed on the support whereas in Au/TiO<sub>2-x</sub>N<sub>x</sub>, the majority of gold particles were less than 3 nm. This implies that the nature of the support affects the average gold particle size and indeed nitrogen doping of TiO<sub>2</sub> lowered the average gold particle size to well below 3 nm.

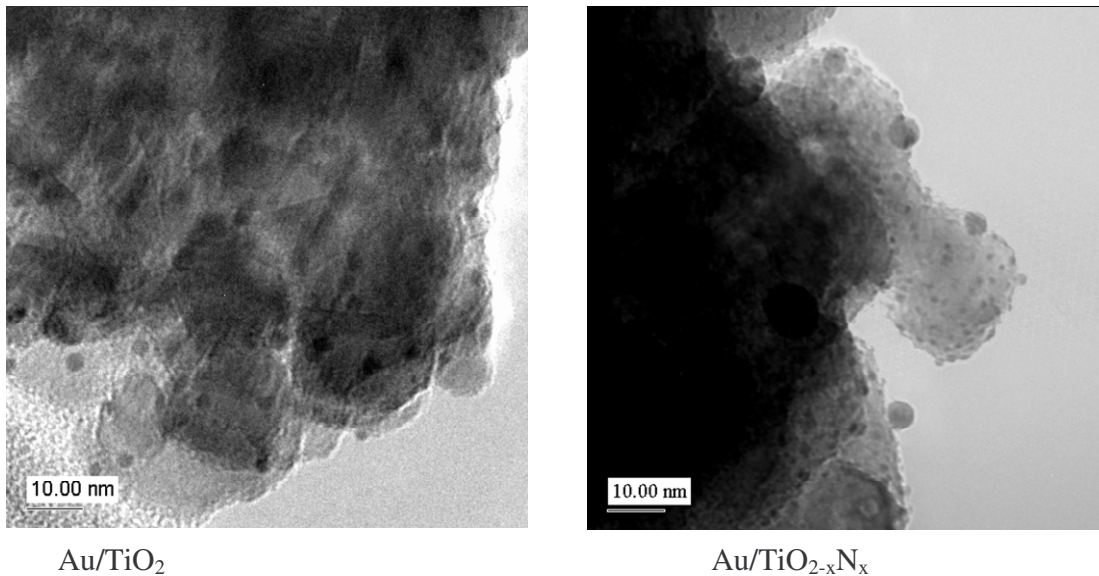


**Figure 3:** HR-TEM pictures of Au/TiO<sub>2</sub> and Au/TiO<sub>2-x</sub>N<sub>x</sub>.

### 5.2.2 Optical properties

Figure 4 shows DRS-UV vis spectra of TiO<sub>2-x</sub>N<sub>x</sub> and TiO<sub>2</sub>. It discloses that TiO<sub>2</sub> absorbs light in the UV region (< 400 nm) whereas TiO<sub>2-x</sub>N<sub>x</sub> absorbs in the visible region at around 450 nm wavelength. This was evidence that nitrogen was indeed introduced into the lattice of TiO<sub>2</sub>; the observation agrees with reported literature that nitrogen doping of TiO<sub>2</sub> alters its electronic properties [17]. Au loading on these supports did not bring about any change in the observed DRS-UV vis spectra.

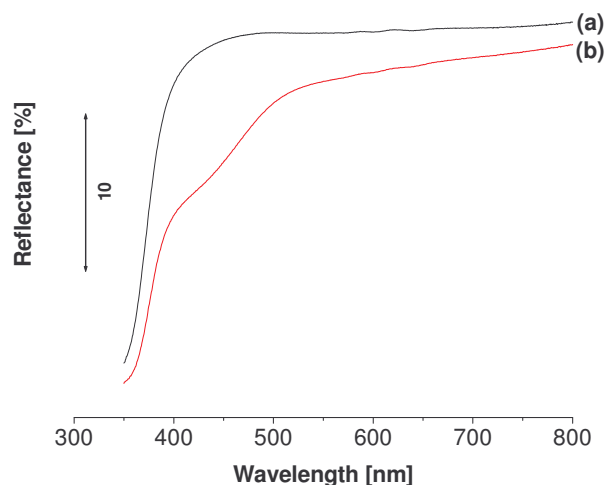


**Figure 4:** DRS-UV vis spectra of (a)  $\text{TiO}_2$  and (b)  $\text{TiO}_{2-x}\text{N}_x$ .

### 5.2.3 Ability of oxygen uptake by the supports

To examine the oxygen uptake ability of the supports, TPO (Temperature programmed oxidation) studies were carried out over the pure supports,  $\text{TiO}_{2-x}\text{N}_x$  and  $\text{TiO}_2$  (Figure 5). The TPO results reveal that  $\text{TiO}_2$  started losing oxygen from the lattice at temperatures above 175 °C with a maximum at 300 °C. On the other hand  $\text{TiO}_{2-x}\text{N}_x$  showed a low temperature oxygen uptake peak at around 100 °C with shoulder peaks between 300 and 400 °C. At high temperatures, a strong oxygen uptake peak around 600 °C and a weak peak around 750 °C were observed. The yellowish  $\text{TiO}_{2-x}\text{N}_x$  sample became white after TPO studies indicating complete oxidation. According to literature [18] accounts, annealing of  $\text{TiO}_{2-x}\text{N}_x$  at above 300 °C in an oxygen rich atmosphere leads to loss of lattice nitrogen due to oxidation and  $\text{TiO}_2$  is formed in the process. The TPO results support the reported DFT (density functional theory) calculations which claimed that the  $\text{TiO}_{2-x}\text{N}_x$  material has a high density of oxygen vacancies [12, 13]; hence why it showed high oxygen uptake ability as compared to  $\text{TiO}_2$ .

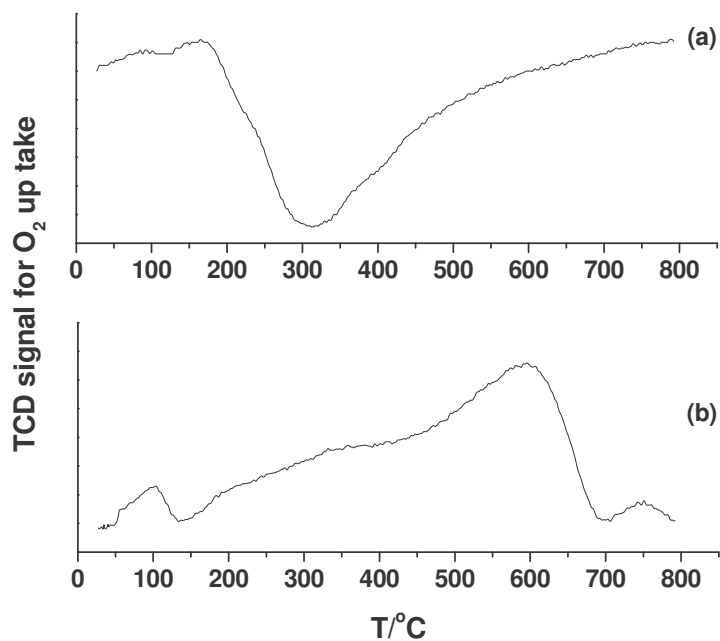


**Figure 5:** Temperature programmed oxidation (TPO) of (a)  $\text{TiO}_2$  and (b)  $\text{TiO}_{2-x}\text{N}_x$ .

## 5.2.4 Oxidation of CO

### 5.2.4.1 Effect of pre-treatment

It has been reported that pre-treatment of gold catalysts in different gaseous atmospheres and at different temperatures affects the metal particle size, its dispersion on the support, the metal support interaction and the ionic and metallic nature of gold on the support [4]. These changes subsequently bring about changes in the catalytic behaviour of gold catalysts in the CO oxidation reaction. Here, we present the CO oxidation results of  $\text{Au/TiO}_2$  and  $\text{Au/TiO}_{2-x}\text{N}_x$  obtained using different pre-treatment conditions.

### A. Without pre-treatment

Figure 6 shows the catalytic CO oxidation reaction, carried out at 70 °C, with time on stream for the as-prepared Au/TiO<sub>2</sub> and Au/TiO<sub>2-x</sub>N<sub>x</sub> catalysts. After 1 h of time-on-line both catalysts started deactivating. It is worth noting that the Au/TiO<sub>2-x</sub>N<sub>x</sub> catalyst underwent deactivation relatively faster than Au/TiO<sub>2</sub>.

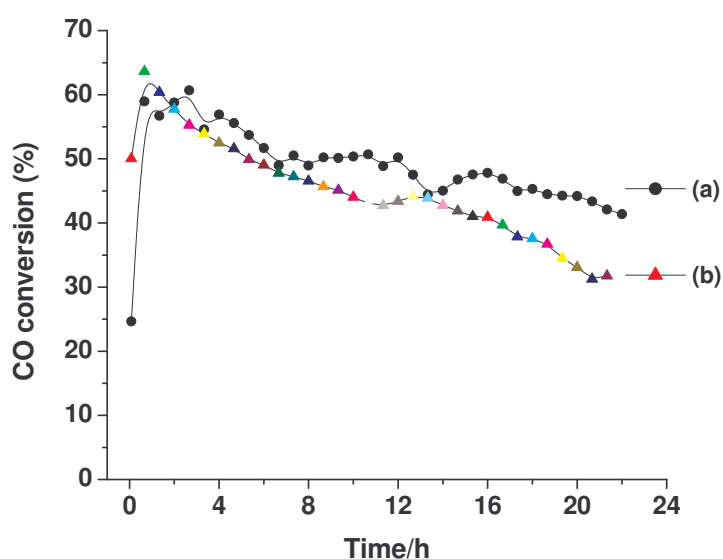


**Figure 6:** Deactivation of the as-prepared catalysts during time-on-line of CO oxidation: (a) Au/TiO<sub>2</sub> and (b) Au/TiO<sub>2-x</sub>N<sub>x</sub>. Reactions were run at 70 °C.

### B. H<sub>2</sub>/O<sub>2</sub> pre-treatment

Pre-treatment of gold catalysts in either reducing (H<sub>2</sub>) or oxidizing (O<sub>2</sub>) atmospheres is not uncommon in Au catalysis [19]. It has also been reported that both ionic and metallic forms of gold are essential for the CO oxidation reaction [20], and certainly the stability of these species could be affected by the pre-treatment and nature of the support. CO oxidation activity results obtained at 40 °C for the catalysts pre-treated in O<sub>2</sub> atmosphere are shown in Figure 7. Au/TiO<sub>2-x</sub>N<sub>x</sub> showed higher initial activity than Au/TiO<sub>2</sub>.

However, the former deactivated faster than the latter catalyst, indicating that nitrogen doping of anatase TiO<sub>2</sub> accelerates the deactivation process. A similar trend was observed for catalysts pre-reduced in H<sub>2</sub> (Figure 8), where Au/TiO<sub>2</sub> was the more active and stable of the two catalysts.

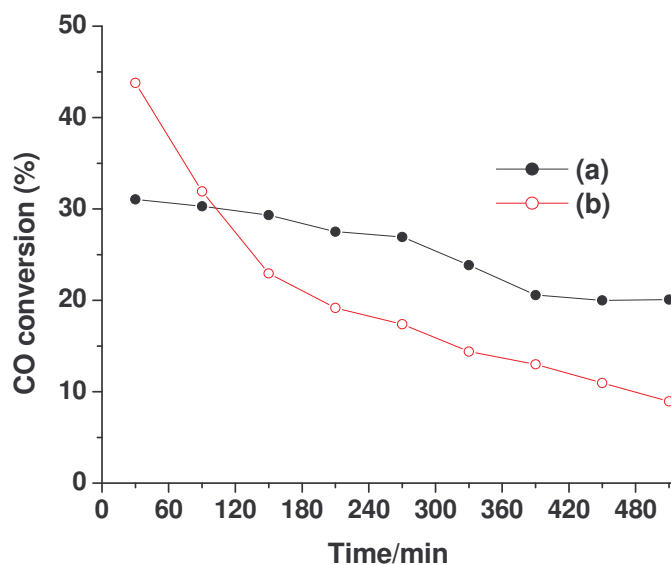


**Figure 7:** Deactivation of catalysts pre-treated at 300 °C in 5 % O<sub>2</sub> (balance He): (a) Au/TiO<sub>2</sub> and (b) Au/TiO<sub>2-x</sub>N<sub>x</sub>. Reactions were run at 40 °C.

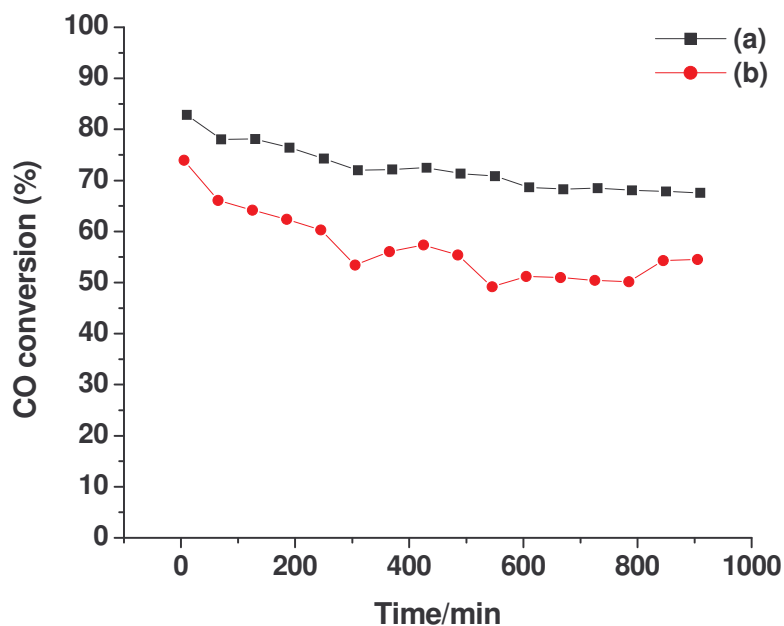


**Figure 8:** CO oxidation activity of catalysts pre-treated at 300 °C in 5 % H<sub>2</sub> (balance He): (a) Au/TiO<sub>2</sub> and (b) Au/TiO<sub>2-x</sub>N<sub>x</sub>. Reactions were run at 70 °C.

#### 5.2.4.2 Effect of moisture

It has been reported that moisture and surface hydroxyl groups on the Au/TiO<sub>2</sub> catalyst surface promote the CO oxidation reaction and prevent deactivation by removal of carbonate/bicarbonate species that might accumulate as a result of the reaction [4]. After pre-treatment of the catalysts Au/TiO<sub>2</sub> and Au/TiO<sub>2-x</sub>N<sub>x</sub> at 300 °C in O<sub>2</sub>/H<sub>2</sub> atmosphere, the reaction was carried out at 70 °C with moisture as a co-feed in the reactant gas mixture. The results obtained are depicted in Figure 9. As seen from the figure, Au/TiO<sub>2</sub> exhibited high catalytic activity without any sign of deactivation when moisture was introduced in the reactant gas mixture from the start of reaction. Hydrogen pre-treatment of Au/TiO<sub>2</sub> further enhanced the catalytic activity compared with oxygen pre-treatment. It was reported that in the case of Au/Al<sub>2</sub>O<sub>3</sub>, the catalytic activity loss could be restored with either hydrogen or water treatment [21, 22]. On the other hand, moisture did not either promote the catalytic activity or prevent the deactivation of Au/TiO<sub>2-x</sub>N<sub>x</sub> (Figure

9b). This suggested that even a small amount of nitrogen doping of TiO<sub>2</sub> inhibits any role that moisture might play in promoting the reaction.

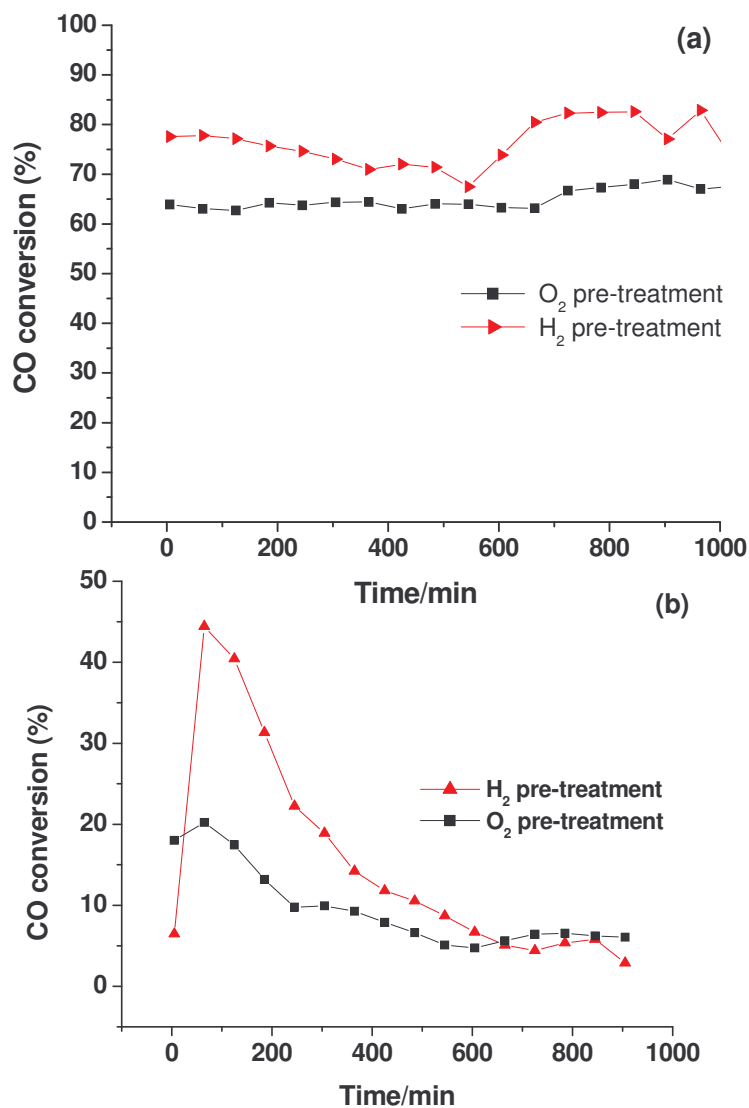


**Figure 9:** Effect of moisture on the catalytic activities of catalysts pre-treated in different atmospheres: (a) Au/TiO<sub>2</sub> and (b) Au/TiO<sub>2-x</sub>N<sub>x</sub>. Reactions were run at 70 °C.

### 5.2.4.3 Regeneration of activity

To investigate the stability and regenerability of activity/active sites of Au/TiO<sub>2-x</sub>N<sub>x</sub>, the catalyst was pre-treated first in an O<sub>2</sub> atmosphere at 300 °C for 1 h and then the reaction

was carried out at 70 °C (Figure 10a). As seen from the figure, Au/TiO<sub>2-x</sub>N<sub>x</sub> underwent deactivation very rapidly with time-on-line; the CO conversion level was reduced from 58 % to 5 % after 19 h. With the aim of regenerating the active sites, after 19 h of reaction, the catalyst was re-heated in O<sub>2</sub> at 300 °C for 1 h, then, after cooling down to 70 °C again, the reaction was recommenced. About 38 % of the initial activity was restored but with further time-on-line (4 h) the catalyst continued to deactivate until it was nearly inactive. With subsequent introduction of moisture into the reactant gas mixture, about 21 % of the initial activity was restored within 2 h but then again the catalyst rapidly deactivated.

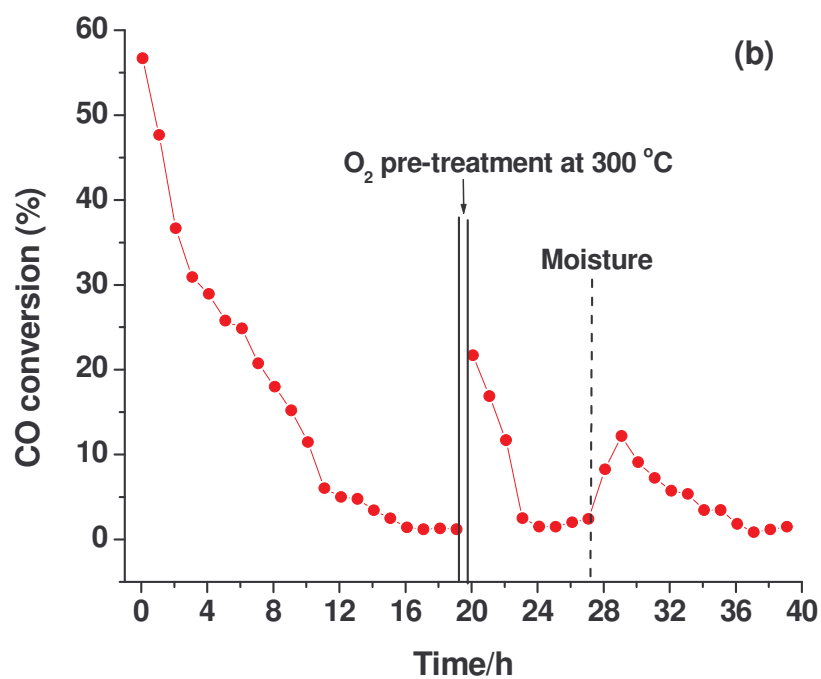
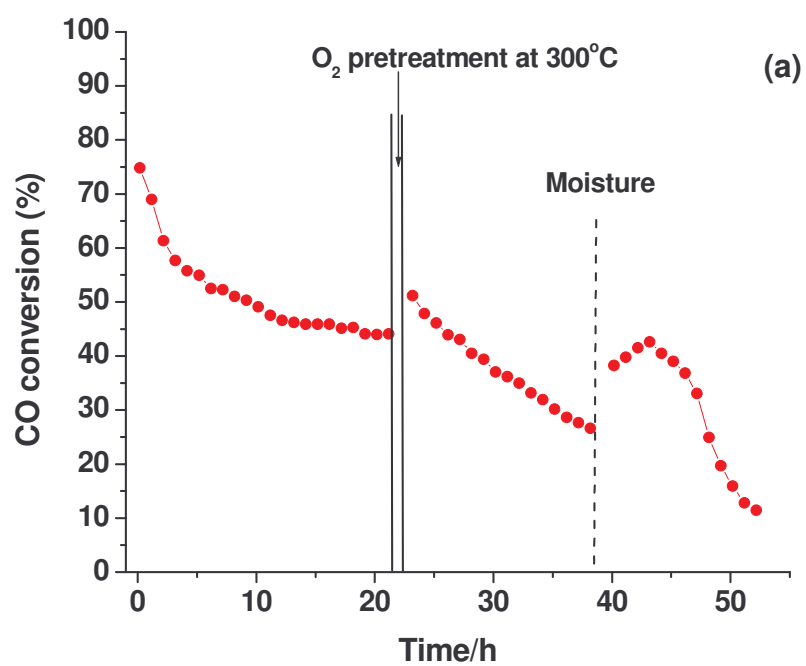


**Figure 10:** Regeneration of catalytic activities of catalysts pre-treated in 5 % O<sub>2</sub> (balance He): (a) Au/TiO<sub>2</sub> and (b) Au/TiO<sub>2-x</sub>N<sub>x</sub>. Reactions were run at 70 °C.

On the other hand, Au/TiO<sub>2</sub> showed relatively slow deactivation after pre-treatment in O<sub>2</sub> at 300 °C (Figure 10a). The CO conversion level decreased from 75 % to 44 % in 21 h. However, this catalyst also could not be fully regenerated with either O<sub>2</sub> or H<sub>2</sub>O.

### 5.2.4.3 Effect of temperature

The as-prepared (without pre-treatment) Au/TiO<sub>2</sub> catalyst showed higher catalytic CO conversion with increasing temperature from 30 to 300 °C than Au/TiO<sub>2-x</sub>N<sub>x</sub> (Figure 11). The latter showed very poor activity up to 50 °C. These results indicate that, without any pre-treatment, Au/TiO<sub>2</sub> is a better catalyst at ambient temperature than Au/TiO<sub>2-x</sub>N<sub>x</sub>.

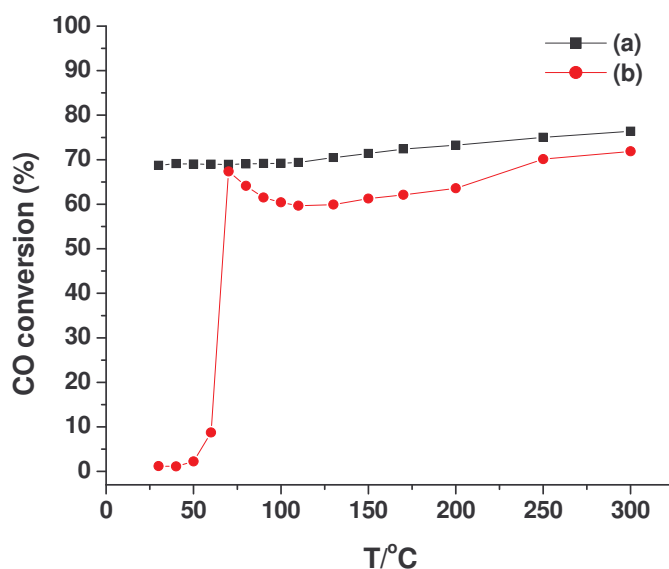


**Figure 11:** CO conversion versus temperature ramp over as-prepared catalysts: (a) Au/TiO<sub>2</sub> and (b) Au/TiO<sub>2-x</sub>N<sub>x</sub>.

Figure 12 shows the activities of the two catalysts as a function of temperature. When both are pre-treated in H<sub>2</sub>, Au/TiO<sub>2</sub> exhibited superior activity to that of Au/TiO<sub>2-x</sub>N<sub>x</sub> at all temperatures. However, the opposite was observed when the catalysts were pre-treated in O<sub>2</sub>. The latter observation contradicts the findings of Centeno et al [23], who reported that Au/TiO<sub>2</sub> showed higher activity than Au/TiO<sub>2-x</sub>N<sub>x</sub> with increasing temperature. The

superior ability of  $\text{TiO}_{2-x}\text{N}_x$  to take up oxygen (Figure 5b) with increasing temperature is a logical explanation of our results.

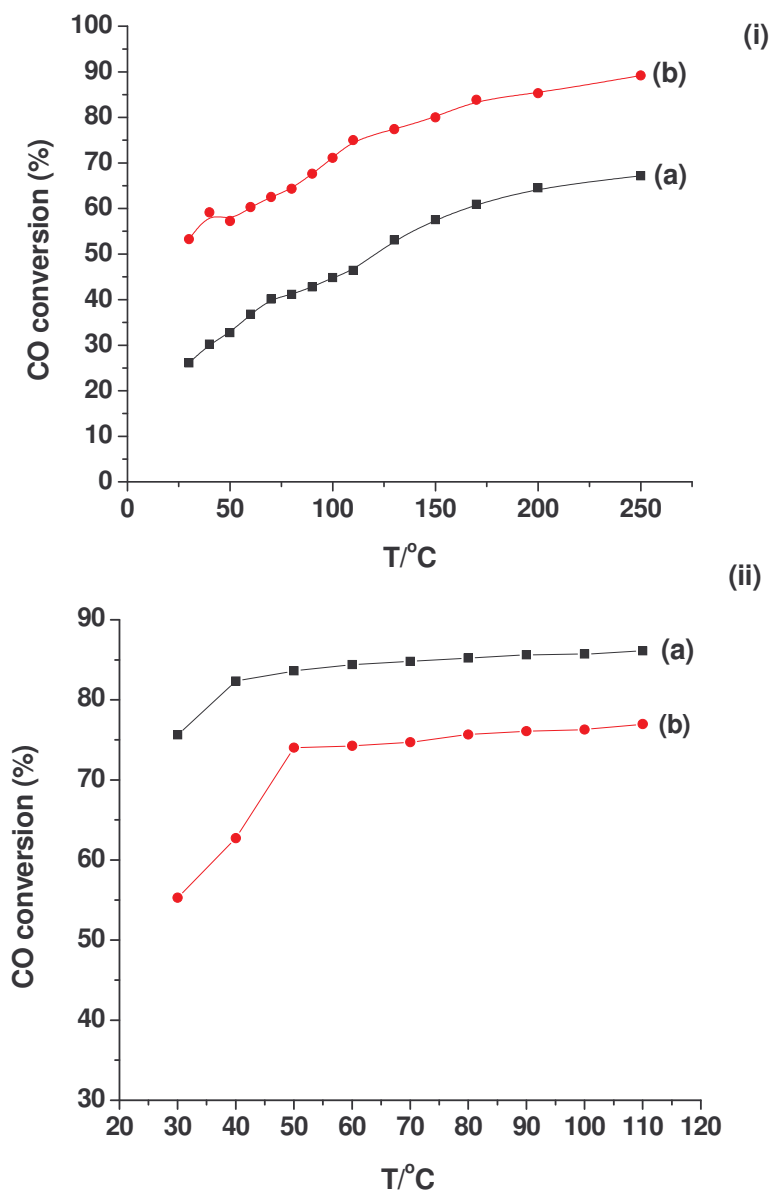


**Figure 12:** CO conversion versus temperature ramp over catalysts pre-treated in (i) 5% O<sub>2</sub>, (ii) 5% H<sub>2</sub> both balance in He: (a) Au/TiO<sub>2</sub> and (b) Au/TiO<sub>2-x</sub>N<sub>x</sub>.

### 5.3. Discussion

The aim of this work was to study the effects of nitrogen doping of anatase  $\text{TiO}_2$ , a material which is commonly utilized as a support for Au catalysts used in the oxidation of carbon monoxide. It is well known that both the electronic state and the structure of Au clusters are dramatically changed depending on which support is selected. In addition, even if the support used is the same, the characteristics of the Au clusters deposited could be different, depending on the surface conditions, such as whether the support has a reduced or oxidised nature [24].

Our results (Figures 4 and 5) confirmed that nitrogen doping of anatase  $\text{TiO}_2$  creates oxygen vacancies (point defects). Defects on metal-oxide supports play an essential role as metal cluster nucleation sites [25]. It has been reported that oxygen vacancies on MgO are essential for the nucleation of active Au clusters [26, 27]. Furthermore, theoretical studies have shown that electron transfer from defects to the Au cluster facilitates CO oxidation [25]. It has recently been reported that (bridging) oxygen vacancies on  $\text{TiO}_2$  are active nucleation sites for Au clusters [28]. It was because of these findings that  $\text{TiO}_{2-x}\text{N}_x$  was prepared and compared with  $\text{TiO}_2$  as the catalyst supports.

In general, the  $\text{Au/TiO}_2$  catalyst system showed superior activity and stability to that of the  $\text{Au/TiO}_{2-x}\text{N}_x$  catalyst. The vast differences seen in the activities of the two catalysts might have largely been due to differences in their Au particle morphology. Figure 3 shows that  $\text{Au/TiO}_{2-x}\text{N}_x$  had smaller Au nano-particles than  $\text{Au/TiO}_2$ . The differences in particle size distribution is not surprising because, in general, the morphology of metal particles on oxide surfaces depends to a large extent on defects, particularly point defects such as oxygen vacancies [28-32]. The finding that  $\text{Au/TiO}_{2-x}\text{N}_x$  had poor activity (compared to  $\text{Au/TiO}_2$ ) despite its smaller Au particle sizes was not a unique result. It has been reported that Au particle size is not an overriding factor in determining the catalytic activity of supported Au nanoparticles [33 and references therein]. The support and metal-support interaction are immensely important as well.

Both catalyst systems deactivated with time-on-stream, irrespective of the type of pre-treatment (Figures 6-8). However, it is worth noting that Au/TiO<sub>2-x</sub>N<sub>x</sub> in all cases deactivated more rapidly than Au/TiO<sub>2</sub>. Once deactivated, neither catalyst could be regenerated to their original activity either by O<sub>2</sub> pre-treatment at 300 °C or by H<sub>2</sub>O. Possible reasons reported for the intrinsic deactivation of Au catalysts include growth of metal particles (sintering), blockage of active sites by carbonate species and/or depletion of surface hydroxyl groups [33]. The accumulation of carbonate species seems to be the plausible reason for deactivation in the case of Au/TiO<sub>2</sub> because the system lost about 20 % of its original activity after 8 h compared to about 79 % loss of activity in the same time period of Au/TiO<sub>2-x</sub>N<sub>x</sub> (Figure 6). The irreversible deactivation of Au/TiO<sub>2-x</sub>N<sub>x</sub> is so rapid that one is tempted to think that its deactivation is not only due to carbonates.

It is not totally unthinkable that nitrogen doping of anatase TiO<sub>2</sub> can affect/alter (negatively) the metal (Au)–support interaction. It has been reported that the introduction of nitrogen into the anionic network of TiO<sub>2</sub> to form TiO<sub>2-x</sub>N<sub>x</sub> alters the properties of the Au-support interface by decreasing the electron density of gold atoms [34]. This decrease of electron density would certainly have an adverse effect on the adsorption/catalytic behaviour of the Au/TiO<sub>2-x</sub>N<sub>x</sub> catalyst. In addition, growth of Au particles was also a likely culprit for the rapid deactivation of this system. Basenbacher and co-workers, using STM, suggested that the diffusion of an oxygen vacancy complex on TiO<sub>2</sub> plays an important role in the formation of larger Au clusters [28]. With the larger number of oxygen vacancies, it is possible that these dynamic point defects “move around” with Au anchored on them and in the process Au particles agglomerate under reaction conditions, irreversibly reducing the activity of Au/TiO<sub>2-x</sub>N<sub>x</sub>.

Figure 9 perhaps underlines the huge contrast in the behaviour and properties of the two catalyst systems. When introduced from the on-set of reaction, moisture prevented the deactivation of Au/TiO<sub>2</sub>. However, irrespective of the type of pre-treatment, moisture had no (positive) effect on the Au/TiO<sub>2-x</sub>N<sub>x</sub> catalyst system. The catalyst continued to deactivate with time-on-line just as in the absence of moisture. The effect of moisture on Au catalysts has been investigated mainly for CO oxidation, since moisture has a

remarkable effect. From comprehensive quantitative analyses, it has been found that moisture enhances the catalytic activities of Au catalysts up to two orders of magnitude and that the effect of moisture depends on the type of metal oxide support used [33]. Our results indicate that the metal-support interaction was not necessarily similar in the two catalysts, and hence the reason that moisture had such contrasting effects on their respective catalytic activities.

The morphology of the Au cluster, (e.g. whether it has a spherical or hemispherical shape), affects the surface charge density distribution that is related to the catalytic activity of Au catalysts and the presence of H<sub>2</sub>O molecules plays an important role in the modification of the electronic state of Au clusters [24]. This implies that on Au/TiO<sub>2</sub>, molecules of H<sub>2</sub>O can positively modify the electronic state of Au clusters; in the process, promoting the reaction and preventing deactivation by accumulation of carbonate species on active sites. However, the different metal-support properties of Au/TiO<sub>2-x</sub>N<sub>x</sub> compared with those of Au/TiO<sub>2</sub> probably do not allow for the same synergy of H<sub>2</sub>O and Au cluster charge to result in the promotion of oxidation of CO.

In addition, the vast differences in catalytic behaviour of the two catalysts cannot be accounted for by the differences in their surface areas (Table 1). Work done by Yeung et al. [7] showed that for anatase TiO<sub>2</sub> supported Au catalysts, surface area played no significant role in terms of catalytic activity.

In retrospect, it is evident that a great deal of mechanistic work needs to be done to decipher the origins of the fundamental differences in the catalytic behaviour of the two catalyst systems. The difference might largely lie in the fact that the one support (TiO<sub>2-x</sub>N<sub>x</sub>) has more oxygen vacancies than the other (TiO<sub>2</sub>). The manner in which the support 'activates' the oxygen molecule is often left unspecified; however, there are indications that these molecules may be activated on oxide ion vacancies as O<sub>2</sub><sup>-</sup> [35-37]. The superoxide ion might then migrate to, and dissociate at, the Au particle edge before reacting [36]. The specific role played by the oxide ion vacancies has been reinforced by the reports that they are blocked by 'spectator' carbonate species, thus, making them

unavailable to oxygen molecules and inevitably leading to deactivation [8, 33, 36]. *In situ* infrared spectroscopy experiments would be invaluable in terms of studying the rate of accumulation of these carbonate species and the effect of moisture on their stability on the two catalyst systems. The toxicity of chloride ion can also be understood by its occupation of anion vacancies [33]. For future work, one would need to do *in situ* IR experiments to study the nature and rate of accumulation of different carbonate species on the two catalyst systems.

#### **5.4. Conclusions**

- (1) Au/TiO<sub>2</sub> is more active and stable than Au/TiO<sub>2-x</sub>N<sub>x</sub> for the oxidation of CO.
- (2) Water promotes catalytic CO oxidation over Au/TiO<sub>2</sub> and inhibits deactivation of the catalyst when introduced from the start of the reaction.
- (3) Water has no lasting observable effect on Au/TiO<sub>2-x</sub>N<sub>x</sub>.

## 5.5. References

1. M. Haruta, *Catal. Today*, **1997**, 36, 153.
2. M. Valden, X. Lai and D. W. Goodman, *Science*, **1998**, 281, 1647.
3. R. Meyer, C. Lemire, Sh. K. Shaikhutdinov and H.-J. Freund, *Gold Bulletin*, **2004**, 37/1–2, 72.
4. G.C. Bond and D.T. Thompson, *Catal. Rev. Sci. Eng.*, **1999**, 41, 319.
5. S. Tsubota, M. Haruta, T. Kobayashi, A. Ueda, Y. Nakahara, in: G. Poncelet, et al. (Eds.), *Preparation of Catalysts*, vol. V, Elsevier, Amsterdam, **1991**, pp. 695–704.
6. M. Haruta, S. Tsubota, T. Kobayashi, H. Kageyama, M. Genet, B. Delmon, *J. Catal.*, **1993**, 144, 175.
7. K. Y. Ho and K. L. Yeung, *Gold Bulletin*, **2007**, (40/1), 15.
8. M. Haruta, *CATTECH*, **2002**, 6(3), 102.
9. K. Okazaki, S. Ichikawa, Y. Maeda, M. Haruta, M. Kohyama, *Appl. Catal. A: General*, **2005**, 291, 45.
10. J. C. Frost, *Nature*, **1988**, 334, 577.
11. M. Okumura, Y. Kitagawa, M. Haruta and K. Yamaguchi, *Applied Catalysis A: General*, **2005**, 291, 37.
12. Di Valentin, C.; G. Pacchioni, A. Selloni, S. Livraghi and E. Giamello, *J. Phys. Chem. B*, **2005**, 109, 11414.
13. E. Sutter, P. Sutter, E. Fujita and J. Muckerman, *Abstracts of the European. Materials Research Society Spring Meeting*, Nice, France, **2006**. Page, M-14.
14. M. A. Centeno and M. J. Lloret, *Mat. Sci. Forum*, **2002**, 383, 111.
15. R. van de Krol and A. Goossens, *J. Vac. Sci. Technol. A*, **2003**, 21, 76.
16. T. Ohsaka, F. Izumi, Y. Fujiki, *J. Raman Spectrosc*, **1978**, 7, 321.
17. Y. Kuroda, T. Mori, K. Yagi, N. Makihata, Y. Kawahara, M. Nagao and S. Kittaka, *Langmuir*, **2005**, 21, 8026.
18. S.H. Mohameda, O. Kappertza, T. Niemeiera, R. Dresea, M. M. Wakkadb, M. Wuttiga, *Thin Solid Films*, **2004**, 468, 48– 56.

19. C. Andreea, Gluhoi, S. Huib, Vreeburg, J. W. Bakker, B. E. Nieuwenhuys  
*Applied Catalysis A: General*, 2005, 291, 145-150.
20. J. Guzman, B. Gates, *J. Phys. Chem. B*, **2002**, 106, 7659.
21. M. C. Kung, C. K. Costello and H. H. Kung, in *Specialist Periodical Reprints: Catalysis*, J. J. Spivey and G. W. Roberts, (eds.) Roy. Soc. Chem., London, **2004**, Vol. 17, p. 152.
22. C. K. Costello, M. C. Kung, H. S. Oh and K. H. Kung, *Appl. Catal. A: Gen.* **2002**, 232, 159.
23. M. A. Centeno, I. Carrizosa and J. A. Odriozola, *Appl. Catal. A: Gen.*, **2003**, 246, 365.
24. M. Okumura, M. Haruta, Y. Kitagawa and K. Yamaguchi, *Gold Bulletin*, **2007**, 40/1, 40.
25. W. T. Wallace, B. K. Min and D. W. Goodman, *Journal of Molecular Catal. A*, **2005**, 228, 3.
26. H. Hakkinen, S. Abbet, A. Sanchez, U. Heiz, U. Landman, *Angew. Chem. Int.*, **2003**, 42, 1297.
27. A. Sanchez, S. Abbet, U. Heiz, W-D. Schneider, H. Hakkinen, R. N. Barnett and U. Landman, *J. Phys. Chem. A*, **1999**, 103, 9573.
28. E. Wahlstrom, N. Lopez, R. Schaub, P. Thostrup, A. Ronnau, C. Africh, E. Laegsgaard, J. K. Norskov and F. Besenbacher, *Phys. Rev. Lett.*, **2003**, 90, 026101.
29. B. K. Min, A. K. Santra and D. W. Goodman, *J. Vac. Sci. Technol. B*, **2003**, 21, 2319.
30. M. Baumer and H. J. Freund, *Prog. Surf. Sci.*, **1999**, 61, 127.
31. M. Baumer, M. Frank, M. Heemeier, R. Kuhnemuth, S. Stempel and H. J. Freund, *Surf. Sci.*, **2000**, 454/456, 957.
32. G. Haas, A. Menck, H. Brune, J. V. Barth, J. A. Venebles and K. Kern, *Phys. Rev. B*, **2000**, 61, 11105.
33. G. C. Bond, C. Louis and D. T. Thompson, *Catalysis by Gold*, Imperial College Press, London, **2006**.
34. M. A. Centeno, M. Paulis, M. Montes and J. A. Odriozola, *Appl. Catal. B: Environ.*, **2005**, 61, 77.

35. H. Liu, A. I. Kozlov, A. P. Kozlova, T. Shido, K. Asakura and Y. Iwasawa, *J. Catal.*, **1999**, 185, 252.
36. M. M. Schubert, S. Hackenberg, A. C.v. Veen, M. Muhler and V. Plazk and R. J. Bhem, *J. Catal.*, **2001**, 197, 113.
37. M. Okumura, J. M. Coronado, J. Soria, M. Haruta and J. C. Conesa, *J. Catal.*, **2001**, 203, 168.

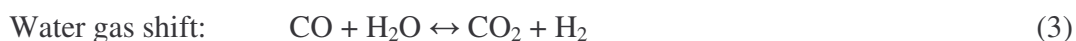
## Chapter 6

### Effect of gold on copper-based catalysts for the direct synthesis of DME from syngas.

#### 6.1 Introduction

The rapid changes and development in modern industry bring with them huge energy demands and major environmental issues. Dimethyl ether (DME) is known as a potential ultra-clean fuel which can be used in diesel engines, households, power generation and for many other purposes [1, 2]. Due to the huge market potential [3, 4], research involving DME is continually on the rise. Commercially, DME is produced mainly from syngas containing CO and H<sub>2</sub> through methanol (MeOH) synthesis and methanol dehydration, known as the two-step process [5, 6].

The principal incentive for developing a single-step syngas-to-DME process is to produce DME at a cost lower than that of the commercial two-step process. The cost penalties of the two-step approach are: (1) limited productivity in the syngas-to-methanol reactor due to equilibrium constraints and (2) the need for a second dehydration reactor and associated technology for separation units [5]. The single-step syngas-to-DME reaction system allows for greater productivity in a single reactor because of the synergy among the three reactions involved (Reactions 1-3).



However, downstream separation in the single-step process is much more complex and costly. This trade-off makes it necessary to optimize the productivity of the reactor in order to produce DME at a lower cost. In other words, the one step process will be able to

produce DME at a cost lower than the two-step process only if the methanol productivity of the reactor in the one-step process is sufficiently higher than the methanol productivity in the two-step process [7].

The key to optimal methanol synthesis is to develop the most effective catalyst. Many research groups are engaged in catalyst preparation using different catalyst compositions and preparation techniques. Although new catalysts based on nickel, copper and their alloys have been reported, copper still remains an important active catalyst component, even though the nature of the active site is yet to be fully understood [8].

Because the methanol synthesis reaction on a Cu-based catalyst is a structurally sensitive reaction, it is useful to modify its performance using various promoters, which could improve the activity, selectivity and/or stability of the catalyst [8]. Elements such as B, Ga, Co and Mg are some of the many promoters which have been added to copper-based methanol synthesis catalysts [9-12]. These promoters can modify the physico-chemical properties of Cu-based catalysts. More research is being carried out to find new promoters to improve the performance of the Cu-based methanol synthesis catalysts; however, no magic promoter seems to be in sight yet [8].

The promotion of Cu-based methanol synthesis catalysts with a secondary metal is not uncommon in the literature. For M/ZrO<sub>2</sub> (M = Cu, Ag or Au) catalysts, copper and silver were the most selective for methanol formation from CO<sub>2</sub> hydrogenation, with silver being significantly less active than copper [13]. Gold was the most active, but unselective, favoring the undesired reverse-water-gas shift (RWGS) reaction. Promotion of Cu/ZrO<sub>2</sub> with silver resulted in a distinct increase in methanol selectivity while the activity remained unaffected [14]. Spencer et al. [15] also reported that Cu-based catalysts promoted with iron, cobalt and nickel showed increased formation of methane and other long-chain paraffins.

In this work, two Cu-based bifunctional catalysts, promoted with gold, were studied in the syngas-to-dimethyl ether single-step synthesis process. The two methanol synthesis

catalysts studied were CuO-ZnO-Al<sub>2</sub>O<sub>3</sub> (abbreviated Cu-Zn-Al) and CuO-ZnO-Al<sub>2</sub>O<sub>3</sub>-ZrO<sub>2</sub>-Cr<sub>2</sub>O<sub>3</sub>-CeO<sub>2</sub> (abbreviated Cu-S5). These catalysts were characterized by X-ray diffraction (XRD) and temperature programmed reduction (TPR). We also report the activity and selectivity of the catalysts in the single-step DME synthesis process.

## 6.2 Results

### 6.2.1 Surface area

The BET surface areas of various methanol synthesis catalysts used in this study are reported in Table 1. The specific surface area of the pure Cu-Zn-Al catalyst was found to be 182 m<sup>2</sup>/g; however, that of the Au-(Cu-Zn-Al) catalyst was 173 m<sup>2</sup>/g. The decrease in the BET surface area upon Au loading was presumably as a result of the plugging of the pores by crystallites of CuO which were affected by Au as shown by the results of X-ray diffraction (6.2.2).

Table 1: BET surface areas of the various Cu-based methanol synthesis catalysts.

Catalyst	Au wt % <sup>a</sup>	BET surface area m <sup>2</sup> /g	Pore Volume cm <sup>3</sup> /g
Cu-Zn-Al	-	182	0.325
Au-(Cu-Zn-Al)	1.7	173	0.290
Cu-S5	-	56	0.147
Au-(Cu-S5)	1.5	50	0.130

a: Determined by XRF spectroscopy.

### 6.2.2 X-ray analyses

The X-ray diffraction patterns of CuO catalysts supported on mixed oxides supports are shown in Figure 1. In the Cu-Zn-Al samples (Figure 1a), no diffraction lines due to ZnO or Al<sub>2</sub>O<sub>3</sub> were observed in the diffraction pattern. However, XRD reflections due to crystalline CuO are noticed at  $2\theta = 35.5^\circ$  and  $38.7^\circ$ , and the intensities of these reflections are found to decrease with the loading of Au. The same effect of Au loading was observed on the Cu-S5 catalyst (Figure 1b). This fact suggested that Au suppressed the crystallinity of CuO in both catalysts. The XRD patterns also indicate that no characteristic peaks due to the formation of a mixed oxide phase between CuO and the ZnO-Al<sub>2</sub>O<sub>3</sub> support were found in the case of Cu-Zn-Al catalyst. However, in the case of Cu-S5 catalyst there were mixed oxide phases observed. Diffraction patterns due to Au were not observed due to the low Au loading on the various samples.

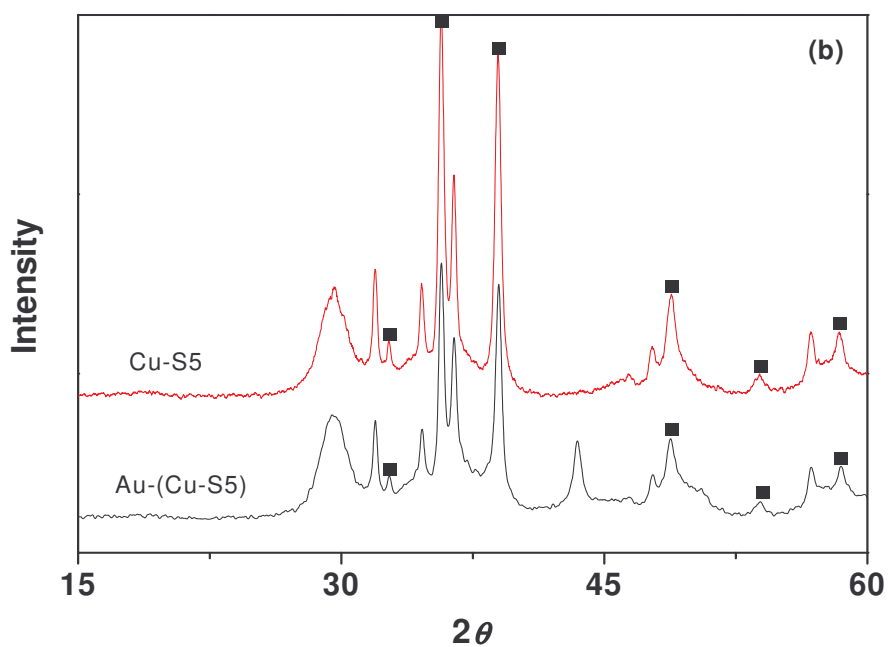
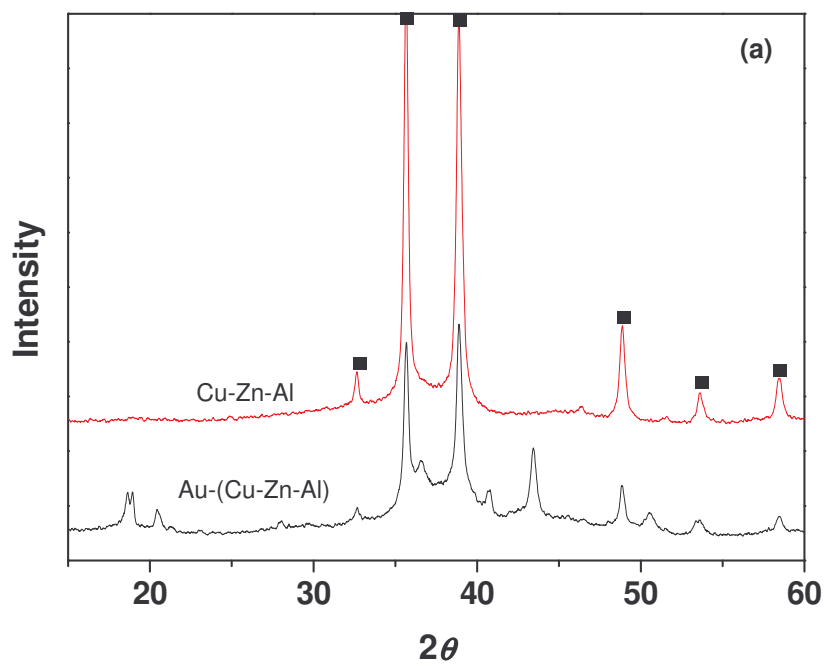


**Figure 1:** X-ray diffractograms of various Cu-based methanol synthesis catalysts (▪ CuO).

### 6.2.3 H<sub>2</sub>-TPR analyses

The reducibility of copper species in the Cu-Zn-Al and Cu-S5 catalysts was investigated by TPR experiments, and the profiles are shown in Figure 2. In both samples, reduction profiles changed with Au loading. In the Cu-S5 catalyst (Figure 2b), two different Cu species were observed. Similar results were found on a Cu-ZSM-5 zeolite catalyst [16]. It has also been reported that surface copper oxide species on the support is more easily reduced than bulk CuO [17-20]. The low temperature reduction peak (257 °C) for Cu-S5 is attributed to the highly dispersed surface CuO and/or Cu<sup>2+</sup> ions with an octahedral environment, and the TPR peak in the high temperature region (303 °C) is attributed to the reduction of bulk CuO [21, 22].

The loading of Au on the Cu-S5 catalyst reduced the crystallinity of CuO species in the catalyst as seen from the XRD results (Figure 1b). This presumably led to more surface CuO species in the Au-(Cu-S5) catalyst as indicated by the increased intensity of the reduction peak at 257 °C, which appears as a shoulder in Figure 2b. Also from Figure 2b it is seen that the loading of Au shifted the reduction peak of bulk CuO species from 303 °C to 290 °C. Such a shift has been reported on Au/CuO-ZnO catalysts used for low temperature water gas shift (WGS) reaction and CO oxidation [23, 24]. It is possible that the presence of gold on the mixed oxides support activates the hydrogen for reduction of CuO at lower temperatures or, alternatively, changes the reducibility of the CuO itself [24]. All the foregoing observations and arguments apply just as well for the Cu-Zn-Al catalyst as confirmed by results in Figures 1a and 2b.

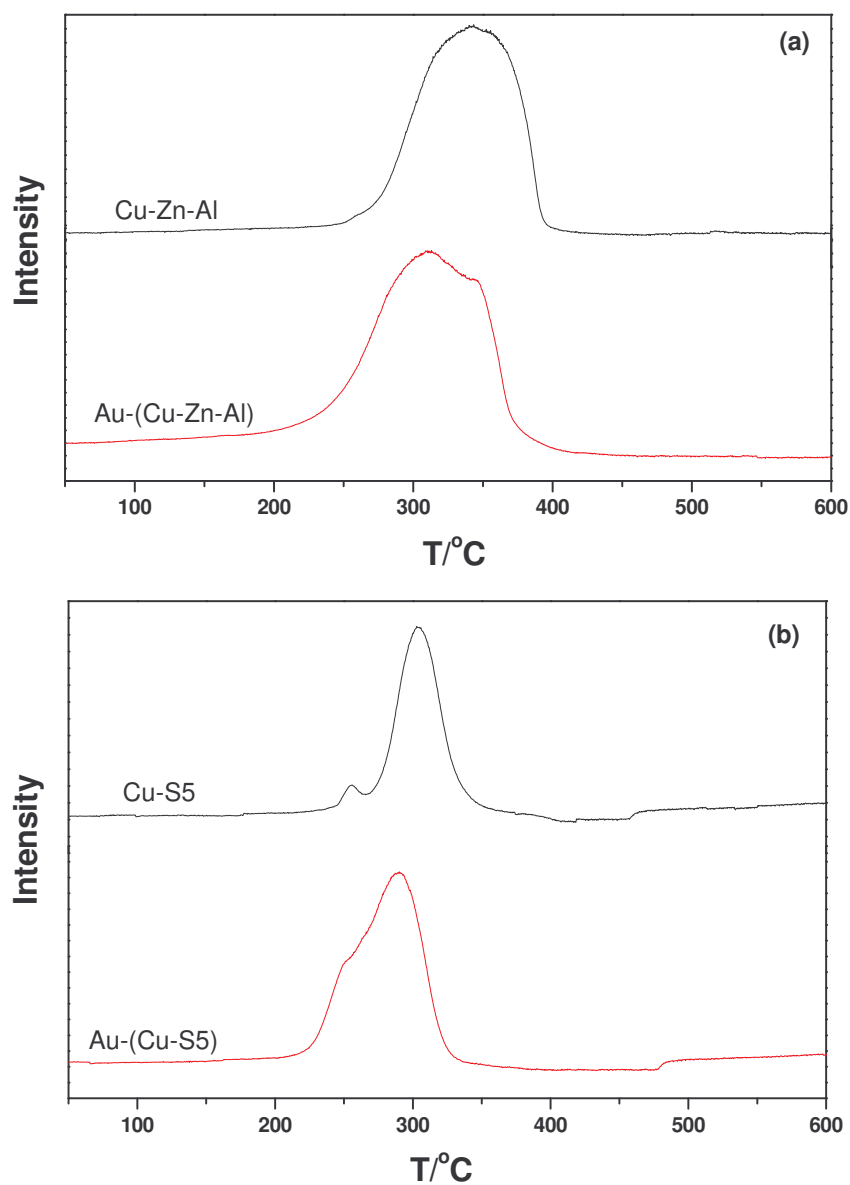


**Figure 2:** Hydrogen temperature-programmed reduction ( $H_2$ -TPR) profiles of various Cu-based methanol synthesis catalysts.

#### 6.2.4 Effect of addition of Au on catalytic activities

The activity and selectivity of different bifunctional catalysts are summarized in Tables 2 and 3. No hydrocarbons (e.g. alkanes, olefins etc.) were detected in any experiments, except methane ( $CH_4$ ). In all cases the conversion of CO increased with the rise in temperature from 250 °C to 300 °C. On Cu-Zn-Al/ $\gamma$ - $Al_2O_3$ , the conversion of CO

increased from 22.8 % at 250 °C to 57 % at 300 °C and throughout that temperature range the main product was DME. However, the selectivity to DME dropped with increasing temperature as methanation and water gas shift (WGS) reactions became more prominent at high temperatures. On the Au-(Cu-Zn-Al)/ $\gamma$ -Al<sub>2</sub>O<sub>3</sub> catalyst, the conversion of CO was higher than that of the 'pure' Cu-Zn-Al/ $\gamma$ -Al<sub>2</sub>O<sub>3</sub> catalyst; however, the selectivity to DME was inferior to that of the latter catalyst. The selectivity to CO<sub>2</sub> (WGS) surpassed that of DME at 300 °C on the Au-loaded catalyst. The loading of Au on Cu-Zn-Al also reduced the methanation reaction at all temperatures investigated.

On Cu-S5/  $\gamma$ -Al<sub>2</sub>O<sub>3</sub> only trace amounts of methane were detected (Table 3). The loading of Au on the Cu-S5 catalyst almost completely inhibited the formation of methane even at high temperatures (300 °C). The Cu-S5/ $\gamma$ -Al<sub>2</sub>O<sub>3</sub> catalyst also showed superior selectivity to DME compared to Cu-Zn-Al/ $\gamma$ -Al<sub>2</sub>O<sub>3</sub>, although it showed lower CO conversion. The differences in CO conversion activity could be attributed to the higher Cu content on Cu-Zn-Al than on the Cu-S5 catalyst (Chapter 3). In general the Cu-S5/ $\gamma$ -Al<sub>2</sub>O<sub>3</sub> catalyst proved to be a better catalyst than Cu-Zn-Al/ $\gamma$ -Al<sub>2</sub>O<sub>3</sub> for the direct synthesis of DME as further shown by the space-time yield (STY) of DME results reported in Figure 3. The loading of Au on both catalysts did not have any significant effect on their productivity of DME at all temperatures investigated, indicative of the fact that Au was neither involved in the methanol synthesis (Reaction 1) nor its dehydration (Reaction 2).

Table 2: Effect of Au loading on the catalytic activity of the Cu-Zn-Al catalyst.

Catalyst	Temp °C	% CO conversion	% Selectivity			
			CH <sub>4</sub>	CO <sub>2</sub>	MeOH	DME
Cu-Zn-Al/ $\gamma$ - Al <sub>2</sub> O <sub>3</sub>	250	22.8	4.7	31.2	2.6	61.5
	275	45.8	7.2	37.3	0	55.5
	300	57.0	13.8	38.8	0	47.4
Au-(Cu-Zn- Al)/ $\gamma$ -Al <sub>2</sub> O <sub>3</sub>	250	25.3	3.5	48.2	0	48.3
	275	48.7	5.9	45.9	0	48.2
	300	67.4	10.6	46.6	0	42.8

Reaction conditions H<sub>2</sub>:CO = 2, GHSV 343 h<sup>-1</sup>, pressure 5.0 MPa.

Table 3: Effect of Au loading on the catalytic activity of Cu-S5 catalyst.

Catalyst	Temp °C	% CO conversion	% Selectivity			
			CH <sub>4</sub>	CO <sub>2</sub>	MeOH	DME
Cu-S5/ $\gamma$ -Al <sub>2</sub> O <sub>3</sub>	250	22.0	0.1	27.0	7.6	65.3
	275	41.4	0.2	26.7	0	73.1
	300	53.1	0.5	25.3	0	74.2
Au-(Cu-S5/ $\gamma$ - Al <sub>2</sub> O <sub>3</sub>	250	27.8	0	35.0	10.0	55.0
	275	48.7	0	42.0	0	58.0
	300	60.5	0.1	32.0	0	67.9

Reaction conditions H<sub>2</sub>:CO = 2, GHSV 343 h<sup>-1</sup>, pressure 5.0 MPa.

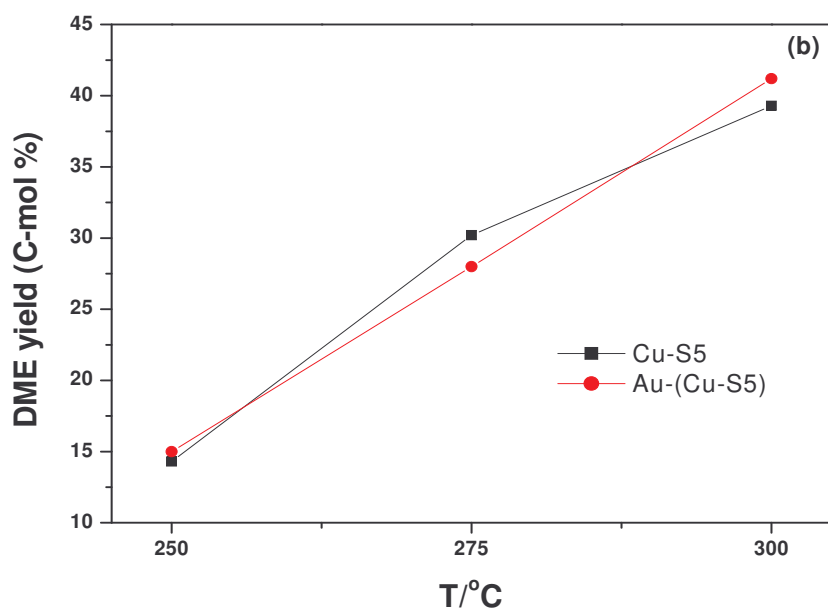
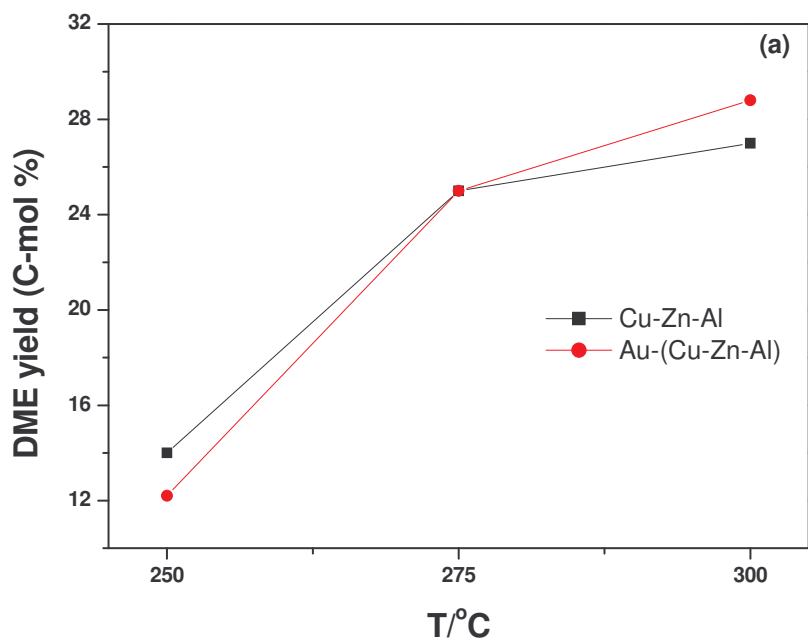


**Figure 3:** Effect of temperature on DME synthesis reaction over various catalysts: all catalysts mixed with  $\gamma$ -Al<sub>2</sub>O<sub>3</sub> (1:1), pressure 5.0 MPa, H<sub>2</sub> : CO = 2, GHSV = 343 h<sup>-1</sup>.

### **6.3 Discussion**

A significant factor in controlling the catalytic activity of many catalysts is the formation of a very fine intimate contact between the noble metal and the support. In the case of Cu-based methanol synthesis catalysts, this is achieved by pre-treating the catalyst at high temperatures in a reducing atmosphere. This is because the structure and catalytic performance of such Cu catalysts depends on the calcination and subsequent reduction [25, 26]. The XRD and TPR results reported in this work (Figures 1 and 2) indicate a possibility of change in the morphology and proportions of amorphous and crystalline forms of CuO upon the loading of Au in the catalysts studied.

However, the reduction process is exothermic and can accelerate the agglomeration of surface active sites; especially at high temperatures. The fact that Au containing Cu catalysts could be reduced at lower temperatures (Figure 2) might have been beneficial for improving Cu<sup>0</sup> dispersion and hence CO conversion activity. Fujita et al. [27] have emphasized the importance and role of low temperature reduction on the dispersion and catalytic activity of Cu-based methanol synthesis catalysts.

Although the Au loaded catalysts showed improved catalytic CO conversion (Tables 2 and 3), one cannot ignore the role that the formation of carbon dioxide (CO<sub>2</sub>) played in the reaction. CO<sub>2</sub> was formed in relatively large quantities on these catalysts, especially at high temperatures. The WGS reaction is kinetically enhanced by an increase in the reaction temperature. It has been reported that metallic gold (Au<sup>0</sup>) supported on various metal oxides is more active than the commercial Cu/ZnO-Al<sub>2</sub>O<sub>3</sub> catalyst for the WGS reaction [28 and refs. therein]. So it is perhaps not surprising that the Au loaded bifunctional catalysts showed higher selectivity towards CO<sub>2</sub> than the 'Au-free' catalysts.

In terms of economic and process implications, the enhanced WGS reaction in the case of Au containing Cu-based catalysts might have its advantages. The kinetics of the WGS reaction (Reaction 3) is much greater than that of the other two reactions (Reactions 1 and 2). This fast reaction provides the ultimate sink to drive the other two reactions away

from equilibrium. In other words, the WGS reaction together with the methanol dehydration has three positive effects on methanol synthesis in the *CO-rich* regime [7]:

- (1) Consuming methanol to expand the equilibrium boundary,
- (2) forming  $H_2$  to replenish the limiting reactant, and
- (3) forming  $H_2$  to slow down the equilibrium.

Also, under CO-rich atmospheres these three effects would be reached to their full extent.

The  $CO_2$  (WGS) formation reaction drives almost all the water into  $H_2$  if the atmosphere is CO-rich as stated already. So it would be advantageous to promote Cu-based catalysts with Au to enhance the removal of  $H_2O$  from the DME product; as it has also been reported that high concentration of  $H_2O$  causes catalyst stability problems [29]. It would also be cheaper in terms of down-stream separation to separate a  $CO_2 + DME$  product than  $H_2O + DME$ ; through refrigeration techniques.

To summarize; the  $CO_2$  formation (WGS) was highest over catalysts containing Au.  $CO_2$  formation over the 'Au-free' bifunctional catalysts was lower but still significant. Methanation did not take place over the Cu-S5/ $\gamma$ - $Al_2O_3$  bifunctional catalyst. On the other hand methane was formed in significant amounts on Cu-Zn-Al/ $\gamma$ - $Al_2O_3$ . The loading of Au on this latter catalyst suppressed the methanation process.

Further studies on the effect of Au loading on the deactivation and subsequent regeneration of the bifunctional catalyst systems are necessary. Also the addition of  $CO_2$  to the feed needs to be studied to determine what its effect would be on both Au loaded and 'Au-free' bifunctional catalysts.

#### **6.4 Conclusions**

- (1) The six component mixed oxide Cu-S5 is a better methanol synthesis component than the Cu-Zn-Al ternary mixed oxide.
- (2) Au lowers the reduction temperature of CuO on the methanol synthesis catalysts.
- (3) Au suppresses the crystallinity of CuO in both methanol synthesis components studied.
- (4) Au promotes the WGS reaction activity of both the bifunctional catalysts studied.
- (5) Au has no effect on the productivity of DME, i.e. it does not play any role in both the methanol synthesis reaction and methanol dehydration reactions on the Cu-based bifunctional catalysts.
- (6) The loading of Au suppresses methanation on both bifunctional catalysts studied.

## 6.5 References

1. V. V. Galvita, G. L. Semin, V. D. Belyaev, T. M. Yurieva and V. A. Sobyenin, *Appl. Catal. A*, **2001**, 216, 85-90.
2. T. L. Tartamella and S. Lee, *Fuel Process. Technol.*, **1997**, 38(4), 228.
3. G. Y. Cai, Z. M. Liu, R. M. Shi, C. Q. He, L. X. Yang, C. L. Sun and Y. J. Chang, *Appl. Catal. A*, **1995**, 125, 29-38.
4. T. Jiang, C. J. Liu, M. F. Rao, C. D. Yao and G. L. Fan, *Fuel Process. Technol.*, **2001**, 73, 143-152.
5. X. D. Peng, A. W. Wang and B. A. Toseland, *Ind. Eng. Chem. Res.*, **1999**, 38, 4381.
6. Y. Adachi, M. Komoto and I. Watanabe, *Fuel*, **2000**, 79, 229.
7. X. D. Peng, U. S. Department of Energy, Topical Report, **2002**.
8. X. M. Liu, G. Q. Lu, Z-F Yang and J. Beltramini, *Ind. Eng. Chem. Res.*, **2003**, 42, 6518-6530.
9. B. J. Liaw and Y. Z. Chen, *Appl. Catal. A*, **2001**, 206, 245.
10. M. Kilo, J. Weigel, A. Wokaun, R. A. Koepfel, A. Stoeckli and A. Baiker, *J. Mol. Catal. A: Chem.*, **1997**, 126, 169.
11. J. Toyir, P. R. De la Piscina, J. L. G. Fierro and N. Homs, *Appl. Catal. B*, **2001**, 29, 207.
12. J. Toyir, P. R. De la Piscina, J. L. G. Fierro and N. Homs, *Appl. Catal. B*, **2001**, 34, 255.
13. A. Baiker, M. Kilo, M. Maciejewski, S. Menzi and A. Wokaun, *Stud. Surf. Sci. Catal.*, **1993**, 75, 1257.
14. C. Froehlich, R. A. Koppel, A. Baiker, M. Kilo and A. Wokaun, *Appl. Catal.*, **1993**, 106, 275.
15. M. V. Twigg and M. S. Spencer, *Appl. Catal. A*, **2001**, 212, 161.
16. I. Yan, D. G. Lee, W. M. H. Sachtler and H. H. Kung, *J. Catal.*, **1996**, 161, 43.
17. G. Fierro, M. L. Jacono, M. Inversi, P. Porta, R. Lavecchia and F. Cioci, *J. Catal.*, **1994**, 148, 709.
18. R. Zhou, T. Yu, X. Jiang, F. Chen and X. Zheng, *Appl. Surf. Sci.*, **1999**, 148, 263.
19. F. S. Delk and A. Vavere, *J. Catal.*, **1994**, 147, 322.

20. L. J. Kundakovic and M. Flytzani-Stephanopoulos, *Appl. Catal. A*, **1998**, 171, 13.
21. M. Shimokawabe, H. Asakawa and N. Takezawa, *Appl. Catal.*, **1990**, 59, 45.
22. W. P. Dow, Y. P. Wang, and T. J. Huang, *J. Catal.*, **1996**, 160, 155.
23. *Chemical Research in Chinese Universities*, **2006**, 22(1), 99.
24. <[www.gold.org/discover/sci\\_indu/gold2003/pdf/s36a1363p994.pdf](http://www.gold.org/discover/sci_indu/gold2003/pdf/s36a1363p994.pdf)> 30<sup>th</sup> July 2007.
25. T. Fujitani and J. Nakamura, *Appl. Catal. A*, **2000**, 191, 111.
26. I. S. Fujita, S. Moribe, Y. Kannamori, M. Kakudate and N. Takezawa, *Appl. Catal. A*, **2001**, 207, 121.
27. I. S. Fujita, Y. Kanamori, A. M. Satriyo, and N. Takezawa, *Catal. Today*, **1998**, 45, 241.
28. G. C. Bond, L. Catherine and D. T. Thompson, *Catalysis by Gold*, Imperial College Press, London **2006**.
29. A. Basu, WO Patent 00/47874, **2000**.

# Chapter 7

## General Conclusions

The low temperature oxidation of carbon monoxide has gained growing interest in the last two decades. Although much work has already been invested into investigating gold catalysts used in this reaction, the reaction kinetics and the mechanism are still under discussion. In Chapter 4 of this thesis we focused on a study of a titanate nanotube supported gold catalyst (Au/TN), prepared by a modified deposition precipitation technique. The CO oxidation activity measurements which were carried out in a micro reactor with on-line GC analytics revealed that this catalyst was not stable, i.e. it suffered a rapid deactivation with time-on-line (Chapter 4). DRIFTS measurements carried out during CO oxidation were presented (Chapter 4) which helped identify the nature of products and possible intermediates or by-products formed during the reaction. These experiments clearly showed that there was bicarbonate species (identified by OH deformation vibration at  $1290\text{ cm}^{-1}$ ) formed during reaction.

In order to correlate the concentration of the bicarbonate species formed during the CO oxidation reaction with measured reaction rates we combined the in situ DRIFTS set-up with an on-line mass spectrometer and our results (Chapter 4) showed that the accumulation of the bicarbonate species led to catalyst deactivation. These bicarbonate species could be simply removed by the addition of water to the feed. Gold was found to be a necessary ingredient to form these bicarbonate species. To consolidate these findings, additional CO<sub>2</sub>-TPD experiments were performed and indeed the results showed there was always a CO<sub>2</sub> desorption peak unique to gold-loaded supports that was absent on the pure supports. It was concluded that this species of CO<sub>2</sub> was most probably stored on gold sites as the bicarbonate observed in the DRIFTS data. Again, moisture inhibited formation of such species. Based on the obtained results we conclude that the bicarbonate species are formed as a result of CO<sub>2</sub> produced from the oxidation of CO on Au/TN leading to the ultimate deactivation of the catalyst.

Non-stoichiometric titanium dioxide ( $\text{TiO}_2$ ) is a well known n-type semiconductor. The defects can be created by reduction in hydrogen or by evacuation at high temperature. However, there is still some controversy regarding the nature of defect sites in non-stoichiometric titania. In Chapter 5 the oxidation of CO over  $\text{TiO}_2$  supported gold was studied to understand the nature and role of defect sites in the  $\text{Au}/\text{TiO}_2$  type catalysts. In the work done in this thesis oxygen vacancies were created on the surface/bulk of  $\text{TiO}_2$  by doping the oxide with nitrogen as confirmed by DRS-UV vis spectroscopy and TPO results (Chapter 5). Oxygen vacancies on the surface of  $\text{TiO}_2$  play an important role in the chemisorption of different adsorbates. This explains the different behaviors of the pure anatase  $\text{TiO}_2$  and the nitrogen-doped titania,  $\text{TiO}_{2-x}\text{N}_x$ , as supports for gold catalysts. The  $\text{Au}/\text{TiO}_{2-x}\text{N}_x$  catalyst system is less stable and less active than  $\text{Au}/\text{TiO}_2$  for the oxidation of CO.

Moisture promotes catalytic CO oxidation over  $\text{Au}/\text{TiO}_2$  and inhibits deactivation of the catalyst when introduced in the feed from the start of reaction. However, on the  $\text{Au}/\text{TiO}_{2-x}\text{N}_x$  catalyst system moisture had no observable lasting effect on its activity in CO oxidation. For future work *in situ* infrared and TPD work will need to be done in order to further understand the reasons for the observed differences in the activity of the two catalysts.

In Chapter 6, the results for the direct synthesis of dimethyl ether (DME) from syngas over gold promoted Cu-based bifunctional are presented. From the data presented it is concluded that the six component mixed oxide, Cu-S5, is a better methanol synthesis catalyst support than the Cu-Zn-Al ternary mixed oxide. The loading of gold onto these Cu-based methanol synthesis catalysts was found to: (1) suppress the crystallinity of CuO, (2) lower the reduction temperature of CuO, (3) promote the water-gas-shift (WGS) reaction activity, and (4) suppress methanation.